NUMERICAL SIMULATIONS OF THE SPIKING ACTIVITY AND THE RELATED FIRST EXIT TIME OF STOCHASTIC NEURAL SYSTEMS

A thesis submitted to the University of Manchester
for the degree of Doctor of Philosophy
in the Faculty of Engineering and Physical Sciences

2011

Hasan Mohammed O Alzubaidi

School of Mathematics

Contents

Word count: 12212

List of Figures

The University of Manchester

Hasan Mohammed O Alzubaidi
Doctor of Philosophy
Numerical simulations of the spiking activity and the related first exit time of stochastic neural systems
September 28, 2011

The aim of this thesis was to study, using numerical simulation techniques, the possible effects of an additive noise on the firing properties of stochastic neural models, and the related first exit time problems. The research is divided into three main investigations. First, using SDELab, mathematical software for solving stochastic differential equations within MATLAB, we examine the influence of an additive noise on the output spike trains for the space-clamped Hodgkin Huxley (HH) model and the spatially-extended FitzHugh Nagumo (FHN) system. We find that a suitable amount of additive noise can enhance the regularity of the repetitive spiking of the space-clamped HH model. Meanwhile, we find the FHN system to be sensitive to noise, requiring that very small values of noise are chosen, in order to produce regular spikes. Second, under additive noise, we use fixed and exponential time-stepping Euler algorithms, with boundary tests, to calculate the mean first exit times (MFET) for one-dimensional neural diffusion models, represented by a stochastic space-clamped FHN system and the Ornstein-Uhlenbeck (OU) model. The strategies and theory behind these numerical methods and their convergence rates in the MFET are also considered. We find that, for different values of noise, these methods with boundary tests can improve the rate of convergence from order one half to order one, which coincides with previous studies. Finally, we look at spatially-extended systems, represented by the Barkley system with additive noise that is white in time and correlated in space, calculating mean nucleation times and mean lifetimes of traveling waves, using an efficient numerical simulation. A simple model of the dynamics of the underlying Barkley model is introduced, in order to compute the mean lifetimes, particulary for interacting waves. The reduced model is easy to use and allows us to explore the full dynamics of the kinks and antikinks, in particular over long periods. One application of the reduced model is to calculate the mean number of kinks at a given time and use this to obtain the probability that the system is excitable at a given position. With these three investigations into the effects of additive noise on stochastic neural models, we have demonstrated some of the interesting results that can be achieved using numerical techniques. We hope to extend this work, in the future, to include the effects of multiplicative noise.

Declaration

No portion of the work referred to in this thesis has been submitted in support of an application for another degree or qualification of this or any other university or other institute of learning.

Copyright Statement

Acknowledgements

First, praise and thanks to almighty Allah, most gracious, most merciful who enabled me to finish this work. I would like to express my sincere thanks and deepest gratitude to my supervisor Dr. Tony Shardlow for his kind guidance, continuous support and encouragement throughout my PhD project. I really appreciate his warm advice and the opportunity he gave me to work with him. I would like to register my gratitude to my officemates and other members of staff and PhD students in the school of mathematics at Manchester university, who have been supportive and helpful during my PhD journey. Finally, I would like to thank my parents, my wife and my daughters for their caring support, patience and constant love.

Chapter 1

Introduction

1.1 Overview

Understanding the mechanism by which information is transmitted between the body's nerve cells has received vigorous interest during the last several years. A nerve cell, or a neuron, which is a basic unit of the nervous system, is responsible for conveying the information via an electrical signal known as a spike or action potential. In simple terms, the neuron produces an action potential when its membrane potential exceeds a firing threshold in response to a strong stimulus (suprathreshold), that is distinguishable from background noise. A neuron that is capable of producing an action potential is said to be excitable. The excitable neuron, in fact, is characterized by three states: the quiescent or rest state, the excited state and the refractory or recovery state [95]. Thus, under a sufficiently strong stimulus, the excitable neuron switches from the quiescent state to the excited state; a short time later it falls into the refractory state, before returning to its quiescent state. The neuron then requires a certain amount of recovery time before it is capable of producing another spike. When the input stimulus is weak (subthreshold), however, the neuron remains quiescent and no spike is generated.

The first landmark model for the generation and propagation of neural spikes was the Hodgkin-Huxley (HH) model, which forms the basis for all models of excitable membrane behaviour, although it was originally developed to describe the spike behaviour in the long giant axon. Alan Hodgkin and Andrew Huxley [38] were awarded the Nobel Prize in Physiology or Medicine in 1963, for this outstanding achievement. FitzHugh [20, 19] later studied the model and reduced it to a two-variable (excitable and recovery) model in order to apply phase plane analysis. Later, Nagumo [68] constructed a circuit using tunnel diodes for the nonlinear channels modeled by the FitzHugh equations, and thus these equations have become known as the FitzHugh-Nagumo (FHN) model.

Many sources of noise can be modeled with these systems [63]. For instance, the noise may come from randomness in the opening and closing times of ionic channels. It may also come from synaptic events in the form of additive noisy synaptic current, which we use for the models in our work.

The aim of our thesis is to study, using numerical simulations, the effects of an additive noise combined with these neural models, both space-clamped models and spatially-extended systems, on the spiking activity of a single neuron and the related first exit time problems.

A noisy neural model is a system of stochastic differential equations (SDEs), whose solution, which represents the membrane potential of a single neuron, can often be approximated by a diffusion process. Unfortunately, being able to solve an SDE explicitly is rare, so accurate numerical solutions play a crucial role. The main approaches to finding a numerical solution are based on discrete-time approximations, and either strong or weak numerical schemes [48]. Strong approximations involve computing individual sample paths, while weak ones involve computing approximations to the probability distribution of the solution or, in general, a functional of the

solution, such as the first or second moment.

Using SDELab, a package for producing strong numerical solutions for SDEs within MATLAB, we begin by examining and analyzing the effects of additive noise on the spiking dynamics of the stochastic space-clamped HH model [86] and the spatially-extended FHN system with space-time white noise. This is described in Chapter 2. The SDELab software was created by Hagen Gilsing and Tony Shardlow [29], with the aim of making the analysis and manipulation of SDEs easily approachable. The software provides different explicit and implicit solvers for Itô and Stratonovich SDEs.

Specifically, we wish, first of all, to explore the firing properties of the space-clamped HH model, in response to the application of a suprathreshold, constant current, and to examine the influence of additive noise on the output spike trains. Repetitive firing in the HH model has been studied and analyzed extensively, particularly in the noiseless case; see, for example [36, 75, 33, 84, 50]. Adding a suitable amount of noise to the HH model may enhance the regularity of the repetitive spiking of the neuron, and this noise-induced phenomenon is known as the coherence resonance [56]. We will hence examine this beneficial effect of noise on the output spike trains of the HH model, using SDELab.

Furthermore, we will regard a FHN system with additive space-time white noise as a parabolic stochastic partial differential equation (SPDE) that can be formulated as an evolution SDE equation in infinite-dimensional space. Based on the theory presented in [70], the existence and uniqueness of the solution of an SDE equation in infinite-dimensional space will be discussed briefly. Following [81], a parabolic SPDE can be discretized spatially, to obtain a system of SDEs, which can be solved numerically using SDELab. We will implement this technique for the FHN system with additive space-time white noise, and evaluate the influence of a small additive

noise on the regularity of output spikes.

Mainly, these neuronal models are modeled and approximated by diffusion processes, due to the well-developed theory on stochastic processes, which enables us to evaluate the firing probabilities of the spiking activity of a single neuron, including the functionals of the so-called first exit time (FET)[46]. There has been significant interest in studying the FET of the membrane potential through a constant firing threshold, since the time to the first spike is believed to hold significant information about the stimulus properties [90, 91]. In Chapter 3, we will study the FET problem, using numerical simulations, for a one-dimensional diffusion, where, in this case, the basic characteristics of such problems, including the distribution of the FET and the boundary behaviour properties, can be calculated explicitly. This has created a strong motivation for research into the first exit phenomenon and the literature on the topic is extensive, for example [46, 40, 3].

We wish to evaluate the effects of additive noise on the systematic errors in the mean FET for the stochastic version of the space-clamped FHN system studied by Tuckwell et al. [89] and for the Ornstein-Uhlenbeck (OU) model studied by Lansky and Lanska [52]. The OU process is the simplest stochastic leaky integrate-and-fire (LIF) model for describing nerve membrane behaviour [51]. It is used to approximate the subthreshold membrane potential of a nerve cell receiving random synaptic inputs, "resulting from the stochastic dendritic currents that are caused by the action potentials of other neurons or by external stimulation in sensory neurons" [53, 54]. The spiking activity of the OU model is identified by the FET of the membrane potential through a constant boundary, which is described completely by its density probability function. Unfortunately, no closed form solution, in general, can be obtained for this density and so numerical techniques and simulation procedures are needed [54]. It is also of interest to evaluate the moments of the FET of the model, in particular the first moment or mean FET (MFET), which can be obtained

analytically using Siegert theory [81]. Indeed, several numerical and simulation techniques for obtaining the distributions of the FET of the OU model and its moments have been discussed in the literature. See, for example, [52, 11, 30, 31, 74] and the references quoted therein.

We restrict our simulation of the MFET of the OU model to the cases studied in [52]. Lansky and Lanska [52] used a fixed time step simulation method (Heun's method), which was found, as is the case with other fixed time step simulation techniques, to overestimate the actual values of the MFET. Decreasing the time step of the simulation can make this overestimation smaller, but the price paid for this is long run-times. Therefore, Lansky and Lanska proposed an adaptive time step algorithm to speed up the simulation and make this overestimation smaller.

Tuckwell et al. [89] used the theory of diffusion processes to obtain partial differential equations for the mean and variance of the FET of a FHN system with Gaussian additive noise. During the elementary stages of the interspike interval, the recovery variable in the FHN system is practically unaffected, and therefore these partial differential equations can be reduced to one-dimensional equations that can easily be solved analytically. Tuckwell et al. compared the results obtained through this analytical framework to computer simulation results obtained using the fixed time-stepping Euler (Euler-Maruyama) method.

However, the error in the mean FET, H_b say, of the one-dimensional diffusion process, $X(t)$, through a constant threshold boundary, b, produced using the Euler method, with fixed time step Δt is found to be proportional to $\Delta t^{\frac{1}{2}}$ [43, 32]. The Euler simulation of the FET for $X(t)$ overestimates the real values, because, under Euler simulation, the continuous sample paths of the Wiener process are approximated by discrete random walks, giving values only at the beginning and end of each time step, and therefore we have no information about the behaviour of the continuous process

during the time step [9]. Thus, we have the possibility that the process reaches the threshold boundary during the time step, but then returns inside the boundary before the time step ends, so that it is within the boundary at the beginning and the end of the time step, and appears not to have crossed the boundary [43, 59, 32]

Mannella [59] dealt with this situation by applying a simple boundary test after each time step using a Brownian bridge, pinned between the beginning and the end of the time step. Later, Gobet [32] proved that this test, when combined with the fixed time-stepping Euler algorithm, could improve the weak order of convergence from $O(\Delta t^{\frac{1}{2}})$ to $O(\Delta t)$ in the evaluation of the functional F of $X(t)$ conditioned on $t < H_b$, with support or regularity conditions on F [32, 8]. Jansons and Lythe [43] (see also Figure 2 in [8]), suggested, on the basis of their own numerical experiments using the fixed time-stepping Euler method with Mannella's boundary test, that this first-order convergence can also be obtained for the case of the exit time. We expect that our numerical experiments for the stochastic FHN system and the OU model will support this observation for different values of noise. Moreover, we will examine the effects of additive noise on the errors in the mean FET for these neural models, both in the presence of the boundary test and without it.

When the time step is a random variable with an exponential distribution, the probability that the boundary has been hit during the time step can also be taken into account using the simple efficient boundary test [43, 42]. Analogously to the fixed time-stepping algorithm, the boundary test for the exponential time-stepping Euler method improves the rate of convergence of the mean FET from $O(\Delta t^{\frac{1}{2}})$ to $O(\Delta t)$, which coincides with our numerical observations for the stochastic FHN system and the OU model.

The final part of our thesis is devoted to examining, using numerical simulations, the effects of additive noise on the spiking activity of one-dimensional spatially-extended neural systems (or, in general, excitable systems) representing the propagation of traveling waves along nerve fiber [80, 95]. In an excitable system, it is possible for waves to be produced through strong changes in the rest state, caused by local nonlinearity and diffusion [61, 95]. Therefore, a generic excitable medium can be represented simply by a two-variable system of reaction-diffusion equations, such as the FHN system or its modification, known as the Barkley model [2].

Here, we are concerned with the Barkley model under the influence of additive noise that is white in time and correlated in space, with homogeneous initial conditions and periodic boundary conditions [82]. In this sub-excitable regime, the system can produce waves when appropriate amounts of noise are added, and consequently no structure can be nucleated under purely deterministic conditions [26]. Specifically, we are interested in exploring the influence of additive noise on the mean lifetime of the traveling waves of the Barkley model, and on their nucleation times, which can be formulated mathematically as FET problems. To this end, we will use the efficient numerical technique presented in [83], where a Wiener process that is white in time and correlated in space, with exponential decay in the spatial correlation, is generated using a fast Fourier transform (FFT), and the Laplacian is approximated using the spectral method. We further apply the exponential Euler method, which is a linearization-preserving integrator, to preserve the eigenvalues of the Laplacian.

The nucleation and dynamics of solitary structures in spatially-extended systems have been studied extensively, in particular for the ϕ^4- equation associated with additive space-time white noise [7]. Such structures are known as kinks, in one-dimensional equations, and their nucleation, propagation and eventual annihilation are worth studying. A kink is defined, for the model in our work, as a boundary with a region close to 0 to its left and a region close to 1 to its right; the opposite case

is called an antikink [58]. In our work, the left (right) sides of front waves and the right (left) sides of back waves are examples of kink (antikink) structures (see Figure 4.1 in Chapter 4). The kinks and antikinks are nucleated at random times and in random positions. They diffuse independently and are annihilated in collision [35]. Habib and Lythe [58, 35] studied a one-space dimensional ϕ^4- equation with space-time white noise, using high resolution numerical simulations, and then introduced a reduced model of kink dynamics that has the ability to predict the rate of nucleation and other physical quantities, such as time and length scales, which led to further understanding of the lifetimes of kinks.

In our work, we also introduce a reduced model of the dynamic behaviour of the stochastic Barkley model, which allows us to calculate the mean lifetimes of the generated traveling waves, even for a large space domain and for interacting waves. This is necessary because, in this case, using the numerical simulation of the Barkley model to calculate the mean lifetime of the interacting waves directly becomes computationally impractical. Under the reduced model, we calculate the mean lifetime of each kink and antikink of each wave, individually. This motivates us to explore the full dynamics of the kinks and antikinks, in particular over longer time periods. One application of the reduced model is to compute the mean number of kinks at a specific time and use this to obtain the probability that a given part of the phase space of the stochastic Barkley system is excited.

1.2 Outline of the thesis

Following this introductory chapter, the rest of the thesis is divided into four chapters and three appendices as follows.

Chapter 2 is devoted to studying the spiking activity of the space-clamped HH model with additive noise and the FHN system with space-time white noise, using

the SDELab package. We begin by introducing the integrators used in SDELab and then explain in detail how the SDEs and SPDEs represented by these neural models can be simulated using the SDELab software. The effects of an additive noise on the output spike trains are also considered.

In Chapter 3, we examine the effects of an additive noise on the FET, for the stochastic version of the space-clamped FHN system and for the OU model, using the fixed time-stepping Euler method with boundary correction and the exponential time-stepping algorithm with boundary test. First of all, we provide a detailed exposition of the strategies behind these methods and the analytical frameworks of relevant functionals of the FETs of the diffusion processes. Finally, we study the effects of the additive noise on the systematic errors in MFETs produced by these simulation techniques.

In Chapter 4, using efficient numerical simulations, we study the mean lifetimes and nucleation times, which can be formulated mathematically as FET problems, of the traveling waves generated under a non-linear spatially-extended system (the Barkley system) with additive noise that is white in time and correlated in space. Furthermore, we introduce a simple model of the dynamics of the underlying model, in order to calculate the mean lifetime efficiently, in particular for interacting waves.

Chapter 5 contains our conclusions and some ideas for future work. In Appendix A, we provide a brief exposition of some commonly-used concepts and foundations for the probability theory and theory of stochastic processes needed throughout the thesis. In Appendix B, we look briefly at Hilbert spaces and some theory that is strongly connected to PDEs, such as linear operator theory. In Appendix C, we include the computer simulation codes used to produce our results.

Chapter 2

Simulation of SDEs and SPDEs from neural systems using SDELab [1]

Various software packages can be used to solve and analyze SDEs. For instance, MATLAB provides an ideal environment for numerical computation. Some examples can be found in [37]. There is also a Maple package which for the symbolic manipulation and numerical analysis of SDEs [79].

Recently, Hagen Gilsing and Tony Shardlow [29] created *SDELab*, a package for producing strong numerical solutions for SDEs within MATLAB. The software provides different explicit and implicit solvers for Itô and Stratonovich SDEs. The current version of SDELab offers several numerical standard methods for computing strong solutions of SDEs (2.1)–(2.2) and generates configurable plots and subplots on demand [29].

SDELab can also be used to solve and analyze some SPDEs, such as the FitzHugh Nagumo (FHN) model with additive space-time white noise. In practice, many kinds

of dynamics that are stochastic in nature can be modeled by SPDEs and the state spaces of their solutions are necessarily infinite dimensional.
A rich body of theoretical work has been developed for SPDEs (see [70, 71]). Nevertheless, few of these equations have analytic solutions, so there is growing interest in producing numerical solutions. For instance, Shardlow [81, 83], Gains [23], Gyongy [34] and Davie and Gains [15] study parabolic SPDEs that are discretized spatially, to obtain a system of SDEs which can be solved by numerical methods. This approach will be implemented here for stochastic FHN equations.

The main aim of the present chapter is to illustrate using the Hodgkin-Huxley (HH) and FitzHugh-Nagumo (FHN) models, how SDEs and SPDEs can be solved numerically, and to give the reader tools to solve their own SDEs and SPDEs in SDELab. Moreover, the influence of the additive noise associated with these neuronal models on the spiking activity is considered.

The chapter is arranged as follows. In Section 2.1, we provide a mathematical description of SDEs and a brief exposition of Itô calculus. We also discuss without proof the existence and uniqueness of strong solutions of SDEs.

In Section 2.2, we introduce discrete-time approximations (integrators) used in the SDELab package and explain in detail how SDELab works. Furthermore, we consider the stochastic HH model with space-clamped technique and study some of the effects of additive noise on output spike trains using the SDELab package.

An evolution SPDE, say a parabolic SPDE can be considered as an evolution SDE in infinite dimensional spaces such as Hilbert spaces. Therefore in Section 2.3, some properties of the Wiener process with values in Hilbert space are briefly sketched. The existence and uniqueness of the solution of an evolution SDE in Hilbert space is also discussed. Moreover, we consider an SPDE system represented by the FHN

model with additive space-time white noise and discuss how we can simulate this system using the SDELab package. The effectiveness of small noise algorithms is also stated. Finally, some of the material in the present chapter has been published in the chapter 12 of the book: Stochastic methods in neuroscience [1].

2.1 SDEs and Itô calculus

Itô calculus is an extension of deterministic calculus and is thus a tool for studying stochastic processes such as the Wiener process. The central result of such a calculus is Itô's formula which is a stochastic counterpart of the chain rule of the deterministic calculus, useful for evaluating the Itô integral. Itô's formula is applied to derive the Itô-Taylor expansion that is used to construct discrete-time approximations of an Itô process. All of these notions will be studied in this section.

2.1.1 SDEs and Wiener process

Wiener process

The standard one-dimensional Wiener process $\beta = \{\beta(t), t \geq 0\}$ is defined as a Gaussian process with continuous sample paths, satisfying

$$\beta(0) = 0 \quad \text{w.p.1}, \quad E(\beta(t)) = 0, \quad Cov(\beta(t), \beta(s)) = \min\{t, s\},$$

for all $0 \leq s \leq t$, and where E and Cov represent mathematical expectation and covariance, respectively. Furthermore, the increments $\beta(t) - \beta(s)$, for all $0 \leq s \leq t$, are normally distributed random variables, with mean 0 and variance $t-s$. Moreover, for $0 \leq s < t < u < v$, the increments $\beta(t) - \beta(s)$ and $\beta(v) - \beta(u)$ are independent. The process $w(t) = (\beta_1(t), \beta_2(t), \cdots, \beta_p(t))$, which appears in SDEs (2.1) and (2.2) below, is defined as an $\mathbb{R}^p$-valued Wiener process with components β_j, $j = 1, 2, \cdots, p$, which are standard Wiener processes and pairwise independent. The Wiener process

is a mathematical description of Brownian motion. Therefore, it is also called a Brownian motion.

Mathematical formulation of SDEs

Mathematically, the Itô SDE is an object of the following type:

$$dX(t) = f(t, X(t))dt + g(t, X(t))dw(t), \qquad X(t_0) = X_0 \tag{2.1}$$

while the corresponding Stratonovich SDE can be written as

$$dX(t) = \underline{f}(t, X(t))dt + g(t, X(t)) \circ dw(t), \qquad X(t_0) = X_0, \tag{2.2}$$

where the notation "$\circ$" in (2.2) denotes the use of Stratonovich calculus. $f, \underline{f} : \mathbb{R} \times \mathbb{R}^d \to \mathbb{R}^d$ are *drift* functions and $g : \mathbb{R} \times \mathbb{R}^d \to \mathbb{R}^{d\times p}$ is a *diffusion* function. $w(t)$ is an $\mathbb{R}^p$-valued Wiener process. The initial condition $X(t_0) = X_0$ is deterministic. The solution $X(t)$ of the above SDEs is a stochastic process satisfying

$$X(t) = X(t_0) + \int_0^t f(s, X(s))ds + \int_0^t g(s, X(s))dw(s) \tag{2.3}$$

and

$$X(t) = X(t_0) + \int_0^t \underline{f}(s, X(s))ds + \int_0^t g(s, X(s)) \circ dw(s), \tag{2.4}$$

in the Itô and Stratonovich senses, respectively. Next, the difference between the Itô and Stratonovich calculi will be discussed further and the definition of stochastic integrals will be given.

The stochastic integral

The second integrals in (2.3) and (2.4) cannot be interpreted as Riemann or Lebesgue integrals because $w(t)$ is nowhere differentiable in the ordinary sense [49].

Therefore, these integrals need to be defined in some way. Itô overcame this problem by defining stochastic integrals using mean-square convergence. Thus, the Itô integral $\int_0^T g dw$ is defined as the mean-square limit of the sum [49]

$$S_n = \sum_{j=0}^{n} g(\tau_j)\{w(t_{j+1}) - w(t_j)\}$$

with evaluation points $\tau_j = t_j$ for partitions $0 = t_0 < t_1 < \cdots < t_{n+1} = T$. In the limit $\delta = \max_{0\leq j\leq n}(t_{j+1} - t_j) \to 0$ and $n \to \infty$. In general, the evaluation point τ_j is

$$\tau_j = (1-\lambda)t_j + \lambda t_{j+1}, \quad 0 \leq \lambda \leq 1.$$

When $\lambda = 0$ this leads to the Itô integral, while the Stratonovich integral $\int_0^T g \circ dw$ as in (2.4) is obtained by setting $\lambda = \frac{1}{2}$ [49]. To understand more about the differences between the two calculi, we set $g = w$ in the sum S_n, yielding [49]

$$\int_0^T w(t)dw(t) = \frac{1}{2}w(T)^2 + (\lambda - \frac{1}{2})T.$$

Thus, in the Itô case ($\lambda = 0$), we have $\int_0^T w(t)dw(t) = \frac{1}{2}w(T)^2 - \frac{1}{2}T$, which contains an additional term $(-\frac{1}{2}T)$ not present in classical calculus. In contrast, Stratonovich calculus ($\lambda = \frac{1}{2}$) gives the same result as classical calculus: $\int_0^T w(t) \circ dw(t) = \frac{1}{2}w(T)^2$. This property of obeying the transformation rules of classical calculus is the main reason for using Stratonovich calculus in many applications, for which white noise is used as an idealization of a real noise process [49]. Meanwhile, Itô calculus is convenient for modeling the external noise arising in many biological and physical systems, in which the noise is independent of the current state [49].

However, it is possible to move between Itô and Stratonovich calculus using a simple transformation, since the solution of the Itô equation (2.1) can be written as the solution of the Stratonovich equation (2.2) with the modified drift function

defined component-wise by [49]

$$\underline{f}^i = f^i - \frac{1}{2}\sum_{j=1}^{d}\sum_{k=1}^{p} g_{jk}\frac{\partial g_{ik}}{\partial x_j} \quad i = 1, 2, \cdots, d.$$

In the case of additive noise, $f = \underline{f}$ and the Itô and Stratonovich SDEs have the same solutions [49, 47].

Since the problems we shall deal with in this chapter, both SDE and SPDE, are modeled with additive noise, we concentrate on Itô calculus in the subsequent sections.

2.1.2 Itô's formula

For each $t \geq t_0$, define a stochastic process

$$Y(t) = U(t, X(t)),$$

where $U(t, X)$ has continuous second order partial derivatives and $X(t)$ is given by [49]

$$dX(t) = f(t)dt + g(t)dw(t), \quad X(t_0) = X_0. \tag{2.5}$$

For simplicity, we write equation (2.5) as

$$dX = fdt + gdw,$$

and consider

$$dY(t) = U(t + dt, X(t) + dX(t)) - U(t, X(t)).$$

Using the Taylor expansion for U yields

$$dY(t) = (\frac{\partial U}{\partial t}dt + \frac{\partial U}{\partial X}dX) + \frac{1}{2}(\frac{\partial^2 U}{\partial t^2}dt^2 + 2\frac{\partial^2 U}{\partial t \partial X}dtdX + \frac{\partial^2 U}{\partial X^2}dX^2) + \cdots,$$

that is

$$dY(t) = \{\frac{\partial U}{\partial t}dt + \frac{\partial U}{\partial X}(fdt+gdw)\} + \frac{1}{2}\{\frac{\partial^2 U}{\partial t^2}dt^2 + 2\frac{\partial^2 U}{\partial t \partial X}dt(fdt+gdw) + \frac{\partial^2 U}{\partial X^2}(fdt+gdw)^2\}.$$

Consequently, we have

$$\begin{aligned} dY(t) = \{&\frac{\partial U}{\partial t}dt + f\frac{\partial U}{\partial X}dt + g\frac{\partial U}{\partial X}dw\} + \frac{1}{2}\{\frac{\partial^2 U}{\partial t^2}dt^2 + 2f\frac{\partial^2 U}{\partial t \partial X}dt^2 \\ &+2g\frac{\partial^2 U}{\partial t \partial X}dtdw + f^2\frac{\partial^2 U}{\partial X^2}dt^2 + 2fg\frac{\partial^2 U}{\partial X^2}dtdw + g^2\frac{\partial^2 U}{\partial X^2}dw^2\}. \end{aligned}$$

Since $E(dw^2) = dt$, $E(dtdw) = 0$ and by considering $E(dt^2) = 0$, we obtain the stochastic version of the chain rule:

$$dY(t) = \{\frac{\partial U}{\partial t} + f\frac{\partial U}{\partial X} + \frac{1}{2}g^2\frac{\partial^2 U}{\partial X^2}\}dt + g\frac{\partial U}{\partial X}dw, \tag{2.6}$$

which is known as Itô's formula [49].

Itô's formula can be generalized to higher dimensional functions. Thus, if we consider

$$dX(t) = f(t)dt + g(t)dw(t), \tag{2.7}$$

where $f : [0,T] \to \mathbb{R}^d$, $g : [0,T] \to \mathbb{R}^{d\times p}$ and $w(t)$ is an $\mathbb{R}^p$-valued Wiener process. In addition, $U : [0,T] \times \mathbb{R}^d \to \mathbb{R}$ has continuous partial derivatives $\frac{\partial U}{\partial t}$, $\frac{\partial U}{\partial X_k}$, $\frac{\partial^2 U}{\partial X_k \partial X_i}$, where $k, i = 1, 2, \cdots, d$. Now, define a stochastic process

$$Y(t) = U(t, X(t)),$$

where $X(t)$ is an $\mathbb{R}^d$-valued stochastic process satisfying equation (2.7). Then Itô's formula can be written as [49]

$$dY(t) = \{\frac{\partial U}{\partial t} + \sum_{k=1}^{d} f_k\frac{\partial U}{\partial X_k} + \frac{1}{2}\sum_{j=1}^{p}\sum_{i,k=1}^{d} g_{ij}g_{kj}\frac{\partial^2 U}{\partial X_i \partial X_k}\}dt + \sum_{j=1}^{p}\sum_{i=1}^{d} g_{ij}\frac{\partial U}{\partial X_i}dw_j. \tag{2.8}$$

2.1.3 Stochastic Taylor expansion

The stochastic Taylor expansion is the stochastic version of the deterministic Taylor expansion and is used to construct numerical methods, as will be shown in Section 2.2. The stochastic Taylor expansion we consider here is called the Itô-Taylor expansion and depends on the repeated use of Itô's formula (2.6). Consider the Itô process X which is the solution of the following one-dimensional Itô SDE in integral form:

$$X(t) = X(t_0) + \int_{t_0}^{t} f(X(s))ds + \int_{t_0}^{t} g(X(s))dw(s), \tag{2.9}$$

for all $t \in [t_0, T]$, where f and g are sufficiently smooth real valued functions, satisfying the linear growth bound (see Assumption 3 in Theorem 2.1.1, for the definition of the linear growth bound).

Let $h : \mathbb{R} \to \mathbb{R}$ be a twice continuously differentiable function. If we apply Itô's formula (2.6) to h, we get [49]

$$h(X(t)) = h(X(t_0)) + \int_{t_0}^{t} (f(X(s))\frac{\partial}{\partial X}h(X(s)) + \frac{1}{2}g^2(X(s))\frac{\partial^2}{\partial X^2}h(X(s)))ds + \int_{t_0}^{t} g(X(s))\frac{\partial}{\partial X}h(X(s))dw(s). \tag{2.10}$$

For simplicity of notation, we consider the following operators:

$$L^0 = f\frac{\partial}{\partial X} + \frac{1}{2}g^2\frac{\partial^2}{\partial X^2}, \quad L^1 = g\frac{\partial}{\partial X}.$$

Consequently, equation (2.10) becomes [49]

$$h(X(t)) = h(X(t_0)) + \int_{t_0}^{t} L^0h(X(s))ds + \int_{t_0}^{t} L^1h(X(s))dw(s). \tag{2.11}$$

The original Itô equation (2.9) can be obtained from (2.11) by setting $h(X) = X$. Hence, $L^0h(X) = f(X)$ and $L^1h(X) = g(X)$.

To derive the Itô-Taylor expansion, we first apply Itô's formula (2.6) to the functions $h = f$ and $h = g$ in (2.9), which yields [49]

$$X(t) = X(t_0) + \int_{t_0}^{t} \{f(X(t_0)) + \int_{t_0}^{s} L^0 f(X(z))dz + \int_{t_0}^{s} L^1 f(X(z))dw(z)\}ds$$
$$+ \int_{t_0}^{t} \{g(X(t_0)) + \int_{t_0}^{s} L^0 g(X(z))dz + \int_{t_0}^{s} L^1 g(X(z))dw(z)\}dw(s). \quad (2.12)$$

It follows that

$$X(t) = X(t_0) + f(X(t_0)) \int_{t_0}^{t} ds + g(X(t_0)) \int_{t_0}^{t} dw(s) + R, \quad (2.13)$$

where

$$R = \int_{t_0}^{t} \int_{t_0}^{s} L^0 f(X(z))dzds + \int_{t_0}^{t} \int_{t_0}^{s} L^1 f(X(z))dw(z)ds$$
$$+ \int_{t_0}^{t} \int_{t_0}^{s} L^0 g(X(z))dzdw(s) + \int_{t_0}^{t} \int_{t_0}^{s} L^1 g(X(z))dw(z)dw(s).$$

Equation (2.13) is the simplest Itô-Taylor expansion and we can continue in this fashion to obtain more terms in the expansion. For instance, we can apply Itô's formula (2.6) to $h = L^1 g$ in equation (2.12) which gives [49]

$$X(t) = X(t_0) + f(X(t_0)) \int_{t_0}^{t} ds + g(X(t_0)) \int_{t_0}^{t} dw(s) + L^1 g(X(t_0)) \int_{t_0}^{t} \int_{t_0}^{s} dw(z)dw(s) + \overline{R} \quad (2.14)$$

where

$$\overline{R} = \int_{t_0}^{t} \int_{t_0}^{s} L^0 f(X(z))dzds + \int_{t_0}^{t} \int_{t_0}^{s} L^1 f(X(z))dw(z)ds + \int_{t_0}^{t} \int_{t_0}^{s} L^0 g(X(z))dzdw(s))$$
$$+ \int_{t_0}^{t} \int_{t_0}^{s} \int_{t_0}^{z} L^0 L^1 g(X(u))dudw(z)dw(s) + \int_{t_0}^{t} \int_{t_0}^{s} \int_{t_0}^{z} L^1 L^1 g(X(u))dw(u)dw(z)dw(s).$$

Similar expansion can be obtained for higher-dimensional Itô processes (see more in [49]). Roughly speaking, "the Itô-Taylor expansion of a sufficiently smooth function of an Itô process is considered to be the sum of a finite number of multiple Itô

integrals, with constant integrands and a remainder term involving a finite number of other multiple integrals with non-constant integrands. The expansion is used to construct discrete-time approximations of Itô processes" [49].

2.1.4 Discrete-time approximations and the concept of strong and weak convergence

Only in limited cases of SDEs can we obtain an explicit solution and thus efficient numerical methods play a crucial role in the remainder. The most efficient numerical approach to solving SDEs is based on discrete-time approximations and either strong or weak numerical schemes. To measure the accuracy of discrete-time approximations, and to assess the usefulness of their schemes, we need certain criteria, such as strong and weak convergence criteria.

Strong convergence criterion

A good pathwise approximation is required in many physical problems, such as direct simulations. The absolute error criterion is suitable in these cases. Let

$$\xi = E(||X(T) - Y(T)||),$$

where $X(T)$ is the Itô stochastic process at time T and $Y(T)$ is the approximation process obtained from the numerical scheme at time T. In fact, the pathwise closeness at T on the time interval $[0, T]$ can be measured by this value. Moreover, it can be said that "a discrete-time approximation Y with maximum step size δ converges strongly to X at time T" [49] if

$$\xi = E(||X(T) - Y(T)||) \to 0 \quad as \quad \delta \to 0.$$

In Section 2.2, discrete-time approximations such as the Euler-Maruyama method and the Milstein method will be used as integrators in SDELab. To compare the methods, their rates of convergence will be used. To be more precise, "a discrete-time approximation Y, with maximum step size δ, converges strongly to X with order γ at time T if there exist a constant $C > 0$, which does not depend on δ, and a δ_0 such that" [49]

$$\xi(\delta) = E(||X(T) - Y(T)||) \leq C\delta^{\gamma}, \quad \text{for each} \quad \delta \in (0, \delta_0).$$

Weak convergence criterion

In some applications, we may be interested in computing approximations to the probability distribution of the solution or an average of a functional of the solution rather than the pathwise approximation. Therefore, the weak convergence criterion is appropriate. Thus, we say that "a discrete-time approximation Y, with maximum step size δ, converges weakly to X at time T with respect to a class $\mathcal{C}$ of test functions φ if

$$\xi = E(||\varphi(X(T)) - \varphi(Y(T))||) \to 0 \quad as \quad \delta \to 0,$$

for all $\varphi \in \mathcal{C}$" [49]. In the same manner as in the strong case, we use the rate of convergence in order to compare different discrete-time approximations. In this way, "a discrete-time method is said to have weak order of convergence equal to β if there exist a constant $C > 0$, which does not depend on δ, and a finite δ_0, such that, for all test functions φ in some class $\mathcal{C}$, we have" [49]

$$\xi(\delta) = E(||\varphi(X(T)) - \varphi(Y(T))||) \leq C\delta^{\beta}, \quad \text{for each} \quad \delta \in (0, \delta_0).$$

In the next section, an example of an SDE from the field of neuroscience will be solved numerically using SDELab. The current version of the software offers strong solutions of SDEs only. Therefore, we discuss the existence and uniqueness of a strong

solution of an Itô SDE (2.1) through the following Theorem 2.1.1(for more details, see [49, 71]).

Theorem 2.1.1. *[49]*

Consider the following assumptions:

1. *$f(t, X)$ and $g(t, X)$ are jointly measurable in $(t, X) \in [t_0, T] \times \mathbb{R}^d$.*

2. *(Lipschitz condition). There exists a constant $K > 0$ such that*

$$||f(t, X) - f(t, Y)|| \leq K||X - Y||$$

and

$$||g(t, X) - g(t, Y)|| \leq K||X - Y||,$$

for all $t_0 \leq t \leq T$ and $X, Y \in \mathbb{R}^d$.

3. *(Linear growth bound). There exists a constant $K > 0$ such that*

$$||f(t, X)||^2 \leq K^2(1 + ||X||^2)$$

and

$$||g(t, X)||^2 \leq K^2(1 + ||X||^2),$$

for all $t_0 \leq t \leq T$ and $X \in \mathbb{R}^d$.

4. *$X(t_0)$ is A_{t_0}-measurable with $E(||X(t_0)||^2) < \infty$.*

Under these assumptions, the SDE of the form (2.1) has a pathwise unique strong solution $X(t)$ on $[t_0, T]$ with

$$\sup_{t_0 \leq t \leq T} E(||X(t)||^2) < \infty.$$

Proof. The proof of this theorem can be found in [49]. □

2.2 How to simulate SDEs using SDELab

2.2.1 SDELab: Introduction

SDELab is a mathematical package, created by Hagen Gilsing and Tony Shardlow [29] to make SDEs as easily accessible. The package provides different explicit and implicit solvers for Itô and Stratonovich SDEs. The current version of SDELab offers several standard numerical methods for the computation of strong solutions to (2.1)–(2.2) and generates configurable plots and subplots as required [29]. Here, we introduce the usage and application of the SDELab package. More details, including usage instructions, can be found at either
www.ma.ac.uk/∼sdelab
or www.mathematik.hu-berlin.de/∼gilsing/sdelab.

SDELab offers three strong numerical methods for solving the Itô SDEs and two strong methods for solving Stratonovich SDEs as follows:

1. Itô SDE methods:
    - α-methods or Euler methods with parameter α.
    - Itô Milstein method.
    - The second-order backward differentiation formula or Itô BDF2 method.
2. Stratonovich SDE methods:
    - The Euler-Heun method.
    - Stratonovich Milstein method.

In the next subsection, we will look more closely at these integrators. However, the problems we will deal with in this chapter are additive noise problems, so we will be concerned more with the Itô Euler methods and BDF2 method and will give only a brief exposition of the others. For further details, see [29].

2.2.2 Integrators used in SDELab

Itô SDE methods

One important class of methods is Euler methods with parameter α; see (2.15) below. When $\alpha = 0$ we obtain the Euler-Maruyama method; when $\alpha = 1/2$ we obtain the trapezium rule; when $\alpha = 1$ we obtain the implicit Euler-Maruyama method. In SDELab, we refer to this class of methods as the *Strong Itô Euler method with parameter* α. Mathematically, the Euler approximation to the Itô process X satisfying (2.1) is defined as the sequence Y_n given by the iterative scheme

$$Y_{n+1} = Y_n + [(1-\alpha)f(t_n, Y_n) + \alpha f(t_{n+1}, Y_{n+1})]\Delta t + g(t_n, Y_n)\Delta w_n, \tag{2.15}$$

where $0 \leq \alpha \leq 1$, $t_n = t_0 + n\Delta t$, and $n = 0, 1, \cdots, N-1$, where $N \in \mathbb{N}$. Δt is the time step and $\Delta w_n = w(t_{n+1}) - w(t_n)$ are increments in the Wiener process, which are normally distributed. $Y_0 = X_0$.

Theorem 2.2.1. *[49]*
Suppose that

1. $$E(||X_0||^2) < \infty,$$

   where X_0 is independent of $w(t)$,

2. $$E(||X_0 - Y_0||^2)^{1/2} \leq k_1 \Delta t^{1/2},$$

3. $$||f(t, X_1) - f(t, X_2)|| + ||g(t, X_1) - g(t, X_2)|| \leq k_2 ||X_1 - X_2||,$$

4. $$||f(t, X)|| + ||g(t, X)|| \leq k_3(1 + ||X||),$$

and

5.

$$||f(s,X) - f(t,X)|| + ||g(s,X) - g(t,X)|| \leq k_4(1 + ||X||)||s - t||^{1/2},$$

for all $s, t \in [t_0, T]$ *and* $X, X_1, X_2 \in \mathbb{R}^d$*, where the constants* k_1*,*k_2*,*k_3 *and* k_4 *do not depend on* Δt*.*

Then

$$E(||X(T) - Y(T)||) \leq k_5 \Delta t^{1/2},$$

where $Y(T)$ *is the Euler approximation to the Itô process* $X(T)$ *at time* T *and* k_5 *is a constant that does not depend on* Δt*.*

Proof. The proof of this theorem can be found in [49]. □

It follows immediately from the above Theorem 2.2.1 that if the drift function f and the diffusion function g are well behaved, then the solution Y_n of (2.15) converges strongly to the solution X of (2.1) at time t_n with order $1/2$, which means that

$$(E[\|X(t_n) - Y_n\|^2])^{1/2} = O(\Delta t^{1/2}), \quad \forall t_0 \leq t_n \leq T,$$

where $E[.]$ denotes expectation with respect to the law of the Wiener process. The Euler scheme is obtained by considering the first three terms of the Itô-Taylor expansion, which was discussed above in Section 2.1.3.

The Euler method represents the simplest strong Taylor approximation. More accurate strong Taylor schemes can be obtained by including further multiple stochastic integrals from the Itô-Taylor expansion into the Euler scheme [49]. The Milstein method is the basic example and is implemented in SDELab as *the Strong Itô Milstein*

method with parameter α [29]

$$Y_{n+1} = Y_n + [(1-\alpha)f(t_n, Y_n) + \alpha f(t_{n+1}, Y_{n+1})]\Delta t + g(t_n, Y_n)\Delta w_n + \sum_{j=1}^{p} \frac{\partial}{\partial Y} g_j(t_n, Y_n)(g(t_n, Y_n)\xi_j), \quad Y_0 = X_0, \tag{2.16}$$

where $g_j(t, Y)$ is the jth column of $g(t, Y)$, $\xi_j = (I_{1j,n}, \cdots, I_{pj,n})^T$ and

$$I_{ij,n} = \int_{t_n}^{t_{n+1}} \int_{t_n}^{r} dw_i(s) dw_j(r).$$

To derive this method, one more term is added to the Euler scheme, which raises the strong convergence order to 1 under regularity on f and g [49, 37]. More information about implementing this method and approximating ξ_j can be found in [29].

SDELab also provides an efficient method for small noise problems, called the *second order Backward Differentiation Formula*, referred to as *Strong Itô BDF2* in SDELab:

$$Y_{n+1} = \frac{4}{3}Y_n - \frac{1}{3}Y_{n-1} + \frac{2}{3}f(t_{n+1}, Y_{n+1})\Delta t + g(t_n, Y_n)\Delta w_n - \frac{1}{3}g(t_{n-1}, Y_{n-1})\Delta w_{n-1}, \tag{2.17}$$

for $n \geq 2$ and with initial values given by

$$Y_1 = Y_0 + \left[\frac{1}{2}f(t_0, Y_0) + \frac{1}{2}f(t_1, Y_1)\right]\Delta t + g(t_0, Y_0)\Delta w_0, \quad Y_0 = X_0.$$

Thus, if we consider (2.1) with diffusion function $\sigma g(t, X)dw$, where σ is a small parameter, then its solution Y_n, obtained from the Euler method with $\alpha = 0.5$ and the BDF2 method, satisfies

$$(E[\|X(t_n) - Y_n\|^2])^{1/2} = O(\Delta t^2 + \sigma\Delta t + \sigma^2\Delta t^{1/2}), \quad \forall t_0 \leq t_n \leq T.$$

So if the noise $\sigma \ll \Delta t$ then the error is of order $O(\Delta t^2 + \sigma \Delta t)$, where $O(\sigma^2 \Delta t^{1/2})$ becomes negligible [29].

Stratonovich SDE methods

Two Stratonovich integrators are implemented in SDELab: the Euler-Heun method and the Stratonovich Milstein method. The former is referred to as *the strong Stratonovich Euler-Heun method with parameter* α in SDELab and takes the following form: [29]

$$\begin{aligned} Y_{n+1} = Y_n + [(1-\alpha) f(t_n, Y_n) + \alpha f(t_{n+1}, Y_{n+1})] \Delta t \\ + \frac{1}{2} [g(t_n, Y_n) + g(t_n, Y_n^{aux})] \Delta w_n \quad Y_0 = X_0 \end{aligned} \tag{2.18}$$

with predicted value $Y_n^{aux} = Y_n + g(t_n, Y_n) \Delta w_n$.

The second method is *the strong Stratonovich Milstein method with parameter* α: [29]

$$\begin{aligned} Y_{n+1} = Y_n + [(1-\alpha) f(t_n, Y_n) + \alpha f(t_{n+1}, Y_{n+1})] \Delta t + g(t_n, Y_n) \Delta w_n \\ + \sum_{j=1}^{p} \frac{\partial}{\partial Y} g_j(t_n, Y_n)(g(t_n, Y_n) \xi_j), \quad Y_0 = X_0, \end{aligned} \tag{2.19}$$

where $\xi_j = (J_{1j,n}, \cdots, J_{pj,n})^T$ for the iterated Stratonovich integral

$$J_{ij,n} = \int_{t_n}^{t_{n+1}} \int_{t_n}^{r} dw_i(s) \circ dw_j(r).$$

Since our problems in this chapter are modeled with additive noise, we will restrict our attention to Itô SDE methods, in particular Itô Euler methods and the Itô BDF2 method. For this reason, we touched only a few aspects of Stratonovich SDEs methods; for deeper discussion, we recommend references [29].

2.2.3 Stochastic HH model with space-clamped technique

The HH model is a mathematical description of electrical excitation and propagation along a nerve axon. In response to a stimulus, the cell membrane elicits an action potential (spike), which propagates along the nerve axon. The current flow across the cell membrane depends on the capacitance of the membrane and the conductance of the ion channels, in particular the voltage-dependent conductances (sodium and potassium) and leakage conductance. The voltage and the current flow are assumed to obey Ohm's law. In this section, we consider the HH model without the extra complication of spatial variation in the membrane potential (known as the space-clamped technique) and with additive Gaussian noise input current. In the literature, there has been interest in the stochastic activity of neurons in generating spikes with regards to understanding neuronal information processing [86]. Several works have been studied the effects of noise on the HH model. See, for example, [87, 90, 88, 39, 69, 94, 77]. Here, we consider the following stochastic version of the HH model [86]:

$$\begin{aligned} C_m dv &= (\overline{g}_k n^4(v_k - v) + \overline{g}_{N_a} m^3 h(v_{N_a} - v) + \overline{g}_l(v_l - v) + \mu)dt + \sigma dw(t) \\ \frac{dn}{dt} &= \alpha_n(v)(1-n) - \beta_n(v)n \\ \frac{dm}{dt} &= \alpha_m(v)(1-m) - \beta_m(v)m \\ \frac{dh}{dt} &= \alpha_h(v)(1-h) - \beta_h(v)h, \end{aligned} \tag{2.20}$$

where μ and σ are constants representing the input current and the noise intensity respectively, and $\{w(t), t \geq 0\}$ is an $\mathbb{R}$-valued Wiener process.

The fractions of potassium channel activation, sodium channel activation and sodium channel inactivation are represented by $n(t)$, $m(t)$ and $h(t)$ respectively (see Figure 2.1). The values of these conductance variables are between 0 and 1. C_m is the membrane capacitance in $\mu F/cm^2$ and $v(t)$ is the membrane potential in mV. $\overline{g}_k$, $\overline{g}_{N_a}$ and $\overline{g}_l$ represent the maximal values of the membrane conductance constants for

potassium, sodium and leakage ions respectively. v_k, v_{N_a} and v_l are the corresponding reversal potentials. The α and β functions are given by [38]

$$\alpha_n(v) = \frac{10 - v}{100(e^{(10-v)/10} - 1)}, \quad \beta_n(v) = \frac{1}{8}e^{-v/80},$$

$$\alpha_m(v) = \frac{25 - v}{10(e^{(25-v)/10} - 1)}, \quad \beta_m(v) = 4e^{-v/18},$$

$$\alpha_h(v) = \frac{7}{100}e^{-v/20}, \quad \beta_h(v) = \frac{1}{e^{(30-v)/10} + 1}.$$

Following [38], we set the parameters of this model to $C_m = 1\mu F/cm^2$, $\overline{g}_k = 36mS/cm^2$, $\overline{g}_{N_a} = 120mS/cm^2$, $\overline{g}_l = 0.3mS/cm^2$, $v_k = -12mV$, $v_{N_a} = 115mV$ and $v_l = 10.613mV$, and hence the resting potential is $0mV$.

To solve the HH system using SDELab, we rewrite the model in the form (2.1),

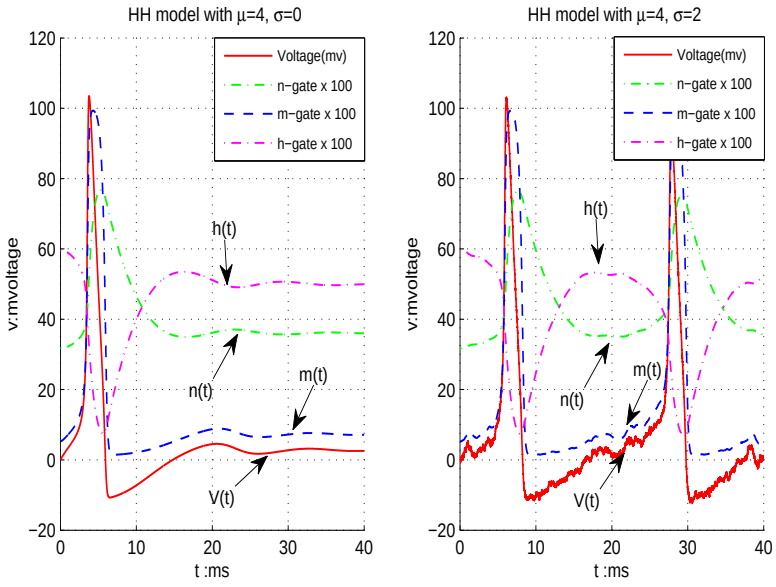

Figure 2.1: The conductance variables $n(t)$, $m(t)$ and $h(t)$ for the HH model with $\mu = 4$ and (a) $\sigma = 0$, and (b) $\sigma = 2$.

where $p = 1$ and $d = 4$:

$$dX(t) = f(t, X(t))dt + g(t, X(t))dw, \tag{2.21}$$

where $X = [v, n, m, h]^T$, the drift function is

$$f(t, X) = \begin{bmatrix} C_1 n^4 (v_k - v) + C_2 m^3 h (v_{N_a} - v) + C_3 (v_l - v) + \mu / C_m \\ \alpha_n(v)(1 - n) - \beta_n(v) n \\ \alpha_m(v)(1 - m) - \beta_m(v) m \\ \alpha_h(v)(1 - h) - \beta_h(v) h \end{bmatrix}$$

and the diffusion function is $g(t, X) = [\sigma / C_m, 0, 0, 0]^T$. We use the initial condition $X_0 = [v_0, n_0, m_0, h_0]^T$, where $v_0 = 0$,

$$n_0 = \frac{\alpha_n(v_0)}{\alpha_n(v_0) + \beta_n(v_0)},$$

$$m_0 = \frac{\alpha_m(v_0)}{\alpha_m(v_0) + \beta_m(v_0)}$$

and

$$h_0 = \frac{\alpha_h(v_0)}{\alpha_h(v_0) + \beta_h(v_0)}.$$

The constants are $C_1 = \overline{g}_k / C_m$, $C_2 = \overline{g}_{N_a} / C_m$ and $C_3 = \overline{g}_l / C_m$.

Note that the noise intensity σ in the HH model is often large [87, 90], and that the system is stiff, so the appropriate integrators are semi implicit ($\alpha = 1/2$) or fully implicit ($\alpha = 1$) methods. Since we have chosen additive noise, the order of strong convergence of the Euler Scheme is 1 under appropriate smoothness assumptions on the drift function [49]. Moreover, the Milstein scheme in case of additive noise is reduced to the Euler scheme which involves no multiple stochastic integrals. Hence, in this case, the Euler method should be selected.

Solving the HH system using SDELab

The codes used in SDELab for the HH model (Code 2.1), its drift (Code 2.2) and its diffusion functions (Code 2.3) are shown below. For simplicity, a and b are used in these codes instead of α and β.

To start using SDELab within MATLAB, type

```
sdelab_init.
```

To find approximate paths (strong approximations) of (2.1) and (2.2), the following function can be used:

```
[t,Y]= sdesolve_strong_solutions (fcn,tspan,Y0,p,opt,params),
```

which requires basic information (arguments) in order to solve SDEs appropriately and returns values in $[t, Y]$. In the following SDELab codes for the HH model, we describe the functions and their arguments; more detail can be found in [29].
Code 2.1, for the HH model, can be described as follows:

1. The first step involves setting up the problem dimension, time interval and initial data

   ```
   d = 4; %dimension of Y
   p = 1; % dimension of w(t)
   tspan = [0,40];   % time interval
   %%%%%%%%%%%%%%%%%%%%%%%%%%%%%%%%%%%%%%%%%%%%%%%%%%%%%%%%%%%%
   % compute initial data Y0
   a0_n=0.1/(exp(1)-1); b0_n=0.125; a0_m=2.5/(exp(2.5)-1); b0_m=4;
   a0_h=0.07; b0_h=1/(exp(3)+1);
   Y0=[0;a0_n/(a0_n+b0_n);a0_m/(a0_m+b0_m);a0_h/(a0_h+b0_h)]
   ```

   The above information is used later in the function

`sdesolve_strong_solutions(fcn,tspan,Y0,p,opt,params),`

where the time interval, initial value Y_0 and the dimension p of $w(t)$ are represented by the second, third and fourth arguments respectively.

2. The second step involves defining the drift f and diffusion g functions, which are specified by the single structure **fcn**. These coefficient functions can be specified using two different styles in SDELab: MATLAB-style functions and Dynamic Library (DL)-style functions. Here, we concentrate on MATLAB-style functions, which can be passed as the first argument to **sdesolve_strong_solutions (fcn,tspan,y0,p,opt,params)**, by setting

   `fcn.drift='HH_drift' and fcn.diff_noise='HH_diff_noise',`

   where **HH_drift** and **HH_diff_noise** are the names of the m-files of the drift and diffusion functions of the HH model (see Codes 2.2 and 2.3 below).

3. Define the parameters of the drift and diffusion functions, which are the last argument of **sdesolve_strong_solutions** and are specified as **params**.

   `params.Mu=2.5; params.sigma=0.`

4. The fifth argument is **opt**, which is a MATLAB structure whose fields set the SDELab options. In our code, we set

   `opt.IntegrationMethod='StrongItoEuler',`
   `opt.StrongItoEuler.Alpha=0.5, opt.MaxStepSize=1e-3 and`
   `opt.MSIGenRNG.SeedZig = 23,`

   where the first option sets the integration method and the second sets the parameter α of the Euler method. In SDELab, the default integration method is **StrongItoEuler** and the options are [29]

`StrongItoMilstein, StrongItoBDF2, StrongStratoEulerHeun, and StrongStratoMilstein.`

The parameter α in the Euler and Milstein methods for the Itô and the Stratonovich equations is controlled by

`StrongItoEuler.Alpha, StrongItoMilstein.Alpha, StrongStratoEulerHeun.Alpha, StrongStratoMilstein.Alpha.`

The third option (**MaxStepSize**) represents the maximum value of the time step Δt, which in our code is equal to 10^{-3}. If it is not specified, the default value $((T - t_0)/100)$ is used.
The last option used in our code is the seed for the random number generator. In fact, there are many other options which can be used to control the nonlinear solver and its output and plot behaviour. For further information, see [29].

5. Finally, we find the strong numerical solutions using the solver function **sdesolve_strong_solutions** with the above arguments. As mentioned above, it returns values in $[t, Y]$. t represents the time points and Y is a matrix of state vectors obtained as follows:

```
[t,Y]= sdesolve_strong_solutions (fcn,tspan,Y0,m,opt,params).
```

Moreover, if $[t, Y]$ is omitted, the MATLAB figure appears and the approximate paths are plotted as they are computed. The output plot of these results can be produced using a set of configurable options which are passed using an option structure as an argument to the calling SDELab function. For instance, the plot types can be controlled using the following options: [29]

```
opt.OutputPlotType='sdesolve_plot_path'  %path plot (default)
```

```
opt.OutputPlotType='sdesolve_plot_phase'        %phase plot
opt.OutputPlotType='sdesolve_plot_time_phase'%time-phase plot
opt.OutputPlotType='sdesolve_plot_phase3'       %phase3 plot.
```

Code2.2: m-file of the drift function of the HH model:

```
function z=HH_drift(t,Y,varargin)
Mu=varargin{2}.Mu;     % Extract parameters
%%%%%%%%%%%%%%%%%%%%%%%%%%%%%%%%%%%%%%%%%%%%%%%%%%%%%%%%%%%%
% conductance variables of potassium,sodium and leakage
%%%%%%%%%%%%%%%%%%%%%%%%%%%%%%%%%%%%%%%%%%%%%%%%%%%%%%%%%%%%
g_k=36;g_Na=120;g_L=0.3;
C_m=1;                      % the membrane capacitance

C1=g_k/C_m;C2=g_Na/C_m;C3=g_L/C_m;
%%%%%%%%%%%%%%%%%%%%%%%%%%%%%%%%%%%%%%%%%%%%%%%%%%%%%%%%%%%%
% Constants of resting potential of such ions
v_k=-12;v_Na=115; v_L=10.613;
a_n=(10-Y(1))/(100*(exp((10-Y(1))/10)-1)); b_n=exp(-Y(1)/80)/8;
a_m=(25-Y(1))/(10*(exp((25-Y(1))/10)-1)); b_m=4*exp(-Y(1)/18);
a_h=(7*exp(-Y(1)/20))/100; b_h=1/(exp((30-Y(1))/10)+1);
%%%%%%%%%%%%%%%%%%%%%%%%%%%%%%%%%%%%%%%%%%%%%%%%%%%%%%%%%%%%
%Compute drift function of HH model
%%%%%%%%%%%%%%%%%%%%%%%%%%%%%%%%%%%%%%%%%%%%%%%%%%%%%%%%%%%%
z1=(C1*(v_k-Y(1))*(Y(2)^4))+(C2*(v_Na-Y(1))*(Y(3)^3)*Y(4))
      +(C3*(v_L-Y(1)))+ Mu/C_m;
z2=a_n*(1-Y(2))-b_n*Y(2); z3=a_m*(1-Y(3))-b_m*Y(3);
z4=a_h*(1-Y(4))-b_h*Y(4);
```

```
z=[z1;z2;z3;z4];   %Return values of the drift function
%%%%%%%%%%%%%%%%%%%%%%%%%%%%%%%%%%%%%%%%%%%%%%%%%%%%%%%%
```

The MATLAB-style function describing the drift function of the HH model satisfies the call syntax

```
function z=HH_drift(t,Y,varargin)
```

whose arguments are the time value t, a real vector Y of length d representing the current state value, and a list of optional arguments **varargin**. The returned value z is a real vector of length d which represents the value of f at $(t,\ Y)$ [29]. The solution of a stiff system with a nonlinear drift requires a nonlinear equation solver as we are using an implicit method. SDELab uses the freeware package MinPack-1.3, which provides software for solving nonlinear equations [29]. To speed up the solver MinPack-1.3, the user may provide spatial derivatives of the drift function, which can be utilized in SDELab as the function **drift_dY**, which returns the *Jacobian* matrix of f with entries $\partial f_i(t,Y)/\partial Y_j$ for $i,j = 1,2,\cdots,d$ [29]. The MATLAB-style function describing the spatial derivatives of the drift f satisfies the call syntax

```
function z=HH_drift_dY(t,Y,varargin)
```

and can be passed as an argument to **sdesolve_strong_solutions** by setting **fcn.drift_dY='HH_drift_dY'**, where **HH_drift_dY** is the name of the m-file of the spatial drift of the HH model. However, **drift_dY** is optional, so if no spatial derivatives of f are passed, the algorithm uses forward-difference approximations of the spatial derivative [29].

Code2.3: m-file for the diffusion function of the HH model

```
function z=HH_diff_noise(t,Y,dw,flag,varargin)
sigma=varargin{2}.sigma; %extract parameters
B=[sigma;0;0;0];        % comput the diffusion
```

```
if(flag)
    z=B;
else z=B*dw; end
%%%%%%%%%%%%%%%%%%%%%%%%%%%%%%%%%%%%%%%%%%%%%%%%%%%%%%%%%%%%
```

The MATLAB-style function describing the diffusion function of the HH model satisfies the call syntax

```
function z=HH_diff_noise(t,Y,dw,flag,varargin)
```

whose arguments are the time value t, a real vector Y of length d representing the current state value, a real vector of length p representing the Wiener increment values, a flag indicator, and a list of optional arguments **varargin**. The returned value z is either a real vector of length d if flag=0, representing the value of gdw (which is beneficial for sparse diffusion matrices), or if the flag is not zero, it is the same size as the matrix g. More details on implementation for both Itô and Stratonovich integrators can be found in [29].

2.2.4 The effectiveness of noise at generating spikes

Repetitive firing in the space-clamped HH model, in response to an applied current, has been studied and analyzed in the literature, particularly in the noiseless case; see, for example [36, 75, 33, 84, 50]. Here, we present a numerical simulation in this context, for the standard HH model. Our results can be summarized as follows:

1. In the absence of noise($\sigma = 0$):

   The minimal current required to fire at least one spike is $\mu = 2.5\mu A/cm^2$, while the threshold current required to elicit an infinite train of spikes is $I_0 = 6.25\mu A/cm^2$. See Figure 2.2.

According to [36, 75, 33, 84], over a range of constantly applied current μ, the HH equations have limit cycle solutions when $I_0 < \mu < I_2$, where $I_2 = 154\mu A/cm^2$ [36]. If $\mu < I_0$, no limit cycle solutions occur and the initial conditions go to a fixed point (see Figure 2.3a for $\mu = 3 < I_0$). When μ is increased to greater than I_0, the HH equations start to generate an infinite train of spikes. I_0 is considered a critical current at which the firing frequency jumps sharply from zero to over 50 spikes/s [84], as shown in Figure 2.5.

Between I_0 and I_1, where $I_1 \cong 9.8 < I_2$ [36], the solutions either decay to the stable fixed point or grow to a stable limit cycle, depending on the initial conditions. This coexistence of stability may demand the existence of a surface containing unstable limit cycles which separate the domains of attractions of these two stable states. See [36, 75] for further details. If μ is increased towards I_1, the domain of attraction of the fixed point becomes smaller and decreases to zero when μ reaches I_1, as shown in Figure 2.3b and Figure 2.3c. Therefore, the system has only periodic solutions for the current range $I_1 < \mu < I_2$ [75]. See Figure 2.3c and Figure 2.4a, for the example where $\mu = 20$.

As μ is increased above I_1, the spiking frequency also increases, as shown in Figure 2.5. However, there is a limited range of frequencies, of $53 - 138$ spikes/s [50]. Thus, if μ is further increased towards I_2, the frequency begins to decrease and, when μ passes I_2, the nerve becomes blocked after a few spikes [84]. This behavior is due to the high injected current in the axon, which causes the membrane to fail to repolarize sufficiently, between spikes, to relieve sodium inactivation. The membrane shows oscillatory behavior but no true action potentials [50], as shown in Figure 2.4b. The system has a stable fixed point. See Figure 2.3d. For further details about the dynamic behavior of solutions to the HH equations, and an analysis of the stability near the parameter $I_k, k = 0, 1, 2$, see [36, 41].

2. To investigate the influence of noise on the firing frequency of the HH model, different values of μ are chosen relative to the critical values I_0, I_1 and I_2, with different levels of noise σ. For $\mu < I_0$, we take $\mu = 0, 3, 5$ and 6; for μ between I_0 and I_1, we choose $\mu = 6.5$ and 8; for $I_1 < \mu < I_2$, we choose $\mu = 10, 12$ and 15, all of which are close to I_1 in order to avoid the decrease in frequency when μ is very high. The results of our simulation are summarized in Figure 2.5, where the mean of the firing frequency is plotted against the current μ for different values of noise intensity $\sigma = 0, 2, 5, 10$ and 15. The results are obtained from 25 trials for each value of μ over an interval of time $[0, 250]$.

   In the absence of noise, no limit cycles are generated when $\mu < I_0$, and if μ is increased above I_0, the firing frequency jumps from 0 to over 50 spikes/s. This discontinuity in the firing frequency (the dashed line in Figure 2.5 for the curve where $\sigma = 0$) is eliminated when suitable noise is added, as shown by the curves in Figure 2.5 for other values of $\sigma = 2, 5, 10$ and 15. Thus, with noise, the input is strong enough to generate spikes with non-zero average frequency, even when $\mu < I_0$ [50, 77], as shown in Figure 2.6. Furthermore, it is clear that additive noise also increases the frequency for values of μ above I_0 (see Figure 2.5).

2.3 Simulating SPDEs using SDELab

SPDEs are PDEs modeled with a noise term. The analysis and study of SPDEs has strong connections with probability theory, functional analysis and PDE theory. Thus, if SPDE is an evolution equation, such as a parabolic or hyperbolic equation, then it can be formulated as an evolution SDE equation in infinite dimensional spaces, Hilbert space, for example. Some preliminaries and relevant material on Hilbert space and Fourier analysis are presented in Appendix B; see [73, 5] for more detail. Given this, we first expose briefly some properties of the Wiener process with values in

Hilbert space.

2.3.1 Hilbert-space-valued Wiener process

Definition 2.3.1. [70] Let H be a separable Hilbert space with inner product $(.,.)_H$. Then the linear operator, denoted by $f \otimes g$, for $f, g \in H$, is defined as

$$[f \otimes g]h := f(g,h)_H, \quad \text{for} \quad h \in H.$$

Definition 2.3.2. [70][**Covariance operator**]
Let $(\Omega, \mathcal{A}, \mathbf{P})$ be a probability space, and consider $X, Y \in L^2(\Omega, \mathcal{A}, \mathbf{P}; H)$, where H is a separable Hilbert space. Then the *covariance operator* of X and the *correlation operator* of (X, Y) are defined by

$$Cov(X) = E[(X - E[X]) \otimes (X - E[X])]$$

and

$$Cor(X,Y) = E[(X - E[X]) \otimes (Y - E[Y])]$$

respectively, where $E[X] = \int_\Omega X(\omega)\mathbf{P}(d\omega)$ denotes the expectation.

$Cov(X)$ is a symmetric, non-negative and nuclear operator with [70]

$$trCov(X) = E[|X - E[X]|^2],$$

where tr represents trace of the operator (see Appendix B). Thus, if $\{e_j, j \in \mathbb{N}\}$ is a complete orthonormal basis in H and $E[X] = 0$, then [70]

$$\begin{aligned} trCov(X) &= \sum_{j=1}^{\infty} (Cov(X)e_j, e_j) \\ &= \sum_{j=1}^{\infty} \int_\Omega |(X(\omega), e_j)|^2 \mathbf{P}(d\omega) = E[|X|^2]. \end{aligned}$$

Now, if we suppose $Q \in L(H)$ is a non-negative and symmetric operator with $trQ < \infty$, then there exists a complete orthonormal system $\{e_j, j \in \mathbb{N}\}$ in H and a bounded sequence of non-negative real numbers λ_j, such that [70]

$$Qe_j = \lambda_j e_j, \quad j = 1, 2, \cdots .$$

The λ_j, where $j = 1, 2, \cdots$, represent the eigenvalues of Q. The e_j, where $j = 1, 2, \cdots$, are the corresponding eigenfunctions [70, 71].

Definition 2.3.3. [70][**Q-Wiener process**]
An H-valued stochastic process $w(t), t \geq 0$ is said to be a *Q-Wiener process* if

1. $w(0) = 0$,
2. w has continuous trajectories,
3. w has independent increments and
4. $w(t) - w(s) \sim \mathcal{N}(0, (t-s)Q), \quad t \geq s \geq 0.$

The following proposition is very important, stating that the Hilbert-space-valued Wiener process is a Gaussian process and can also be represented in terms of a real-valued Wiener process.

Proposition 2.3.1. *[70, 71] Let w be a Q-Wiener process, with $trQ < \infty$. Then, we have the following:*

1. *w is a Gaussian process on H with*

$$E(w(t)) = 0 \quad and \quad Cov(w(t)) = tQ, \quad for \quad t \geq 0.$$

2. *For arbitrary t, w has the expansion*

$$w(t) = \sum_{j=1}^{\infty} \sqrt{\lambda_j}\beta_j(t)e_j, \tag{2.22}$$

where

$$\beta_j(t) = \frac{1}{\sqrt{\lambda_j}}(w(t), e_j), \quad j = 1, 2, \cdots,$$

are real valued Wiener processes, mutually independent on $(\Omega, \mathcal{A}, \mathbf{P})$*, and the series (2.22) is convergent in* $L^2(\Omega, \mathcal{A}, \mathbf{P})$.

Proof. See [70, 71] for the proof of this proposition. □

2.3.2 Existence and uniqueness of the solutions of SDEs in infinite dimensional space

Definition 2.3.4. [73][C_0**-semigroup**]

A family $S(t), t \geq 0$ of bounded linear operators on a separable Hilbert space H (or, in general, a Banach space) is said to be *a* C_0*-semigroup* or strongly continuous semigroup of bounded linear operators, if the following statements hold:

- $S(0) = I$, where I is the identity operator on H.
- $S(s + t) = S(s)S(t)$ for all $s, t \geq 0$.
- For all $u \in H$, the H-valued function $t \mapsto S(t)u$, $t \geq 0$, is continuous. In fact, it is enough to hold the continuity at $t = 0$ (i.e. for all $u \in H, ||S(t)u - u|| \to 0$ as $t \to 0$) and use the uniform boundedness principle to show that $S(.)$ is continuous at $t \geq 0$.

Definition 2.3.5. [73][**infinitesimal generator**]

Let $S(t), t \geq 0$, be a C_0-semigroup of bounded linear operators on a separable Hilbert space H. Then, *the infinitesimal generator* of the semigroup $S(t)$ is the operator A (linear and usually unbounded), defined as follows:

$$Au = \lim_{h \to 0^+} \frac{S(h)u - u}{h} \quad \text{for all} \quad u \in D(A),$$

where $D(A) = \{u \in H : \text{there exists} \lim_{h \to 0^+} \frac{S(h)u - u}{h}\}$.

Now consider the following nonlinear additive noise SDE on a time interval $[0, T]$:

$$\begin{aligned} du(t) &= (Au(t) + f(u(t)))dt + \sigma dw \\ u(0) &= u_0, \end{aligned} \tag{2.23}$$

where $A : D(A) \subset H \to H$ is the infinitesimal generator of C_0-semigroup $S(t) = e^{At}, 0 \leq t \leq T$, u_0 is an $\mathcal{A}_0$-measurable H-valued random variable, σ is the noise intensity and $f : H \to H$ satisfies the Lipschitz and linear growth conditions. Thus, $\forall u, v \in H$, $\exists C > 0$ such that

$$||f(u) - f(v)|| \leq C||u - v|| \tag{2.24}$$

and

$$||f(u)||^2 \leq C^2(1 + ||u||^2), \tag{2.25}$$

where $||.||$ is the norm on H.

To make sense of this nonlinear case, we need to work with a mild solution defined as follows.

Definition 2.3.6. [70][**mild solution**]

A predictable H-valued process $u(t), t \in [0, T]$, (see Definition A.0.5 of the predictable process), is called *a mild solution* of (2.23) if

$$P(\int_0^T ||u(s)||^2 ds < \infty) = 1$$

and, for $0 < t < T$,

$$u(t) = S(t)u_0 + \int_0^t S(t-s)f(u(s))ds + \int_0^t S(t-s)\sigma dw(s). \tag{2.26}$$

Theorem 2.3.2. *[70]*

Let u_0 be an $\mathcal{A}_0$-measurable H-valued random variable and

$f : H \to H$ satisfies conditions (2.24) and (2.25). Then

1. *there exists a unique mild solution to (2.23) in the form of (2.26) and it has a continuous modification (see Definition A.0.3) and*

2. *for any $p \geq 2$ there exists $C_p > 0$ such that*

$$\sup_{0 \leq t \leq T} E||u(t)||^p \leq C_p(1 + E||u_0||^p).$$

Proof. The proof of this theorem can be found in [70]. □

2.3.3 The FHN model with additive space-time white noise

Consider the FHN model with additive space-time noise

$$\begin{aligned} du &= (D\Delta u + F(u,v) + \mu)dt + \sigma dw(t,x) \\ dv &= G(u,v)dt \end{aligned} \tag{2.27}$$

and with boundary conditions $u(t,0) = u(t,1) = 0$, initial values $u(0,x) = u_0$ and $v(0,x) = v_0$ and $F, G : \mathbb{R}\times\mathbb{R} \to \mathbb{R}$. μ and σ are real numbers. The Laplacian $\Delta = \frac{\partial^2}{\partial x^2}$, and $D\Delta u$ represents the propagation of the potential u at a rate determined by diffusion coefficient D. $w(t,x)$ is a Wiener process with covariance Q. To understand this, consider $\{e_j = \sqrt{2}\sin(j\pi x),\ j = 1, 2, \ldots\}$, a complete orthonormal system for $L^2(0,1)$ as shown in Theorem B.0.9. Then, the Wiener process $w(t,x)$ with covariance Q can be written in terms of its Fourier series. If Q has eigenvalues $\alpha_j > 0$ and corresponding eigenfunctions $\sin(j\pi x)$, then

$$w(t,x) = \sum_{j=1}^{\infty} (\sqrt{2}\sqrt{\alpha_j}\sin(j\pi x)\beta_j(t)),$$

where $\beta_j(t)$ is a sequence of independent real valued Wiener processes. For our work, we consider a space-time white noise, so $Q = I$, where I is the identity operator, and

thus $\alpha_j = 1$, $\forall j = 1, 2, \ldots$ Thus

$$w(t,x) = \sum_{j=1}^{\infty} (\sqrt{2}\sin(j\pi x)\beta_j(t)).$$

Following [20], the function $F(u,v)$ is a cubic function that can be written as $F(u,v) = u(1-u)(u-a) - v$, where $0 < a < 1$, and $G(u,v) = b(u - \gamma v)$, where $b, \gamma \in \mathbb{R}$ [86]. To obtain a suitable suprathreshold response, the parameter a should be less than $1/2$ [88]. The variable u represents the fast (voltage-like) variable and v represents the slow or recovery variable (potassium gating variable). The initial values are chosen to be the resting value of u ($u_0 = 0$) and the equilibrium state of v ($v_0 = n_0$).

To discuss the existence and uniqueness of the solution of the system (2.27), we regard the system as an evolution equation of form (2.23) in a separable Hilbert space H and apply Theorem 2.3.2. However, F in system (2.27) is a nonlinear polynomial, an as a result does not satisfy the global Lipschitz condition. To deal with this situation, we consider equation(2.23) on a smaller state space, E, on which F is well defined (locally Lipschitz continuous). E is a Banach space that is continuously, densely and, as a Borel subset, embedded in H. To guarantee the existence and uniqueness of a mild solution to equation (2.23) in this case, some assumptions need to be satisfied; see Theorem 7.10 and assumptions 7.35, 7.36 and 7.37 in [70, pp 197-198]. In our example, we take $H = L^2(0,1)$ and $E = C([0,1])$, similarly to Example 7.11 in [70]. For further details of the general case, see chapter 7 and Appendices A and D in [70].

We now discuss how to discretize the FitzHugh-Nagumo model spatially, to get a system of SDEs which can be solved by SDELab. To do this, consider a time step Δt and a grid size $\Delta x = \frac{1}{d+1}$, where $d \in \mathbb{N}$. The Wiener process $w(t,x)$ can be approximated by truncating its Fourier expansion after d terms [81], so we consider

the $\mathbb{R}^d$-valued process $\tilde{w}(t)$, with components

$$\tilde{w}_i(t) = \sum_{j=1}^{d} (\sqrt{2} \sin j\pi x_i \beta_j(t)),$$

where $x_i = i\Delta x, i = 1, 2, \cdots, d$, is the spatial grid. Moreover, the standard three-point finite difference approximation A is used to approximate the Laplacian Δ, where A is a tridiagonal matrix $\in \mathbb{R}^d \times \mathbb{R}^d$ and $A_{ii} = -2$, $A_{i+1,i} = 1$ for $1 \leq i \leq d-1$ and $A_{i-1,i} = 1$ for $2 \leq i \leq d$. This leads to the following spatial discretization scheme:

$$\begin{aligned} d\tilde{u} &= [D\frac{1}{(\Delta x)^2} A\tilde{u} + F(\tilde{u}, \tilde{v}) + \mu]dt + \sigma d\tilde{w}(t) \\ d\tilde{v} &= G(\tilde{u}, \tilde{v})dt, \end{aligned} \tag{2.28}$$

where $\tilde{u} \in \mathbb{R}^d$ with components $\tilde{u}_i = u(t, i\Delta x)$ and $\tilde{v} \in \mathbb{R}^d$ with components $\tilde{v}_i = v(t, i\Delta x)$. $F(\tilde{u}, \tilde{v})$ and $G(\tilde{u}, \tilde{v}) : \mathbb{R}^d \times \mathbb{R}^d \to \mathbb{R}^d$ with components

$$F_i = (\tilde{u}_i(1 - \tilde{u}_i)(\tilde{u}_i - a) - \tilde{v}_i)$$

and

$$G_i = b(\tilde{u}_i - \gamma\tilde{v}_i),$$

where $i = 1, 2, \cdots, d$. $d\tilde{w}(t) = Qd\beta(t)$ where $Q \in \mathbb{R}^d \times \mathbb{R}^d$ with components

$$Q_{ij} = \sqrt{2} \sin(ij\pi\Delta x),$$

and $d\beta(t)$ is $\mathbb{R}^d$-valued Wiener process since $d\beta(n) = [d\beta_1(t), d\beta_2(t), \cdots, d\beta_d(t)]^T$.

Numerical simulation of SPDEs of FHN model using SDELab

Spatially discretizing the system (2.27) of SPDEs for the FHN model yields the system (2.28) of SDEs, which can be solved by SDELab. Firstly, we rewrite these as

$$dY = f(t, Y)dt + g(t, Y)d\beta(t), \tag{2.29}$$

where $Y = [\tilde{u_1}, \tilde{u_2}, \ldots, \tilde{u_d}, \tilde{v_1}, \tilde{v_2}, \ldots, \tilde{v_d}]^T \in \mathbb{R}^{2d}$, the drift function

$$f(t, Y) = \begin{bmatrix} D\frac{1}{(\Delta x)^2}A\tilde{u} + F(\tilde{u}, \tilde{v}) + \mu \\ G(\tilde{u}, \tilde{v}) \end{bmatrix},$$

where $F(\tilde{u}, \tilde{v})$ and $G(\tilde{u}, \tilde{v})$ are interpreted as vectors with entries $F(\tilde{u}_1, \tilde{v}_1)$, $F(\tilde{u}_2, \tilde{v}_2)$, etc. and $g = \begin{bmatrix} \sigma Q \\ 0 \end{bmatrix}$ is a diffusion function, with initial condition

$Y_0 = \begin{bmatrix} u_0 \\ v_0 \end{bmatrix} \in \mathbb{R}^{2d}$ since $u_0 = \begin{bmatrix} 0 \\ 0 \\ \vdots \\ 0 \end{bmatrix} \in \mathbb{R}^d$ and $v_0 = \begin{bmatrix} n_0 \\ n_0 \\ \vdots \\ n_0 \end{bmatrix} \in \mathbb{R}^d$.

The codes for the FHN equations and their drift and diffusion functions are shown in Appendix C as codes C.1.1, C.1.2 and C.1.3 respectively. The parameters of the model are specified as $D = 0.01, a = 0.05, \mu = 0.5, \gamma = 0.5$ and $b = 0.008$ with time step $\Delta t = 0.01$ and spatial grid $\Delta x = 0.1$.

To avoid problems with stability and to deal efficiently with a small intensity of noise for the FHN model where $\sigma \ll 1$, either the Euler method with $\alpha = 1/2$ or the BDF2 method would be suitable.

Trajectories

To investigate the influence of the additive noise intensity σ on the trajectories of the fast variable u using our SDELab codes, different values are chosen for σ, holding the other parameters fixed. The results of the numerical simulations can be summarized as follows:

- When σ is very small, as shown in Figure 2.8 for $\sigma = 0.001$, the paths are close to the deterministic case (shown in Figure 2.7).
- If the noise parameter is increased to $\sigma = 0.01$, for example, spikes can be realized, although the paths are erratic, as illustrated in Figure 2.9.
- When the noise is further increased to $\sigma = 0.1$, the irregularity in paths is also increased. This is shown in Figure 2.10, where the paths are very erratic and it is difficult to recognize the spikes.

The above numerical experiments provide evidence of the sensitivity of this type of model to noise. Therefore, the noise should be very small, $\sigma \ll 1$, in order to produce regular spikes.

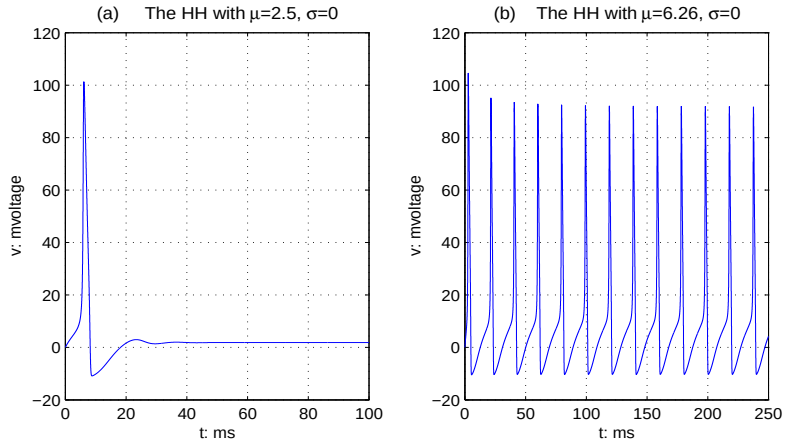

Figure 2.2: In absence of noise: (a) shows the current needed to fire a spike ($\mu = 2.5$) and (b) shows the current required to produce an infinite train of spikes must be greater than $I_0 = 6.25$. In the figure: $\mu = 6.26$ is just above I_0.

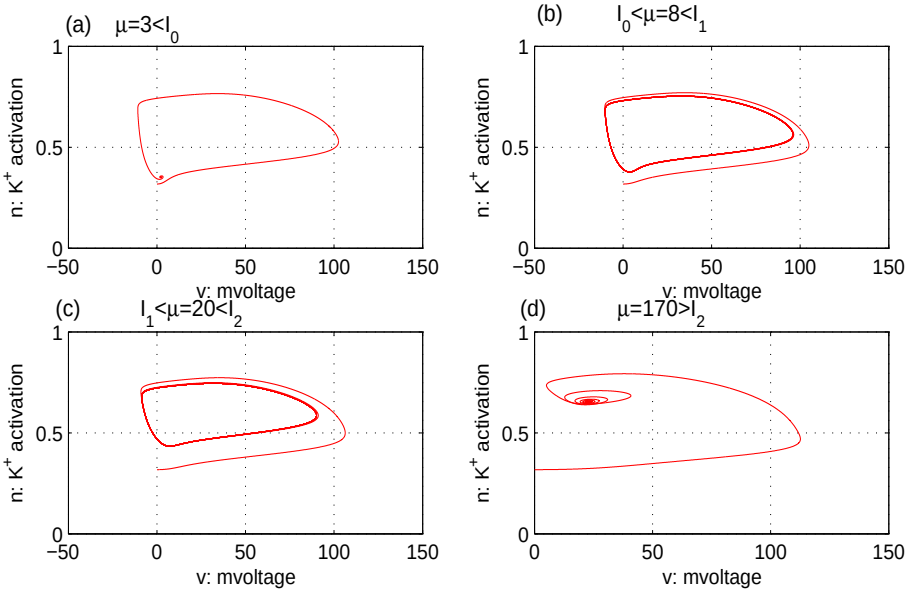

Figure 2.3: Examples for the dynamic behavior that the solutions of the HH equations can display: (a) $\mu = 3 < I_0$ (b) $I_0 < \mu = 8 < I_1$ (c) $I_1 < \mu = 20 < I_2$ and (d) $\mu = 170 > I_2$.

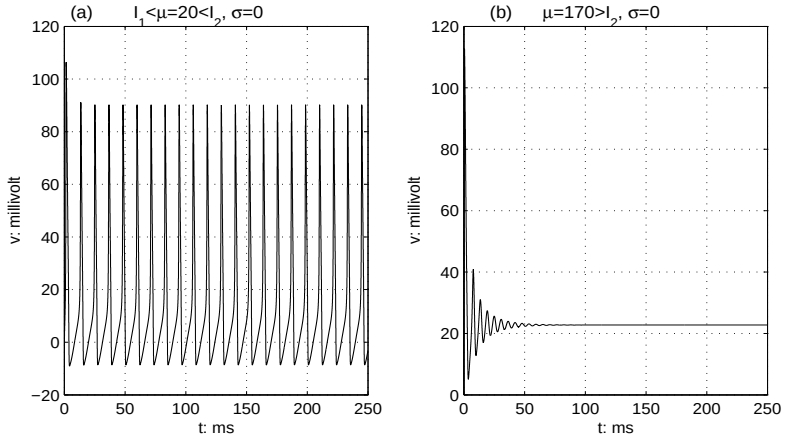

Figure 2.4: (a) Periodic solutions that the system has when $I_1 < \mu < I_2$. (b) The case when $\mu > I_2$ where the system shows oscillatory behavior but no true spikes due to the blocking of nerve after few spikes.

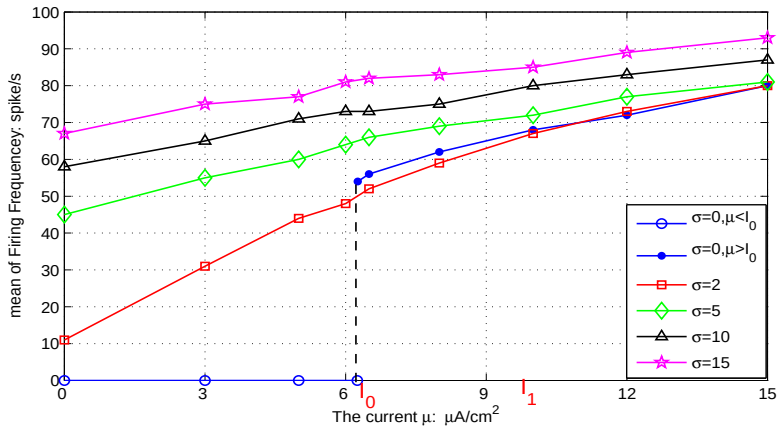

Figure 2.5: The mean firing frequency versus the current μ for different values of noise σ.

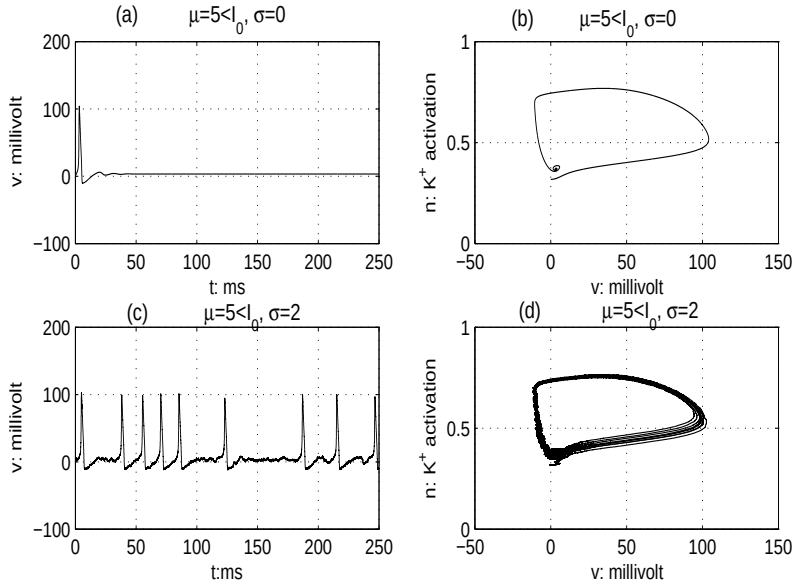

Figure 2.6: Trajectories of voltage variable v of the HH system when $\mu = 5$ (less than the critical value I_0) with (a) $\sigma = 0$ (c) $\sigma = 2$, and (b) and (d): the projection v vs n for the corresponding cases, respectively.

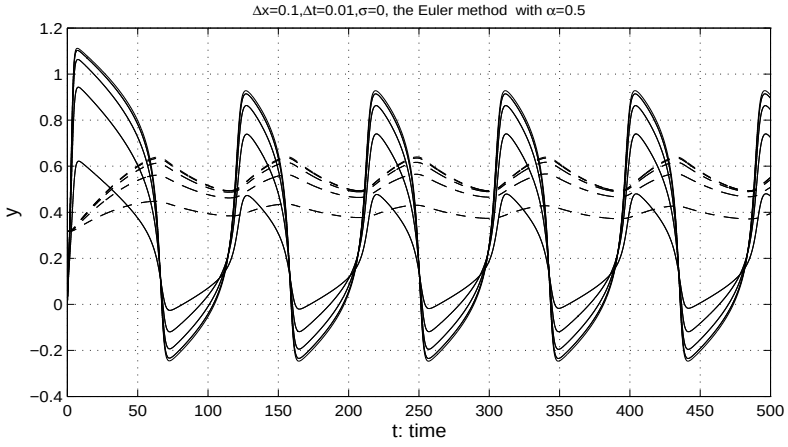

Figure 2.7: An illustration of the spikes generated by numerical simulation of SPDEs for the FHN system using the Euler method ($\alpha = 0.5$) with $\Delta t = 0.01, \Delta x = 0.1$ and $\sigma = 0$. The fast variable $u(i\Delta x, t)$ where $i = 1, 2, \cdots, d = 9$ is represented by sold lines and the recovery variable $v(i\Delta x, t)$ where $i = 1, 2, \cdots, d$ by dashed lines.

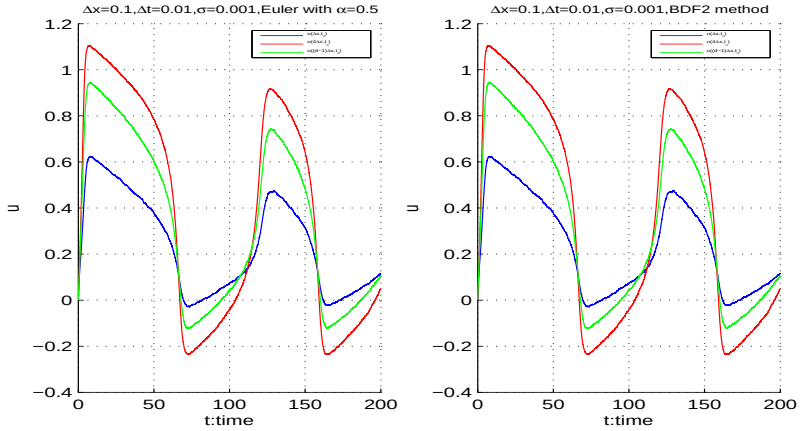

Figure 2.8: Numerical simulation of the FHN model when $\sigma = 0.001 \ll 1$, for which the trajectories are very close to the deterministic case. The figure shows the trajectories of the fast variable: (a) when using the Euler method with $\alpha = 0.5$. (b) when using the BDF2 method.

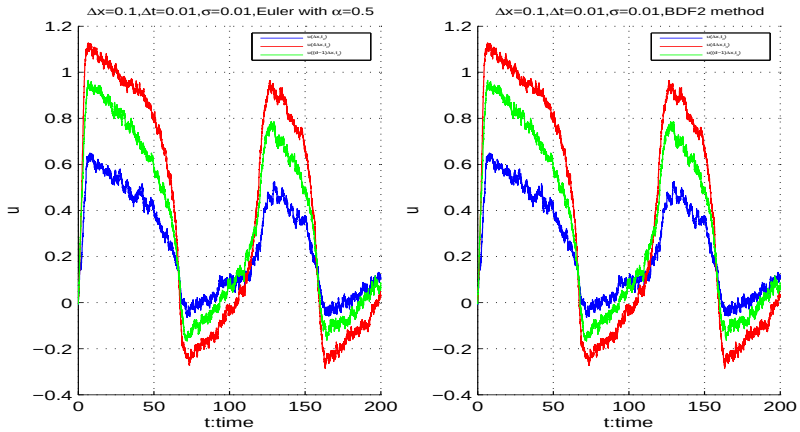

Figure 2.9: Trajectories of the fast variable u when $\sigma = 0.01$. (a) Using the Euler method with $\alpha = 0.5$ and (b) using the BDF2 method. The spikes can be recognized despite of irregularity in their paths.

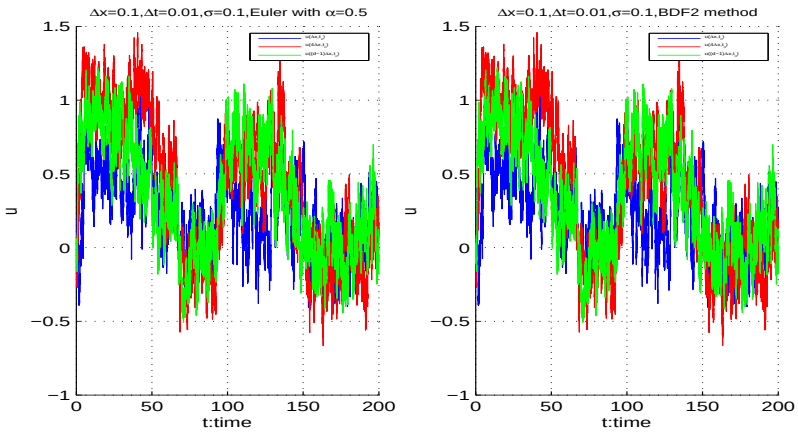

Figure 2.10: Erratic paths of the fast variable u when $\sigma = 0.1$:(a) Using the Euler method ($\alpha = 0.5$). (b) Using BDF2 method. The noise is dominant so it is difficult to recognize the spikes.

Chapter 3

Simulation of first exit time problems of one-dimensional neural diffusion models

There is no doubt that the first exit time (FET) or the first passage time (FPT) of one-dimensional diffusion through a constant threshold is one of the classical problems in probability theory with important applications in many scientific areas such as physics and neurobiology. The basic characteristics of such problems, including the first passage probabilities and the boundary behavior properties, can be calculated explicitly and thus have created a strong motivation for the extensive studies of the theory of first exit phenomena in the literature, for example [46, 40, 3].

In neurobiology, for instance, there has been significant interest in studying the aspect of neuronal spiking activity, in particular the first exit time of the membrane potential through a fixed threshold. In fact, the time to the first spike, for example in cortical neurons, is implicated as coding much of the information about stimulus properties [90]. For more detail, see [91] and the references therein. Therefore, this problem has received a lot of attention in the literature, in particular for the basic

diffusion neuronal models such as [52] for the Ornstein Uhlenbeck (OU) process, [90] for the Hodgkin Huxley (HH) model and [89] for the FitzHugh Nagumo (FHN) model.

However, finding the analytical results for the first exit time problems, in general, is a hard task and success can be limited, although closed forms can be obtained in some cases. Therefore, numerical and particularly simulation approaches are often used in this context. For more information, see [89, 90, 52, 67] and the references given there. The simulation of the FET through threshold boundary using the fixed time step Euler method overestimates the actual values due to the possibility that the threshold boundary is reached during the time step. Decreasing the time step of the simulation can make this overestimation smaller. However, the price paid is the long run time [67]. Mannella [59] treated this situation by applying a simple test after each time step to calculate the probability of the boundary being hit during the time step.

When the time step is a random variable with an exponential distribution, the probability that the boundary has been hit during the time step can also be taken into account using the simple boundary test [43, 42]. In the present chapter, both the fixed time step Euler algorithm and the exponential time-stepping Euler method, with boundary tests, are used to simulate the FET of the FHN equation presented in [89] and the OU process studied in [52].

The chapter is organized as follows. In Section 3.1, we briefly sketch the main properties of diffusion processes that are needed in the subsequent sections. Section 3.2 presents some facts and theory of the FET of the one-dimensional diffusion through constant boundaries referring to [46, 76] for a more thorough treatment. In Section 3.3, we look more closely at the exponential and the fixed time-stepping methods, with boundary tests and the relevant theory. Thus in Section 3.3.1, we recall the fixed time-stepping Euler method introduced in Chapter 2 and use it to simulate the

FET of one-dimensional diffusion. Moreover, the main idea of the boundary test of Mannella associated with the Euler algorithm is clarified and analyzed. In Section 3.3.2, following [43], we provide a detailed exposition of the strategy of the exponential timestepping algorithm with boundary test and an analytical framework of relevant functionals of the FET of the diffusion processes. In last section, we include numerical experiments concerning the FHN equation and the OU model, to compare the properties of the exponential time-stepping Euler method with those of the fixed time-stepping algorithm.

3.1 Diffusion processes

First of all, we present some basic definitions related to continuous time Markov processes with continuous state space, before defining a diffusion process.

Definition 3.1.1. [49][**Markov property, Markov process, transition probability, transition density**]
Let $X(t)$, $t \geq 0$ be a continuous time process with continuous state space $I \subseteq \mathbb{R}$. *The Markov property* of the process $X(t)$ is defined as

$$\mathbf{P}(X(t+h) \in B | X(t) = x, X(t_1) = x_1, ..., X(t_n) = x_n) = \mathbf{P}(X(t+h) \in B | X(t) = x),$$

where $0 < t_1 < t_2 < \cdots < t_n < t$, $h > 0$, $x_1, x_2, \cdots, x_n, x \in I$ and $B \subseteq I$ is a Borel subset of $\mathbb{R}$. A process $X(t)$ with this property is called a *Markov process* with *transition probabilities* given by

$$P(B, t+h|x, t) = \mathbf{P}(X(t+h) \in B | X(t) = x), \tag{3.1}$$

and with *transition densities* $p(\cdot, t+h|x, t)$(if they exist) defined by

$$P(B, t+h|x, t) = \int_B p(y, t+h|x, t)dy. \tag{3.2}$$

Definition 3.1.2. [65][**stopping time**]
Consider a stochastic process $X(t)$ defined on the filtered probability space $(\Omega, \mathcal{F}, \mathcal{F}_t, \mathbf{P})$. The *stopping time* (or Markov time) of the process $X(t)$ is a random variable $\tau : \Omega \to [0, \infty]$ for which the event $\{\tau \leq t\} \in \mathcal{F}_t$ for all $t \geq 0$. The first passage time or first exit time

$$H_b = \inf\{t \geq 0 : X(t) = b\},$$

which will be discussed in the next section, is an example of a stopping time.

Definition 3.1.3. [65][**strong Markov property**]

The *strong Markov property* is a generalization of the Markov property defined above, in which t is replaced by a stopping time τ.

We clarify this concept using the case of the Wiener process. The Wiener process starts afresh at each deterministic time instance meaning that it satisfies the Markov property [65, Theorem 2.3]. Moreover, the Wiener process is called a strong Markov process since it obeys the Markov property for a class of random times called stopping times. Mathematically, if $w(t), t \geq 0$ is a standard Wiener process, then for all finite stopping times τ (w.p.1), the process $w(\tau + t) - w(\tau)$, for all $t \geq 0$ is also a standard Wiener process independent of $w(t)$ (see [65, Theorem 2.16]). Clearly, the strong Markov property implies the Markov property, but not vice versa. One important application of the strong Markov property is *the reflection principle* as stated in the following theorem:

Theorem 3.1.1. ***Reflection principle*** *If τ is a stopping time and $w(t), t \geq 0$ is a standard Wiener process then the process*

$$w^*(t) = \begin{cases} w(t), & if \quad t \leq \tau, \\ 2w(\tau) - w(t) & if \quad t > \tau, \end{cases} \tag{3.3}$$

is also a standard Wiener process. In other words, the Wiener process reflected at some stopping time τ is still a Wiener process.

Proof. The proof of this theorem can be found in [65]. □

Lemma 3.1.2. *Suppose $w(t), t \geq 0$ is a standard Wiener process and $H_b = \inf\{t : w(t) = b\}$ is a stopping time of $w(t)$ at a constant boundary b. Then*

$$\mathbf{P}(H_b < t) = 2\mathbf{P}(w(t) > b).$$

Proof. For the proof, we follow [18]. First, if $w(t) > b$ then by the continuity of the

path of the Wiener process, we get $H_b < t$. It follows that

$$\mathbf{P}(w(t) > b) = \mathbf{P}(w(t) > b, H_b < t).$$

By the strong Markov property and since H_b is a stopping time, $w(t+H_b)-w(H_b), t \geq 0$ is also a standard Wiener process, independent of $w(t)$. Then the symmetry for the Wiener process yields

$$\mathbf{P}(w(t) - w(H_b) > 0 | H_b < t) = \mathbf{P}(w(t) > b | H_b < t) = \frac{1}{2}.$$

Now, we have

$$\begin{aligned} \mathbf{P}(w(t) > b) &= \mathbf{P}(w(t) > b, H_b < t), \\ &= \mathbf{P}(w(t) > b | H_b < t)\mathbf{P}(H_b < t), \\ &= \frac{1}{2}\mathbf{P}(H_b < t). \end{aligned}$$

□

We now turn to the case of diffusion processes. Basically, the *diffusion process* is defined as a continuous time Markov process with continuous sample paths. To be more precise, we present the mathematical description of the diffusion process as follows:

Definition 3.1.4. [49, 46, 3, 28][**diffusion process**]
Consider a Markov process $X(t)$, $t \geq 0$ defined on the state $I = [l, r] \subseteq \mathbb{R}$ with $-\infty \leq l < r \leq \infty$. Then the process $X(t)$ is said to be *a diffusion process* if the following limits exist:

1. $\lim_{h \downarrow 0} \frac{1}{h}\mathbf{P}(|X(t+h) - X(t)| > \xi | X(t) = x) = 0, \quad \text{for any} \quad \xi > 0,$
2. $\lim_{h \downarrow 0} \frac{1}{h} E[X(t+h) - X(t) | X(t) = x] = \mu(x, t),$
3. $\lim_{h \downarrow 0} \frac{1}{h} E[(X(t+h) - X(t))^2 | X(t) = x] = \sigma^2(x, t),$

where μ and σ are Lipschitz functions.

By condition (1), the diffusion process $X(t)$ avoids any instantaneous jumps and consequently $X(t)$ has continuous sample paths [49, 46]. The functions $\mu(x,t)$ and $\sigma^2(x,t)$ represent the drift and diffusion parameters of the diffusion process $X(t)$, respectively, and they are, generally, continuous in t and x [46].

Definition 3.1.5. [46][**homogeneous diffusion process**]
A diffusion process $X(t)$, $t \geq 0$ is said to be *homogeneous* if

$$\mathbf{P}(X(t+h) \in B | X(t) = x) = \mathbf{P}(X(h) \in B | X(0) = x), \tag{3.4}$$

for all Borel subsets $B \in I$, $x \in I$ and $h, t \geq 0$.

In this case the process depends only on the increment of time rather than the specific time t, and the drift $\mu(x,t)$ and diffusion $\sigma^2(x,t)$ are time independent. Thus,

$$\mu(x,t) = \mu(x) = \lim_{h \downarrow 0} \frac{1}{h} E[X(h) - x | X(0) = x], \tag{3.5}$$

and

$$\sigma^2(x,t) = \sigma^2(x) = \lim_{h \downarrow 0} \frac{1}{h} E[(X(h) - x)^2 | X(0) = x]. \tag{3.6}$$

Definition 3.1.6. [46, 76][**regular diffusion process**]
Let $X(t)$, $t \geq 0$ be a diffusion process defined on state space $I = [l, r]$, where $-\infty \leq l < r \leq \infty$. Then $X(t)$ is called *regular* if, for all $x \in (l, r)$ and $b \in I$, we have

$$\mathbf{P}(H_b < \infty | X(0) = x) > 0. \tag{3.7}$$

The behavior of the regular time homogeneous diffusion process $X(t)$ defined on the state space $I = [l, r]$ is expressed by its *infinitesimal generator*, given by [46, 3]

$$Lf(x) = \mu(x) \frac{df(x)}{dx} + \frac{1}{2} \sigma^2(x) \frac{d^2 f(x)}{dx^2}, \tag{3.8}$$

where $f(x)$ is a twice continuously differentiable on I, $l < x < r$, and

$$L = \mu(x)\frac{d}{dx} + \frac{1}{2}\sigma^2(x)\frac{d^2}{dx^2}$$

is a differentiable operator. From now on, we shall consider a regular homogeneous diffusion process, unless otherwise stated.

Definition 3.1.7. [46, 76][**scale density, scale function**]
Let $s(x) : \mathbb{R} \to \mathbb{R}$ be a function given by

$$s(x) = \exp(-\int_l^x 2\mu(\xi)\sigma^{-2}(\xi)d\xi), \quad l < x < r, \tag{3.9}$$

where the state space is as defined above, and with the assumption that $\sigma^2(x) > 0$. Then $s(x)$ is said to be a *scale density* of the process $X(t)$. Furthermore, a *scale function* of the process $X(t)$ is a continuous strictly increasing C^2-function $S(x)$ on $\mathbb{R}$ defined by

$$S(x) = \int_l^x s(\eta)d\eta, \quad l < x < r. \tag{3.10}$$

Definition 3.1.8. [46, 76][**speed density**]
A function $m(x) : \mathbb{R} \to \mathbb{R}$ given by

$$m(x) = \frac{2}{\sigma^2(x)s(x)}, \quad l < x < r, \tag{3.11}$$

is known as the *speed density* of the process $X(t)$.

One efficient technique for solving (3.8) is to express the differential operator L as consecutive differentiations with respect to $s(x)$ and $m(x)$. We have

$$\frac{s'(x)}{s(x)} = -\frac{2\mu(x)}{\sigma^2(x)},$$

and consequently equation (3.8) can be written as

$$Lf(x) = \big(\frac{1}{m(x)}\big)\frac{d}{dx}\left[\frac{1}{s(x)}\frac{df(x)}{dx}\right]. \tag{3.12}$$

Now, we have $dS(x) = s(x)dx$ and $dM(x) = m(x)dx$, where M is called *the speed measure*. Substituting these quantities into equation (3.12) yields

$$Lf(x) = \frac{d}{dM}\left[\frac{df(x)}{dS}\right], \tag{3.13}$$

which is known as the *canonical representation* of the differential operator associated with diffusion process $X(t)$ [46].

The properties related to the diffusion process and to its infinitesimal generator, presented in this section, will be used to study the FET problem of one-dimensional diffusion in the following sections.

3.2 First exit time problem of one-dimensional diffusion

The first time for reaching a point or exiting a region plays a crucial role in the study of one-dimensional diffusion processes. First, let $X(t)$, $t \geq 0$ be a regular time homogeneous diffusion process, defined on the state space $I = [l, r]$ where $-\infty \leq l < r \leq \infty$, and define the first exit time for $X(t)$ through a fixed point $b \in I$ given by

$$H_b(x) = \inf\{t \geq 0 : X(t) = b | X(0) = x\}.$$

In addition, denote by

$$H = H_a \wedge H_b = \min(H_a, H_b)$$

the first time $X(t)$ reaches either a or b where $l \leq a < b \leq r$. We here restrict our attention to the problems of mean first exit for $X(t)$ of constant boundaries, beginning with the following general problem.

Lemma 3.2.1. *Suppose*

$$U(x) = E[f(\int_0^H g(X(s))ds)|X(0) = x] = E_x[f(\int_0^H g(X(s))ds)], \quad a < x < b, \tag{3.14}$$

where $H = H_a \wedge H_b$, $f \in C^2[a, b]$ and g is a piecewise smooth function assumed to be bounded and continuous. Then, $U(x)$ satisfies the boundary value problem

$$LU(x) + g(x)V(x) = 0, \quad U(a) = U(b) = f(0), \tag{3.15}$$

where $V(x) = E_x[f'(\int_0^H g(X(s))ds)]$ and $LU(x) = \mu(x)U'(x) + \frac{1}{2}\sigma^2(x)U''(x)$.

Proof. We follow [46] to prove this lemma. First, verification of the boundary conditions is straightforward from the definition of H. Given $0 < h < H$, and assuming

$h \to 0$, the Taylor expansion implies

$$\begin{aligned} U(x) &= E_x[f(\int_0^h g(X(s))ds + \int_h^H g(X(s))ds)] \\ &= E_x[f(\int_h^H g(X(s))ds) + f'(\int_h^H g(X(s))ds) \int_0^h g(X(s))ds] + O(h^2). \end{aligned}$$

As g is continuous at x, we have

$$U(x) = E_x[f(\int_h^H g(X(s))ds) + hg(x)f'(\int_h^H g(X(s))ds)] + o(h), \tag{3.16}$$

where $o(h)$ is of smaller order than h. Using the property of the conditional expectation (A.14) and the Markov property, we obtain

$$\begin{aligned} E_x[f(\int_h^H g(X(s))ds) + hg(x)f'(\int_h^H g(X(s))ds)] & \\ &= E_x[E_{X(h)}[f(\int_h^H g(X(s))ds)] \\ &+ hg(x)E_{X(h)}[f'(\int_h^H g(X(s))ds)]] \\ &= E_x[U(X(h))] + hg(x)E_x[V(X(h))]. \end{aligned}$$

Consequently (3.16) is rewritten as

$$U(x) = E_x[U(X(h))] + hg(x)E_x[V(X(h))] + o(h). \tag{3.17}$$

By the continuity of the sample paths of the diffusion process X, as $h \to 0$, $X(h) \to X(0) = x$. Expanding then about x yields

$$E_x[U(X(h))] = U(x) + U'(x)E_x[X(h) - x] + \frac{1}{2}U''(x)E_x[(X(h) - x)^2] + o(h), \tag{3.18}$$

and

$$E_x[V(X(h))] = V(x) + o(h). \tag{3.19}$$

Substituting from (3.18) and (3.19) into (3.17) gives

$$U(x) = U(x)+U'(x)E_x[X(h)-x]+\frac{1}{2}U''(x)E_x[(X(h)-x)^2]+hg(x)V(x)+o(h), \quad (3.20)$$

which means

$$0 = U'(x)E_x[X(h) - x] + \frac{1}{2}U''(x)E_x[(X(h) - x)^2] + hg(x)V(x) + o(h). \quad (3.21)$$

The result then follows from dividing (3.21) by h, letting h tends to zero and substituting μ and σ^2 into equation (3.21) from the infinitesimal equations

$$\mu(x) = \lim_{h\downarrow 0} \frac{1}{h} E_x[X(h) - x]$$

and

$$\sigma^2(x) = \lim_{h\downarrow 0} \frac{1}{h} E_x[(X(h) - x)^2].$$

□

We restrict ourselves here to discussing two important special cases of the problem introduced by Lemma 3.2.1. The first is when $f(x) = x^n$, so $f'(x) = nx^{n-1}$, and consequently the n^{th} moment of $\int_0^H g(X(s))ds$ is given by

$$U_n(x) = E_x[(\int_0^H g(X(s))ds)^n],$$

which satisfies

$$\mu(x)U_n'(x) + \frac{1}{2}\sigma^2(x)U_n''(x) + ng(x)U_{n-1}(x) = 0, \quad U(a) = U(b) = 0. \quad (3.22)$$

The first moment or the mean of the first time the diffusion reaches either a or b is thus obtained by setting $n = 1$ and $g(x) \equiv 1$ giving

$$T(x) = U_1(x) = E_x[H_{a,b}], \quad a < x < b,$$

which satisfies the associated boundary value problem

$$LT(x) = -1, \quad a < x < b, \quad T(a) = T(b) = 0. \tag{3.23}$$

The second important special case, which arises in many applications, is $f(x) = \exp(-\lambda x)$, $\lambda > 0$ and $g(x) \equiv 1$. Obviously, $f'(x) = -\lambda f(x)$. Here, we are interested in the problem of the first time the diffusion reaches a single barrier, b say. Thus we will concentrate on the problem of the mean FET from the region $(-\infty, b)$ with $X(0) = x$. As a result, from Lemma 3.2.1, the mean or the Laplace transformation of the first exit time H_b,

$$\varphi(x) = E_x[\exp(-\lambda H_b)], \tag{3.24}$$

is the solution of the following differential equation:

$$L\varphi(x) - \lambda\varphi(x) = \mu(x)\varphi'(x) + \frac{1}{2}\sigma^2(x)\varphi''(x) - \lambda\varphi(x) = 0, \quad \varphi(b) = 1. \tag{3.25}$$

For a deeper discussion of this case, see for example [46, 76, 40]; here, however, we touch on a few aspects of the theory related to this problem. First, we remark that a one-dimensional diffusion process, starting at state a, say, and reaching state b, must visit all intermediate points. Using this and the strong Markov property implies the following important lemma [46].

Lemma 3.2.2. *For $l < a < c < b < r$ and for each $\lambda > 0$, we have*

1.

$$E_a[\exp(-\lambda H_b)] = E_a[\exp(-\lambda H_c)]E_c[\exp(-\lambda H_b)], \tag{3.26}$$

and

2.

$$E_b[\exp(-\lambda H_a)] = E_b[\exp(-\lambda H_c)]E_c[\exp(-\lambda H_a)], \tag{3.27}$$

Proof. We refer to [46] for the proof of this lemma. □

Now, for each $\lambda > 0$, define the functions [76]
$\psi^{\uparrow}(x)$: $[l, r) \to (0, \infty)$ and $\psi^{\downarrow}(x)$: $(l, r] \to (0, \infty)$ by

$$\psi^{\uparrow}(x) \equiv \begin{cases} E_x[\exp(-\lambda H_c)], & x \leq c, \quad x \in (l, r) \\ \\ \dfrac{1}{E_c[\exp(-\lambda H_x)]}, & x \geq c, \quad x \in (l, r) \end{cases}$$

and

$$\psi^{\downarrow}(x) \equiv \begin{cases} E_x[\exp(-\lambda H_c)], & x \geq c, \quad x \in (l, r) \\ \\ \dfrac{1}{E_c[\exp(-\lambda H_x)]}, & x \leq c, \quad x \in (l, r) \end{cases}$$

where $c \in (l, r)$ and $\psi^{\uparrow}(l) = \psi^{\downarrow}(r) = 0$. The functions $\psi^{\uparrow}(x)$ and $\psi^{\downarrow}(x)$ are well defined due to the regularity of the homogeneous diffusion process $X(t)$ which means that $E_c[\exp(-\lambda H_x)] > 0$.

Lemma 3.2.3. *1. For $b > x$,*

$$E_x[\exp(-\lambda H_b)] = \frac{\psi^{\uparrow}(x)}{\psi^{\uparrow}(b)}, \tag{3.28}$$

and

2. for $b < x$,

$$E_x[\exp(-\lambda H_b)] = \frac{\psi^{\downarrow}(x)}{\psi^{\downarrow}(b)}. \tag{3.29}$$

Moreover, $\psi^{\uparrow}(x)$ and $\psi^{\downarrow}(x)$ are strictly increasing and strictly decreasing functions

of x respectively, and also satisfy

$$L\psi(x) = \lambda\psi(x), \quad \psi(b) = 1. \tag{3.30}$$

Proof. We first prove statement(1), and statement (2) follows similarly. From Lemma 3.2.2, we have for $x < c < b$,

$$E_x[\exp(-\lambda H_b)] = E_x[\exp(-\lambda H_c)]E_c[\exp(-\lambda H_b)]. \tag{3.31}$$

The definitions of $\psi^{\uparrow}(x)$ and $\psi^{\downarrow}(x)$ imply that

$$E_x[\exp(-\lambda H_c)] = \psi^{\uparrow}(x), \quad \text{where} \quad x < c,$$

and

$$E_c[\exp(-\lambda H_b)] = \frac{1}{\psi^{\uparrow}(b)}, \quad \text{where} \quad b > c.$$

(1) then follows immediately by substituting these quantities into (3.31). From this, we have for, $x < b$,

$$E_x[\exp(-\lambda H_b)]\psi^{\uparrow}(b) = \psi^{\uparrow}(x),$$

and since $0 < E_x[\exp(-\lambda H_b)] < 1$, it follows that $\psi^{\uparrow}(x) < \psi^{\uparrow}(b)$. Hence, $\psi^{\uparrow}(x)$ is a strictly increasing function of x. In the same manner, we can see that $\psi^{\downarrow}(x)$ is a strictly decreasing function of x. Now, by Lemma 3.2.1, $\varphi(x) = E_x[\exp(-\lambda H_b)]$ is the solution of

$$L\varphi(x) = \lambda\varphi(x), \quad \varphi(b) = 1, \tag{3.32}$$

and from (3.28), we have

$$E_x[\exp(-\lambda H_b)] = \frac{\psi^{\uparrow}(x)}{\psi^{\uparrow}(b)} = \frac{\psi^{\uparrow}(x)}{constant}.$$

Consequently, (3.32) is also satisfied for $\psi^{\uparrow}(x)$. □

However, explicit solutions of the first exit problems of one-dimensional diffusions are limited to a few simple cases and therefore, in general, accurate numerical solutions are required. We will introduce two of these numerical approaches in the next section.

3.3 Numerical simulations of exit time problems

We present here two numerical simulation algorithms in order to study the FET problem of the one-dimensional diffusion process. The first technique is the standard Euler (or Euler-Maruyama) method, introduced in Chapter 2, where the time step is taken to be constant. The second approach is called the exponential time-stepping Euler method, which is analogous to the standard Euler algorithm but with an exponentially distributed random time step [43]. The boundary corrections used to improve the accuracy of the mean exit times estimated by these methods will also be considered.

3.3.1 Standard Euler method with boundary correction

Definition 3.3.1. [3, 6][**Brownian bridge**]
Let $w(t)$, $t \geq 0$ be a standard Wiener process. Then *the Brownian bridge* or *tied-down Wiener process* from 0 to 0 on $[0, T]$, where $T > 0$, is defined as the continuous Gaussian process

$$Y(t) = w(t) - \frac{t}{T} w(T),$$

with zero mean and covariance $Cov(Y(t), Y(s)) = s - \frac{st}{T}, 0 \leq s < t \leq T$. The distribution probability of the Brownian bridge is thus the conditional probability of the Wiener process $w(t)$, given that $w(0) = w(T) = 0$.

A scaled stochastic integral

$$X(t) = \int_0^t \frac{T-t}{T-u} dw(u), \quad 0 \leq t \leq T,$$

that satisfies the stochastic differential equation

$$dX(t) = \frac{-X(t)}{T-t} dt + dw(t),$$

is a Gaussian process with the same mean and covariance as the Brownian bridge $Y(t)$, and therefore $X(t)$ can also be said to be a Brownian bridge from 0 to 0 [6]. Generally, the Brownian bridge from x to y on $[0, T]$, where $x, y \in \mathbb{R}$ is defined as the continuous Gaussian process

$$X(t) = x + \frac{(y-x)t}{T} + \int_0^t \frac{T-t}{T-u} dw(u),$$

with mean

$$E[X(t)] = x + \frac{(y-x)t}{T},$$

and covariance

$$Cov(X(t), X(s)) = s - \frac{st}{T}, \quad 0 \leq s < t \leq T,$$

and is characterized as the pathwise unique solution of the SDE

$$dX(t) = \frac{y - X(t)}{T-t} dt + dw(t), \quad X(0) = x.$$

With these preliminaries in place, we can now proceed to describe the standard Euler method with boundary correction. First, let $X(t)$ be a regular homogeneous diffusion process satisfying the SDE

$$dX(t) = \mu(X(t))dt + \sigma dw, \quad X(0) = x. \tag{3.33}$$

Then the fixed time-stepping Euler method (standard Euler method) for simulating such an equation takes the form [49]

$$X(t_n + \Delta t) = X(t_n) + \mu(X(t_n))\Delta t + \sigma\sqrt{\Delta t}\eta_n, \quad n = 0, 1, 2, \cdots \tag{3.34}$$

where Δt is the fixed time step, $t_n = n\Delta t$ and each η_n is an i.i.d standard Gaussian random variable ($\eta_n \sim N(0, 1)$). However, simulating exit time problems using this approach may cause large errors in the calculation of the probability of the first time the diffusion reaches a boundary point, b say, or exits a region [43]. This is due to the possibility that the process may attain the boundary and come back, within the time step [9]. Approximating the continuous sample paths of Brownian motion using discrete random walks gives the values only at the beginning and the end of the time step and so we have no information about the behavior of the continuous process during the time step [9]. Mannella [59] dealt with this situation by applying a simple hitting test after each time step using the distribution of the Brownian bridge from $X(0) = x$ to $X(\Delta t) = y$. Later, Gobet [32] proved that this test, when combined with the fixed time-stepping Euler algorithm, can improve the weak order of convergence from $O(\Delta t^{\frac{1}{2}})$ to $O(\Delta t)$ in evaluation of the functional $F(X(t))$ conditioned on $t < H_b$, with support or regularity conditions on F [9]. Jansons and Lythe [43] suggested according to their own numerical experiments using the fixed time-stepping Euler method with Mannella boundary test that the first order convergence also applies to the case of the exit time, consistent with our numerical observations that will be presented in the next section. Basically, Mannella's boundary test associated with the fixed time-stepping Euler method requires calculating the probability

$$\mathbf{P}(H_b < \Delta t | X(0) = x, X(\Delta t) = y),$$

where H_b is the first time that the process $X(t)$ reaches the level b. To this end, we first calculate this probability for the diffusion process with constant coefficients as

demonstrated by the following lemma.

Lemma 3.3.1. *Let $B(t)$, $t \geq 0$ be a Wiener process with constant drift defined by*

$$B(t) = x + \mu t + \sigma w(t), \quad B(0) = x,$$

where μ and $\sigma > 0$ are real constants. Also let $H_b^B = \inf\{t \geq 0 : B(t) = b\}$ be the first exit time of $B(t)$ through constant boundary b, then

$$\mathbf{P}(H_b^B < t | B(0) = x, B(t) = y) = \exp(\frac{-2(b-x)(b-y)}{\sigma^2 t}),$$

provided $y < b$.

Proof. We follow [9] to prove this lemma. The proof starts with the observation that

$$\mathbf{P}(H_b^B < t | B(0) = x, B(t) = y) = \mathbf{P}(\sup_{0 \leq s \leq t} B(s) \geq b | B(0) = x, B(t) = y),$$

and since the process

$$Z(t) = \frac{B(t)}{\sigma} = \frac{x}{\sigma} + \frac{\mu}{\sigma} t + w(t), \quad Z(0) = \frac{x}{\sigma},$$

is the Wiener process with constant drift $\bar{\mu} = \frac{\mu}{\sigma}$, it follows that

$$\mathbf{P}(H_b^B < t | B(0) = x, B(t) = y) = \mathbf{P}(\sup_{0 \leq s \leq t} Z(s) \geq \frac{b}{\sigma} | Z(0) = \frac{x}{\sigma}, Z(t) = \frac{y}{\sigma}).$$

Now, for simplicity of notation, we set $\bar{b} = \frac{b}{\sigma}$, $\bar{x} = \frac{x}{\sigma}$ and $\bar{y} = \frac{y}{\sigma}$, giving

$$\mathbf{P}(H_b^B < t | B(0) = x, B(t) = y) = \frac{\mathbf{P}(\sup_{0 \leq s \leq t} Z(s) \geq \bar{b}, Z(t) \in d\bar{y} | Z(0) = \bar{x})}{\mathbf{P}(Z(t) \in d\bar{y} | Z(0) = \bar{x})},$$

where $d\bar{y}$ is a tiny interval around $\bar{y}$. Now recalling the formula [6, 2.1.0.6 p.250]

$$\mathbf{P}(Z(t) \in d\bar{y} | Z(0) = \bar{x}) = \frac{1}{\sqrt{2\pi t}} \exp(\frac{-(\bar{y} - \bar{x} - \bar{\mu} t)^2}{2t}) d\bar{y},$$

and [6, 2.1.1.8 p.251]

$$\mathbf{P}(\sup_{0\le s\le t} Z(s) \ge \bar{b}, Z(t) \in d\bar{y} | Z(0) = \bar{x}) = \frac{1}{\sqrt{2\pi t}} \exp(\bar{\mu}(\bar{y}-\bar{x}) - \frac{\bar{\mu}^2 t}{2} - \frac{((\bar{b}-\bar{y})+(\bar{b}-\bar{x}))^2}{2t}) d\bar{y},$$

we obtain

$$\begin{aligned}
\mathbf{P}(H_b^B < t | B(0) = x, B(t) = y) &= \frac{\frac{1}{\sqrt{2\pi t}} \exp(\bar{\mu}(\bar{y}-\bar{x}) - \frac{\bar{\mu}^2 t}{2} - \frac{((\bar{b}-\bar{y})+(\bar{b}-\bar{x}))^2}{2t}) d\bar{y}}{\frac{1}{\sqrt{2\pi t}} \exp(\frac{-(\bar{y}-\bar{x}-\bar{\mu}t)^2}{2t}) d\bar{y}} \\
&= \exp(\bar{\mu}(\bar{y}-\bar{x}) - \frac{\bar{\mu}^2 t}{2} - \frac{(2\bar{b}-\bar{y}-\bar{x})^2}{2t} + \frac{(\bar{y}-\bar{x}-\bar{\mu}t)^2}{2t}) \\
&= \exp(\frac{2t\bar{\mu}(\bar{y}-\bar{x}) - \bar{\mu}^2 t^2 - (2\bar{b}-\bar{y}-\bar{x})^2 + (\bar{y}-\bar{x}-\bar{\mu}t)^2}{2t}) \\
&= \exp(\frac{-4\bar{b}^2 + 4\bar{b}\bar{y} + 4\bar{b}\bar{x} - 4\bar{x}\bar{y}}{2t}) \\
&= \exp(\frac{-4(\bar{b}-\bar{x})(\bar{b}-\bar{y})}{2t}) \\
&= \exp(\frac{-2(b-x)(b-y)}{\sigma^2 t}).
\end{aligned}$$

□

The diffusion process $X(t)$ defined by (3.33), conditioned on $X(t) = x$ and $X(t+\Delta t) = y$, on the interval $[t, t+\Delta t]$ where $\Delta t \to 0$, behaves like the Wiener process $B(t)$ with constant coefficients, and therefore, as a result of Lemma 3.3.1, the distribution of the FET with respect to the bridge pinned at $X(t) = x$ and $X(t+\Delta t) = y$ can be expressed as [9, 59]

$$P_{x,b,y} = \mathbf{P}(H_b < \Delta t | X(t) = x, X(t+\Delta t) = y) = \exp(\frac{-2(b-x)(b-y)}{\sigma^2 \Delta t}). \quad (3.35)$$

The fixed time-stepping Euler method with boundary test is thus divided into two main parts [32]:

- The trajectories $\{X(t_{n+1}) : n = 0, 1, 2, \cdots\}$ are generated according to equation (3.34).
- After each time step, a simple boundary test (Mannella's boundary test) is

performed to check the possibility that the boundary b was reached during the time step, by generating a uniformly distributed random variable $u \sim \mathbf{U}(0,1)$ and comparing it to the probability $P_{x,b,y}$ defined by (3.35). To be precise, an excursion during the time step is deduced if

$$X(t+\Delta t) \geq b \quad \text{or} \quad u < P_{x,b,y}. \tag{3.36}$$

3.3.2 Exponential time-stepping Euler method with boundary test

Under the exponential time-stepping method [43, 42], the time step δt is an exponentially distributed random variable so that

$$\mathbf{P}(\delta t > t) = \exp(-\lambda t), \quad t \geq 0, \quad \lambda > 0. \tag{3.37}$$

In our work, we consider the exponential time-stepping Euler method [43, 42] for the regular homogeneous diffusion process $X(t)$ defined by (3.33). The strategy of this algorithm is based on calculating the conditional probability of a given boundary being hit during the time step and the density of the random variable $X(t+\delta t)-X(t)$. Due to the independence of all quantities of the starting time, we assume the process starts at $t = 0$, and hence we need only to compute the density of $X(\delta t)$ and the probability of the FET of $X(t)$ through a certain boundary, b say, occurring before δt [43].

The first task is thus to calculate the density of $X(\delta t)$:

$$R(x,y) = \frac{d}{dy}\mathbf{P}(X(\delta t) < y | X(0) = x), \tag{3.38}$$

and then to write it in terms of $\psi^{\uparrow}(x)$ and $\psi^{\downarrow}(x)$. To this end, consider first the second-order ordinary differential equation:

$$\mathcal{L}u = Lu - \lambda u = f, \quad l < x < r, \tag{3.39}$$

with homogeneous boundary conditions

$$u(l) = u(r) = 0, \tag{3.40}$$

where L is the differential operator given by (3.25), $\lambda > 0$, and $f : (l, r) \to \mathbb{R}$ is a continuous function. By taking $f = 0$ in (3.39), we obtain the corresponding homogeneous equation

$$\mathcal{L}u = 0 \Leftrightarrow Lu = \lambda u. \tag{3.41}$$

Definition 3.3.2. [46, 12][**Green's function**]
A Green's function $G(x, y)$ for the homogeneous equation (3.41) is defined as satisfying the following conditions:

1. For fixed y, $G(x, y)$ is continuous in x on $[l, r] \times [l, r]$, and the first and second derivatives of G for $x \neq y$ are also continuous.

2. For all $y \in (l, r)$ and $x \neq y$, $\mathcal{L}G(x, y) = 0$.

3. For all $y \in (l, r)$, $G(l, y) = G(r, y) = 0$.

4. The first derivative of G has a jump discontinuity at $x = y$:

$$\frac{\partial G(y+, y)}{\partial y} - \frac{\partial G(y-, y)}{\partial y} = \frac{2}{\sigma^2(y)}, \quad l < y < r.$$

Lemma 3.3.2. *Suppose that the homogeneous equation (3.41) with boundary conditions (3.40), admits only trivial solutions. Then (3.39) with boundary conditions*

(3.40) has a unique solution of the form

$$u(x) = \int_l^r G(x,y)f(y)dy, \quad l < x < r, \tag{3.42}$$

where $G(x,y)$ is the Green's function of the equation (3.41).

Proof. See [12]. □

Construction of Green's function

First, by Lemma 3.2.3, the functions $\psi^{\uparrow}(x)$ and $\psi^{\downarrow}(x)$ are a pair of fundamental solutions of (3.41) (i.e. nonzero and linearly independent solutions), with initial conditions [46]

$$\psi^{\uparrow}(l) = 0, \quad \frac{d\psi^{\uparrow}(l)}{dx} > 0, \quad \text{and} \quad \psi^{\downarrow}(r) = 0, \quad \frac{d\psi^{\downarrow}(r)}{dx} < 0.$$

In fact, $\psi^{\uparrow}(x)$ and $\psi^{\downarrow}(x)$ are linearly independent due to the assumption that the homogeneous equation (3.41) has only trivial solutions satisfying the homogeneous boundary conditions (3.40). We now construct the Green's function of (3.41) by first setting G to

$$G(x,y) = \begin{cases} Z_1\psi^{\uparrow}(x), & l \le x \le y \le r, \\ Z_2\psi^{\downarrow}(x), & l \le y \le x \le r, \end{cases}$$

where Z_1 and Z_2 are unknowns that need to be determined. By the first property of a Green's function (continuity), we have for $x = y$

$$Z_1\psi^{\uparrow}(y) - Z_2\psi^{\downarrow}(y) = 0, \tag{3.43}$$

and on account of the jump condition (the fourth property), we obtain

$$Z_1\frac{d\psi^{\uparrow}(y)}{dy} - Z_2\frac{d\psi^{\downarrow}(y)}{dy} = \frac{-2}{\sigma^2(y)}. \tag{3.44}$$

We thus solve the system of equations (3.43) and (3.44) with respect to Z_1 and Z_2. To this end, we first calculate the determinant Δ of this system:

$$\Delta = \begin{vmatrix} \psi^{\uparrow}(y) & -\psi^{\downarrow}(y) \\ \frac{d\psi^{\uparrow}(y)}{dy} & -\frac{d\psi^{\downarrow}(y)}{dy} \end{vmatrix} = -W(y),$$

where $W(y) = \psi^{\uparrow}(y)\frac{d\psi^{\downarrow}(y)}{dy} - \psi^{\downarrow}(y)\frac{d\psi^{\uparrow}(y)}{dy}$ is the Wronskian of the functions $\psi^{\uparrow}(x)$ and $\psi^{\downarrow}(x)$.

It is easy to check that $W(y) \neq 0$, for all $y \in (l, r)$. To do this, we suppose that $W(y) = 0$, for some $y \in (l, r)$. That is,

$$W(y) = \psi^{\uparrow}(y)\frac{d\psi^{\downarrow}(y)}{dy} - \psi^{\downarrow}(y)\frac{d\psi^{\uparrow}(y)}{dy} = 0.$$

Consequently

$$\frac{d}{dy}\frac{\psi^{\uparrow}(y)}{\psi^{\downarrow}(y)} = \frac{-W(y)}{(\psi^{\downarrow}(y))^2} = 0,$$

and so

$$\frac{\psi^{\uparrow}(y)}{\psi^{\downarrow}(y)} = c,$$

where c is an arbitrary constant. From this, $\psi^{\uparrow}(y)$ and $\psi^{\downarrow}(y)$ are linearly dependent, which contradicts the assumption above, and hence $W(y) \neq 0$, for all $y \in (l, r)$.

Now using Cramer's rule to solve the system of equations (3.43) and (3.44), yields

$$Z_1 = \frac{-1}{W(y)} \begin{vmatrix} 0 & -\psi^{\downarrow}(y) \\ \frac{-2}{\sigma^2(y)} & -\frac{d\psi^{\downarrow}(y)}{dy} \end{vmatrix} = \frac{2\psi^{\downarrow}(y)}{W(y)\sigma^2(y)}$$

and

$$Z_2 = \frac{-1}{W(y)} \begin{vmatrix} \psi^{\uparrow}(y) & 0 \\ \frac{d\psi^{\uparrow}(y)}{dy} & \frac{-2}{\sigma^2(y)} \end{vmatrix} = \frac{2\psi^{\uparrow}(y)}{W(y)\sigma^2(y)}.$$

Hence, the Green's function $G(x,y)$ can be written as

$$G(x,y) = \frac{2}{W(y)\sigma^2(y)} \begin{cases} \psi^{\downarrow}(y)\psi^{\uparrow}(x), & l \le x \le y \le r, \\ \psi^{\uparrow}(y)\psi^{\downarrow}(x), & l \le y \le x \le r. \end{cases}$$

We next claim that

$$\frac{1}{2}W(y)\sigma^2(y)m(y) = C,$$

where C is an arbitrary constant and $m(y)$ is the speed measure defined by (3.11). To prove this, first, we have

$$W(y) = \psi^{\uparrow}(y)\frac{d\psi^{\downarrow}(y)}{dy} - \psi^{\downarrow}(y)\frac{d\psi^{\uparrow}(y)}{dy}$$

and

$$\frac{dW(y)}{dy} = \psi^{\uparrow}(y)\frac{d^2\psi^{\downarrow}(y)}{dy^2} - \psi^{\downarrow}(y)\frac{d^2\psi^{\uparrow}(y)}{dy^2},$$

and since $\psi^{\uparrow}(y)$ and $\psi^{\downarrow}(y)$ are fundamental solutions of the equation $\mathcal{L}u = 0$, we get

$$\begin{aligned} \frac{1}{2}\sigma^2(y)\frac{d}{dy}W(y) + \mu(y)W(y) &= \frac{1}{2}\sigma^2(y)(\psi^{\uparrow}(y)\frac{d^2\psi^{\downarrow}(y)}{dy^2} - \psi^{\downarrow}(y)\frac{d^2\psi^{\uparrow}(y)}{dy^2}) \\ &+ \mu(y)(\psi^{\uparrow}(y)\frac{d\psi^{\downarrow}(y)}{dy} - \psi^{\downarrow}(y)\frac{d\psi^{\uparrow}(y)}{dy}) \\ &= \psi^{\uparrow}(y)(\frac{1}{2}\sigma^2(y)\frac{d^2\psi^{\downarrow}(y)}{dy^2} + \mu(y)(\frac{d\psi^{\downarrow}(y)}{dy})) \\ &- \psi^{\downarrow}(y)(\frac{1}{2}\sigma^2(y)\frac{d^2\psi^{\uparrow}(y)}{dy^2} + \mu(y)(\frac{d\psi^{\uparrow}(y)}{dy})) \\ &= \psi^{\uparrow}(y)(\lambda\psi^{\downarrow}(y)) - \psi^{\downarrow}(y)(\lambda\psi^{\uparrow}(y)) \\ &= 0. \end{aligned}$$

Consequently

$$\frac{d}{dy}W(y) = \frac{-2\mu(y)}{\sigma^2(y)}W(y),$$

and so

$$\int_l^y \frac{\frac{d}{dy}W(\xi)}{W(\xi)}d\xi = \int_l^y \frac{-2\mu(\xi)}{\sigma^2(\xi)}d\xi.$$

We thus get

$$\ln(\frac{W(y)}{W(l)}) = \int_l^y \frac{-2\mu(\xi)}{\sigma^2(\xi)} d\xi,$$

and accordingly

$$W(y) = \frac{1}{W(l)} \exp(\int_l^y \frac{-2\mu(\xi)}{\sigma^2(\xi)} d\xi) = \frac{s(y)}{W(l)},$$

where $s(y)$ is the scale density defined by (3.9). We therefore obtain

$$\frac{1}{2} W(y)\sigma^2(y)m(y) = \frac{1}{2}\frac{s(y)}{W(l)}\sigma^2(y)\frac{2}{\sigma^2(y)s(y)} = \frac{1}{W(l)} = C,$$

and consequently

$$\frac{2}{W(y)\sigma^2(y)m(y)} = \frac{1}{C}.$$

Hence, the Green's function can be factorized as

$$G(x,y) = \frac{1}{C} \begin{cases} \psi^{\downarrow}(y)\psi^{\uparrow}(x)m(y), & l \le x \le y \le r, \\ \psi^{\uparrow}(y)\psi^{\downarrow}(x)m(y), & l \le y \le x \le r. \end{cases} \tag{3.45}$$

The definitions of $\psi^{\uparrow}(x)$ and $\psi^{\downarrow}(x)$ tell us that $\psi^{\uparrow}(l) = \psi^{\downarrow}(r) = 0$, and thus it follows immediately that $\mathcal{L}G(l,y) = \mathcal{L}G(r,y) = 0$. It remains only to prove that $\mathcal{L}G(x,y) = 0$ for $x \neq y$ in order to complete the verification that (3.45) is a Green's function. To this end, recall that $\psi^{\uparrow}(y)$ and $\psi^{\downarrow}(y)$ are fundamental solutions of the equation $\mathcal{L}u = 0$, which yields, for $x < y$,

$$\begin{aligned} \mathcal{L}G(x,y) &= \frac{1}{C}\psi^{\downarrow}(y)m(y)(\frac{1}{2}\sigma^2(x)\frac{d^2\psi^{\uparrow}(x)}{(dx)^2} + \mu(x)(\frac{d\psi^{\uparrow}(x)}{dx}) - \lambda\psi^{\uparrow}(x)) \\ &= \frac{1}{C}\psi^{\downarrow}(y)m(y).0 = 0, \end{aligned}$$

and similarly, for $x > y$, we have $\mathcal{L}G(x,y) = 0$.

Theorem 3.3.3. *The density $R(x,y)$ defined by (3.38) can be written in terms of the increasing function $\psi^{\uparrow}(x)$ and the decreasing function $\psi^{\downarrow}(x)$ as*

$$R(x,y) = c_\lambda \psi^\uparrow(x \wedge y)\psi^\downarrow(x \vee y)m(y),$$

where c_λ is a constant dependent on λ, $m(y)$ is the speed measure, defined by (3.11), $x, y \in (l,r)$, and $(x \wedge y) = \min(x,y)$ and $(x \vee y) = \max(x,y)$.

Proof. First, let

$$p(t,x,y) = \frac{d\mathbf{P}(X(t) \le y | x(0) = x)}{dy}$$

be the transition density of the diffusion process $X(t)$ on (l,r). Let $\{S_t, t \ge 0\}$ be a family of semigroup operators defined as $S_t : C([l,r]) \to C([l,r])$, with

$$S_t f(x) = E_x[f(X(t))] = \int_l^r p(t,x,y)f(y)dy, \quad x \in (l,r),$$

and define the associated resolvent operators as the Laplace transforms of S_t with parameter $\lambda > 0$:

$$R_\lambda(x) = \int_0^\infty \exp(-\lambda t)(S_t f)(x)dt, \quad x \in (l,r).$$

Thus,

$$\begin{aligned} R_\lambda(x) &= \int_0^\infty \exp(-\lambda t)(S_t f)(x)dt \\ &= \int_0^\infty \exp(-\lambda t) \int_l^r p(t,x,y)f(y)dydt \\ &= \int_l^r f(y)G_\lambda(x,y)dy, \end{aligned}$$

where $G_\lambda(x,y) = \int_0^\infty \exp(-\lambda t)p(t,x,y)dt$ is a Green's function, which can be factorized using (3.45) into

$$G_\lambda(x,y) = \frac{1}{C} \begin{cases} \psi^\downarrow(y)\psi^\uparrow(x)m(y), & l \le x \le y \le r, \\ \psi^\uparrow(y)\psi^\downarrow(x)m(y), & l \le y \le x \le r. \end{cases} \tag{3.46}$$

Now, recall that δt is an exponentially distributed random variable with parameter λ and density function

$$p_{\delta t}(t) = \lambda \exp(-\lambda t), \lambda > 0, t \geq 0.$$

Then, the density $R(x, y) = \frac{d}{dy}\mathbf{P}(X(\delta t) \leq y | x(0) = x)$, is easily calculated by integrating the transition density $p(t, x, y)$ over the density $p_{\delta t}$ of all possible values of δt:

$$R(x, y) = \int_0^\infty \lambda \exp(-\lambda t) p(t, x, y) dt = \lambda G_\lambda(x, y). \tag{3.47}$$

From (3.46) and (3.47), it follows that

$$R(x, y) = \frac{\lambda}{C} \begin{cases} \psi^{\downarrow}(y)\psi^{\uparrow}(x)m(y), & l \leq x \leq y \leq r, \\ \psi^{\uparrow}(y)\psi^{\downarrow}(x)m(y), & l \leq y \leq x \leq r. \end{cases} \tag{3.48}$$

and by setting $c_\lambda = \frac{\lambda}{C}$ in (3.48), the proof is then complete. □

In order to carry out the exponential time-stepping Euler algorithm, it remains only to calculate the conditional probability of the boundary b being hit during the time step.

First note that the distribution of the diffusion process at the end of the exponential time step δt, conditional on it having hit b during the time step, is the same as if the time step had started with X equal to b [43]. Thus,

$$\mathbf{P}(X(\delta t) < y | H_b(x) < \delta t, X(0) = x) = \mathbf{P}(X(\delta t) < y | X(0) = b). \tag{3.49}$$

"This is a consequence of the fact that the exponential distribution of δt is considered as corresponding to a fixed probability per unit time of the time step coming to an end" [43].

Lemma 3.3.4. *For the process $X(t)$ defined by (3.33), we have*

$$\mathbf{P}(H_b(x) < \delta t) = E_x[\exp(-\lambda H_b)], \tag{3.50}$$

where δt is an exponentially distributed random variable with rate λ.

Proof. We prove this as follows. First, on account of equation (A.10), for two real random variables Y and Z defined on $(\Omega, \mathcal{F}, \mathbf{P})$ and with density functions f_Y and f_Z, we have

$$\mathbf{P}(Z < Y) = \int_{-\infty}^{\infty} \mathbf{P}(Z < y | Y = y) f_Y(y) dy = \int_{-\infty}^{\infty} \mathbf{P}(Y > z | Z = z) f_Z(z) dz.$$

Now, writing $Z = H_b(x)$ and $Y = \delta t$, with $f_Z = \frac{d}{dt}\mathbf{P}(H_b(x) < t) = r(t)$ and $f_Y = \lambda \exp(-\lambda t)$, yields

$$\mathbf{P}(H_b(x) < \delta t) = \int_0^{\infty} \mathbf{P}(\delta t > t | H_b(x) = t) r(t) dt, \quad \text{since } t > 0.$$

As δt and H_b are independent, we obtain

$$\begin{aligned} \mathbf{P}(H_b(x) < \delta t) &= \int_0^{\infty} \mathbf{P}(\delta t > t) r(t) dt, \\ &= \int_0^{\infty} \exp(-\lambda t) r(t) dt, \\ &= E_x[\exp(-\lambda H_b)], \end{aligned} \tag{3.51}$$

which follows from the definition of the Laplace transformation of a density function of a nonnegative random variable. □

According to equations (3.28),(3.29) and (3.51), there is a pair of functions $\psi^{\uparrow}(x)$ and $\psi^{\downarrow}(x)$, the former increasing and the latter decreasing, such that

$$\mathbf{P}(H_b(x) < \delta t) = \frac{\psi^{\uparrow}(x)}{\psi^{\uparrow}(b)}, \quad \text{for } b > x, \tag{3.52}$$

and

$$\mathbf{P}(H_b(x) < \delta t) = \frac{\psi^{\downarrow}(x)}{\psi^{\downarrow}(b)}, \quad \text{for } b < x. \tag{3.53}$$

Lemma 3.3.5. *1. If $x < b$ and $y < b$, then we have*

$$\mathbf{P}(H_b(x) < \delta t | X(\delta t) = y, X(0) = x) = \frac{\psi^{\uparrow}(x \vee y)\psi^{\downarrow}(b)}{\psi^{\uparrow}(b)\psi^{\downarrow}(x \vee y)}, \quad \textit{and} \tag{3.54}$$

2. if $x > b$ and $y > b$, then we obtain

$$\mathbf{P}(H_b(x) < \delta t | X(\delta t) = y, X(0) = x) = \frac{\psi^{\downarrow}(x \wedge y)\psi^{\uparrow}(b)}{\psi^{\downarrow}(b)\psi^{\uparrow}(x \wedge y)}. \tag{3.55}$$

Proof. We will prove (1) and note that (2) can be deduced in the same manner. First, for simplicity of notation, write $\mathbf{P}_x(.)$ for $\mathbf{P}(.|X(0) = x)$, and thus we have

$$\begin{aligned} \mathbf{P}_x(H_b(x) < \delta t | X(\delta t) = y) &= \frac{\mathbf{P}_x(H_b(x) < \delta t, X(\delta t) \in dy)}{\mathbf{P}_x(X(\delta t) \in dy)} \\ &= \frac{\mathbf{P}_x(X(\delta t) \in dy | H_b(x) < \delta t)\mathbf{P}_x(H_b(x) < \delta t)}{\mathbf{P}_x(X(\delta t) \in dy)}. \end{aligned}$$

Now using (3.49) yields

$$\mathbf{P}_x(H_b(x) < \delta t | X(\delta t) = y) = \frac{\mathbf{P}(X(\delta t) \in dy | X(0) = b)\mathbf{P}_x(H_b(x) < \delta t)}{\mathbf{P}_x(X(\delta t) \in dy)},$$

and hence

$$\mathbf{P}_x(H_b(x) < \delta t | X(\delta t) = y) = \mathbf{P}_x(H_b(x) < \delta t)\frac{R(b, y)}{R(x, y)}. \tag{3.56}$$

Now, from Theorem 3.3.3, we obtain

$$R(x, y) = c_\lambda \psi^{\uparrow}(x \wedge y)\psi^{\downarrow}(x \vee y)m(y),$$

and

$$R(b, y) = c_\lambda \psi^{\uparrow}(y)\psi^{\downarrow}(b)m(y),$$

and, from (3.52), we have

$$\mathbf{P}_x(H_b(x) < \delta t) = \frac{\psi^{\uparrow}(x)}{\psi^{\uparrow}(b)},$$

where $x < b$ and $y < b$. Substituting these expressions into (3.56) gives (3.54). □

However, in the exponential time-stepping Euler method, the process $X(t)$ is approximated by a Wiener process with constant drift, with parameters determined at the current position [43]. In fact, when both $\mu(x)$ and $\sigma(x)$ are constants, exact calculations of the required quantities given by expressions (3.38), (3.54) and (3.55) can be obtained. Therefore, we first perform the calculations for the Wiener process with constant drift

$$B(t) = \mu t + \sigma w(t), \quad B(0) = 0, \tag{3.57}$$

where μ and σ are constants, and we then update the exponential time-stepping Euler method for $X(t)$ using these calculations [43]. First, we will determine the explicit expressions for the fundamental solutions $\psi^{\uparrow}(x)$ and $\psi^{\downarrow}(x)$ of the homogeneous second order differential equation

$$\mu\frac{d\psi(x)}{dx} + \frac{1}{2}\sigma^2\frac{d^2\psi(x)}{dx^2} - \lambda\psi(x) = 0, \tag{3.58}$$

where the general solution of which is given by

$$\psi(x) = c_1\psi^{\uparrow}(x) + c_2\psi^{\downarrow}(x),$$

where c_1 and c_2 are arbitrary constants. To this end, we consider the characteristic equation of the homogeneous equation (3.58):

$$\alpha\phi^2(x) + \beta\phi(x) + \gamma = 0, \tag{3.59}$$

where $\alpha = \frac{1}{2}\sigma^2$, $\beta = \mu$ and $\gamma = -\lambda$. The roots of the characteristic equation (3.59)

are then obtained using the quadratic formula

$$\phi_{1,2} = \frac{-\beta \pm \sqrt{\beta^2 - 4\alpha\gamma}}{2\alpha}, \tag{3.60}$$

and consequently

$$\phi_1 = \frac{-\mu}{\sigma^2} + \sqrt{(\frac{\mu}{\sigma^2})^2 + \frac{2\lambda}{\sigma^2}} \quad , \quad \phi_2 = \frac{-\mu}{\sigma^2} - \sqrt{(\frac{\mu}{\sigma^2})^2 + \frac{2\lambda}{\sigma^2}}. \tag{3.61}$$

Then, the solutions $\psi^{\uparrow}(x)$ and $\psi^{\downarrow}(x)$ of equation (3.58) can be written as

$$\psi^{\uparrow}(x) = \exp(\phi_1 x) \quad , \quad \psi^{\downarrow}(x) = \exp(\phi_2 x), \tag{3.62}$$

and hence

$$\psi^{\uparrow}(x) = \exp((N - F)x) \quad , \quad \psi^{\downarrow}(x) = \exp(-(N + F)x), \tag{3.63}$$

where $F = \frac{\mu}{\sigma^2}$ and $N = \sqrt{(\frac{\mu}{\sigma^2})^2 + \frac{2\lambda}{\sigma^2}}$. Now, substituting these expressions for $\psi^{\uparrow}(x)$ and $\psi^{\downarrow}(x)$ into the conditional probabilities (3.54) and (3.55) yields

$$\mathbf{P}(H_b(x) < \delta t | B(\delta t) = y) = \exp(-2N(b - (x \vee y))), \quad \text{for } x < b \text{ and } y < b, \tag{3.64}$$

and

$$\mathbf{P}(H_b(x) < \delta t | B(\delta t) = y) = \exp(-2N((x \wedge y) - b)), \quad \text{for } x > b \text{ and } y > b. \tag{3.65}$$

The density of the increment $B(t+\delta t) - B(t)$ can be obtained either from Theorem 3.3.3 or by using "the fact that the distance traveled by the Wiener process $B(t)$, starting from any fixed point, after a fixed time t, is a Gaussian random variable with mean μt and variance $\sigma^2 t$" [43] and thus the density of $B(t + \delta t) - B(t)$ is evaluated by integrating the Gaussian density over the exponential density of all possible values of δt [43].

Lemma 3.3.6.

$$\begin{aligned}\frac{d}{dx}\mathbf{P}(B(t+\delta t)-B(t)<x) &= \int_0^\infty \lambda\exp(-\lambda t)\frac{1}{\sqrt{(2\pi\sigma^2 t)}}\exp(\frac{-(x-\mu t)^2}{2\sigma^2 t})dt \\ &= \frac{\lambda}{\sigma^2}N^{-1}\exp(-|x|N+Fx). \qquad (3.66)\end{aligned}$$

Proof. We follow [46] to verify (3.66). We first let $s^2=\sigma^2 t$ in the integral above to obtain

$$\begin{aligned}I &= \lambda\int_0^\infty \exp(-\lambda\frac{s^2}{\sigma^2})\frac{1}{\sqrt{(2\pi)}s}\exp(\frac{-(x-\frac{\mu}{\sigma^2}s^2)^2}{2s^2})2\frac{s}{\sigma^2}ds \\ &= \frac{\lambda}{\sigma^2}\sqrt{\frac{2}{\pi}}\int_0^\infty \exp(-[\frac{\lambda}{\sigma^2}s^2+\frac{x^2}{2s^2}-x\frac{\mu}{\sigma^2}+\frac{\mu^2 s^2}{2\sigma^4}])ds \\ &= \frac{\lambda}{\sigma^2}\sqrt{\frac{2}{\pi}}\exp(\frac{\mu}{\sigma^2}x)\int_0^\infty \exp(-[(\frac{2\lambda}{\sigma^2}+\frac{\mu^2}{\sigma^4})\frac{s^2}{2}+\frac{x^2}{2s^2}])ds.\end{aligned}$$

Next, we set $u=s/\sqrt{c}$, where $c=\frac{|x|}{\sqrt{\frac{2\lambda}{\sigma^2}+\frac{\mu^2}{\sigma^4}}}$, which yields

$$I=\frac{\lambda}{\sigma^2}\sqrt{\frac{2c}{\pi}}\exp(\frac{\mu}{\sigma^2}x)\int_0^\infty \exp(-[(\frac{2\lambda}{\sigma^2}+\frac{\mu^2}{\sigma^4})\frac{|x|u^2}{2\sqrt{\frac{2\lambda}{\sigma^2}+\frac{\mu^2}{\sigma^4}}}+\frac{x^2\sqrt{\frac{2\lambda}{\sigma^2}+\frac{\mu^2}{\sigma^4}}}{2u^2}])du.$$

Now, for simplicity of notation, we set $F=\frac{\mu}{\sigma^2}$ and $N=\sqrt{(\frac{\mu}{\sigma^2})^2+\frac{2\lambda}{\sigma^2}}$ in the integral I, which gives

$$\begin{aligned}I &= \frac{\lambda}{\sigma^2}\sqrt{\frac{2c}{\pi}}\exp(xF)\int_0^\infty \exp(-\frac{|x|N}{2}(u^2+\frac{1}{u^2}))du \\ &= \frac{\lambda}{\sigma^2}\sqrt{\frac{2c}{\pi}}\exp(xF)\int_0^\infty \exp(-\frac{|x|N}{2}(u^2-2+\frac{1}{u^2})-|x|N)du \\ &= \frac{\lambda}{\sigma^2}\sqrt{\frac{2c}{\pi}}\exp(xF-|x|N)\int_0^\infty \exp(-\frac{|x|N}{2}(u-\frac{1}{u})^2)du \\ &= \frac{\lambda}{\sigma^2}\sqrt{\frac{2c}{\pi}}\exp(xF-|x|N)(\int_0^1 \exp(-\frac{|x|N}{2}(u-\frac{1}{u})^2)du+\int_1^\infty \exp(-\frac{|x|N}{2}(u-\frac{1}{u})^2)du).\end{aligned}$$

Now, since

$$\int_1^\infty \exp(-\frac{|x|N}{2}(u-\frac{1}{u})^2)du = \int_0^1 \exp(-\frac{|x|N}{2}(u-\frac{1}{u})^2)\frac{1}{u^2}du,$$

it follows that

$$\begin{aligned} I &= \frac{\lambda}{\sigma^2}\sqrt{\frac{2c}{\pi}}\exp(xF-|x|N)(\int_0^1 \exp(-\frac{|x|N}{2}(u-\frac{1}{u})^2)du + \int_0^1 \exp(-\frac{|x|N}{2}(u-\frac{1}{u})^2)\frac{1}{u^2}du) \\ &= \frac{\lambda}{\sigma^2}\sqrt{\frac{2c}{\pi}}\exp(xF-|x|N)\int_0^1 \exp(-\frac{|x|N}{2}(u-\frac{1}{u})^2)(1+\frac{1}{u^2})du \\ &= \frac{\lambda}{\sigma^2}\sqrt{\frac{2c}{\pi}}\exp(xF-|x|N)(\int_0^\infty \exp(-\frac{|x|N}{2}(v^2)dv, \end{aligned}$$

where $v = u - \frac{1}{u}$, thus $dv = (1+\frac{1}{u^2})du$, and so the boundaries of integration become $v = \infty$ and $v = 0$ instead of $u = 0$ and $u = 1$, respectively. Now, the integral $\int_0^\infty \exp(-\frac{|x|N}{2}(v^2)dv$ is a Gaussian integral, and consequently,

$$\int_0^\infty \exp(-\frac{|x|N}{2}(v^2)dv = \frac{1}{2}\sqrt{\frac{2\pi}{|x|N}}.$$

This gives

$$\begin{aligned} I &= \frac{\lambda}{\sigma^2}\sqrt{\frac{2|x|}{N\pi}}\exp(xF-|x|N)\frac{1}{2}\sqrt{\frac{2\pi}{|x|N}} \\ &= \frac{\lambda}{\sigma^2}\frac{1}{N}\exp(xF-|x|N), \end{aligned}$$

which is the desired conclusion. □

Lemma 3.3.7. *Integrating equation (3.66) implies that*

$$\mathbf{P}(B(t+\delta t)-B(t)>0) = \frac{1}{2}(1+\frac{F}{N}). \tag{3.67}$$

Proof. First, from Lemma 3.3.6, we have

$$\mathbf{P}(B(t+\delta t)-B(t)<x) = \int_{-\infty}^x \frac{\lambda}{\sigma^2 N}\exp(yF-|y|N)dy,$$

where $N = \sqrt{U^2 + F^2}$, $U = \sqrt{\frac{2\lambda}{\sigma^2}}$ and $F = \frac{\mu}{\sigma^2}$. Consequently,

$$\begin{aligned}
\mathbf{P}(B(t+\delta t) - B(t) < x) &= \frac{U^2}{2N}\int_{-\infty}^{0} \exp(yF + yN)dy + \frac{U^2}{2N}\int_{0}^{x} \exp(-(yN - yF))dy \\
&= \frac{U^2}{2N}\frac{1}{F+N}\int_{-\infty}^{0} (F+N)\exp((F+N)y)dy \\
&- \frac{U^2}{2N}\frac{1}{N-F}\int_{0}^{x} (-(N-F))\exp(-(N-F)y)dy \\
&= \frac{U^2 + F^2 - F^2}{2N(F+N)}[\exp((F+N)y)]_{-\infty}^{0} \\
&- \frac{U^2 + F^2 - F^2}{2N(N-F)}[\exp(-(N-F)y)]_{0}^{x} \\
&= \frac{N^2 - F^2}{2N(F+N)} - \frac{N^2 - F^2}{2N(N-F)}[\exp(-(N-F)x) - 1] \\
&= \frac{1}{2}(\frac{N-F}{N} + \frac{N+F}{N}) - \frac{1}{2}(\frac{N+F}{N})\exp(-(N-F)x) \\
&= 1 - \frac{1}{2}(1 + \frac{F}{N})\exp(-(N-F)x). \qquad (3.68)
\end{aligned}$$

Accordingly, we obtain

$$\begin{aligned}
\mathbf{P}(B(t+\delta t) - B(t) > x) &= 1 - \mathbf{P}(B(t+\delta t) - B(t) < x) \\
&= 1 - (1 - \frac{1}{2}(1 + \frac{F}{N})\exp(-(N-F)x)) \\
&= \frac{1}{2}(1 + \frac{F}{N})\exp(-(N-F)x),
\end{aligned}$$

and then (3.67) follows directly by setting $x = 0$. □

Now, on account of (3.66), the density of an increment in the Wiener process B, $\Delta B = B(t+\delta t) - B(t)$, is

$$\frac{d}{dx}\mathbf{P}(\Delta B < x) = \frac{\lambda}{\sigma^2}N^{-1}\exp(-|x|N + Fx).$$

Now, denote ΔB^+ for increments in the Wiener process for $x \geq 0$ and ΔB^- for $x < 0$. Then, the density of ΔB^+ is

$$\frac{d}{dx}\mathbf{P}(\Delta B^+ < x) = \frac{\lambda}{\sigma^2}N^{-1}\exp(-(N-F)x) \tag{3.69}$$

and, the density of ΔB^- is

$$\frac{d}{dx}\mathbf{P}(\Delta B^- < x) = \frac{\lambda}{\sigma^2}N^{-1}\exp(-(-N-F)x). \tag{3.70}$$

From (3.67), we also have

$$\mathbf{P}(\Delta B > 0) = \frac{1}{2}(1 + \frac{F}{N}).$$

Now, define a two-points random variable s taking values $+1$ and -1 with probabilities

$$\mathbf{P}(s = 1) = \mathbf{P}(\Delta B > 0) = \frac{1}{2}(1 + \frac{F}{N}),$$

and

$$\mathbf{P}(s = -1) = \mathbf{P}(\Delta B < 0) = 1 - \frac{1}{2}(1 + \frac{F}{N}).$$

Therefore, s can be generated by a uniformly distributed random variable u on $[0, 1]$ as

$$s = \begin{cases} 1 & \text{if} \quad 0 \leq u \leq \frac{1}{2}(1 + \frac{F}{N}), \\ -1 & \text{if} \quad \frac{1}{2}(1 + \frac{F}{N}) < u \leq 1. \end{cases}$$

Thus,

$$s = \text{sign}(\frac{1}{2}(1 + \frac{F}{N}) - u). \tag{3.71}$$

Now, from (3.69), (3.70) and (3.71), ΔB is an exponentially distributed random variable generated by

$$\Delta B = \begin{cases} \frac{p}{N-F} & \text{if} \quad s = 1, \\ \frac{-p}{N+F} & \text{if} \quad s = -1. \end{cases}$$

where p is an exponentially distributed random variable with

$$\mathbf{P}(p > x) = e^{-x},$$

and can be generated using (A.20) as

$$p = -\ln v,$$

where v is a uniformly distributed random variable on $[0, 1]$ and independent of u. Thus,

$$B(t + \delta t) = B(t) + (N - sF)^{-1} sp. \tag{3.72}$$

The exponential time-stepping Euler algorithm with boundary test for the diffusion process $X(t)$ defined by (3.33), is then carried out as follows [43]:

1. Given the value of $X(t)$, we first generate the value of $X(t + \delta)$ using (3.72) with $\mu = \mu(X(t))$. Thus,

$$X(t + \delta t) = X(t) + (N_t - sF_t)^{-1} sp, \tag{3.73}$$

   where $F_t = \sigma^{-2}\mu(X(t))$, $N_t = \sqrt{(F_t)^2 + \frac{2\lambda}{\sigma^2}}$ and $s = \text{sign}(\frac{1}{2}(1 + \frac{F_t}{N_t}) - u)$.

2. Next, we perform a simple test using (3.64) after each time step in order to check the possibility that the boundary $b > X(t)$ (similar treatment for $b < X(t)$) was attained during the time step, where b was reached by the process $X(t)$ during the time step if

$$X(t + \delta t) > b \quad \text{or} \quad z < \exp(-2N_t(b - (X(t) \vee X(t + \delta t)))), \tag{3.74}$$

   where z is a uniformly distributed random variable on $[0, 1]$.

3.4 Numerical experiments

We employ the simulation techniques described above to two neurobiological examples, the FitzHugh Nagumo (FHN) and the Ornstein Uhlenbeck (OU) models.

3.4.1 FitzHugh Nagumo model

Consider a space-clamped FHN system [89]

$$\begin{aligned} dX &= (f(X(t), Y(t)) + I)dt + \sigma dw \\ dY &= \beta(X(t) - \gamma Y(t))dt, \end{aligned} \tag{3.75}$$

with initial conditions $X(0) = x$ and $Y(0) = y$. $X(t)$ represents the voltage variable and $Y(t)$ the recovery variable. $w(t)$ is a standard Wiener process, σ is a noise parameter and I is a constant input current. f is the cubic function

$$f(X, Y) = kX(X - c)(1 - X) - Y, \quad 0 < c < 1.$$

c should be set to less than $\frac{1}{2}$ in order to obtain suitable suprathreshold responses [89]. γ and β are positive constants. We are interested, here, in finding the mean of the first exit time of a one-dimensional diffusion through a constant threshold b. In fact, the recovery variable is practically unaffected during the elementary stages of the interspike interval, and therefore the system (3.75) can be reduced to a one-dimensional equation by considering $Y(t) = y$ to be a constant [89]. The system then takes the form

$$dX = (f(X(t), y) + I)dt + \sigma dw, \tag{3.76}$$

with initial condition $X(0) = x \in (-\infty, b)$. Let $H_b(x)$ be the first time the process $X(t)$ attains the threshold b. Then, by equation (3.23), the mean first exit time

$T = E_x[H_b]$ satisfies the differential equation

$$LT = \frac{\sigma^2}{2}\frac{d^2T(x)}{dx^2} + \mu(x)\frac{dT(x)}{dx} = -1, \quad T(-\infty) = T(b) = 0, \tag{3.77}$$

where $\mu(x) = f(x, y) + I$. To find numerical solutions, we take the domain of starting values to be finite with $x \in (-a, b)$ where $a > 0$ [89]. As $a \to \infty$, all exits occur at $x = b$ rather than at $x = -a$. [89]

The MATLAB function bvp_4C is used to obtain accurate numerical solutions to (3.77). The parameters can be chosen as [89] $c = 0.1$, $k = 0.5$ and $I = 1.5$ with various values of σ, such that $0.1 < \sigma < 5$. The initial values are $x = 0$ and $y = 1$. These solutions are used to check the simulation algorithms discussed above.

In our work, the fixed and exponential time-stepping Euler algorithms with boundary tests are used to simulate the mean first exit time of the FHN equation (3.75). The convergence properties of such algorithms are examined by comparing their simulations to numerical solutions of the boundary value problem (BVP) (3.77). The resultant error is then analyzed and estimated.

Generally, numerical simulation of SDEs produces two main errors. The first is known as *random error or statistical error*, and can be defined as the deviation of the total error from its mean value. It appears as a result of using finite samples in the simulation algorithms and hence can be reduced by carrying out multiple simulation runs and taking the average of the outcomes. The other is *systematic error or constant error*, and is defined as the expectated value of the overall error. Discretizing time in simulation algorithms causes systematic error and, therefore, decreasing the size of the fixed time step Δt or the mean duration of the exponential time step can reduce this error.

Suppose now that T is the theoretical value of the mean first exit time through the constant threshold b, which represents the solution of the BVP (3.77). Following [89], the threshold is chosen as $b = 0.6$. Let $\overline{T}_M = \frac{1}{M}\sum_{j=1}^{M} T_j$ be the estimation of T obtained using the two simulation algorithms discussed above. The error to be calculated and analyzed is then the absolute value of

$$\epsilon = E[\overline{T}_M - T].$$

The total error ϵ occurring in the simulation algorithms could not be computed exactly as these algorithms are subject to statistical errors. Therefore, an estimation of the error, $\hat{\epsilon}$ say, is used to calculate the 95% confidence interval of the error ϵ. In order to estimate ϵ, a number N of independent simulation runs are performed, and the estimation $\hat{\epsilon}$ is taken to be the absolute value of the average of the corresponding errors $\epsilon_1, \epsilon_2, \cdots, \epsilon_N$. The estimation of the error is decomposed into the statistical error ϵ_{stat} and the systematic error ϵ_{sys}:

$$\hat{\epsilon} = \epsilon_{stat} + \epsilon_{sys},$$

and since $E(\epsilon_{stat}) = 0$, we have

$$E(\hat{\epsilon}) = \epsilon_{sys} = \epsilon.$$

The 95% confidence interval of the total error ϵ is therefore

$$[\hat{\epsilon} - 2\sqrt{\frac{\sigma_\epsilon^2}{N}}, \hat{\epsilon} + 2\sqrt{\frac{\sigma_\epsilon^2}{N}}],$$

where

$$\sigma_\epsilon^2 = \frac{1}{N-1}\sum_{i=1}^{N}(\epsilon_i - \hat{\epsilon})^2$$

is the unbiased estimator of the variance of ϵ.

Our numerical results for the exit time of the FHN system (3.75) are as follows: As illustrated in Figure 3.1, the number of samplings M is plotted against the error in the mean exit time. The other parameters are specified as follows: the noise parameter $\sigma = 1$, the number of runs $N = 100$, and $\Delta t = \frac{1}{\lambda} = 0.001$, where $\frac{1}{\lambda}$ is the mean value of the exponential time step δt. δt is a random variable and so its precise value is not known. Therefore, the expectation $E[\delta t] = \frac{1}{\lambda}$ is used in the exponential time-stepping algorithm as an equivalent to Δt in the fixed time-stepping algorithm. The elapsed time after N time steps is a random variable with mean $\frac{N}{\lambda}$, whereas the corresponding quantity for the fixed time-stepping algorithm is $N\Delta t$ [43]. The results obtained using the Euler methods with boundary tests, both exponential and fixed, are shown as empty circles with error bars, and those obtained using such Euler methods without boundary tests are shown as shaded circles with error bars. All of these methods produce statistical errors as indicated by the error bars, which decrease as M increases. Moreover, both Euler methods with boundary tests provide more accurate results than those without.

Figures 3.2, 3.3, 3.4, 3.5, 3.6 and 3.7 display the error in mean exit time as a function of $\Delta t = \frac{1}{\lambda}$, for different values of σ chosen between 0.25 and 10, in order to demonstrate the effect of the additive noise on the systematic error produced by the underlying simulation algorithms. To avoid any influence from the sampling errors, M and N are chosen as 100000 and 100, respectively. In this case, the error bars which represent the statistical errors, are smaller than the plotted symbols, and therefore can be neglected. The figures illustrate that the systematic errors in the mean exit times obtained using both algorithms are increasing functions of $\Delta t = \frac{1}{\lambda}$. Furthermore, when the Euler methods without boundary corrections are used, we find a systematic error in mean exit time proportional to $\Delta t^{\frac{1}{2}}$; however, when the boundary tests are applied, the systematic error is reduced to being proportional to $\Delta t = \frac{1}{\lambda}$. As observed from these figures, for σ taking values between $\sigma = 0.25$ and $\sigma = 10$, the fixed time-stepping Euler method shows greater accuracy than the

exponential time-stepping algorithm in spite of the similarity between their respective rates of convergence.

Figures 3.8 and 3.9 display the error in mean exit time as a function of the noise parameter σ, for different values of $\Delta t = \frac{1}{\lambda}$. As can be observed from these figures, the additive noise has strong effects on the convergence properties of the Euler methods without boundary corrections, whether exponential or fixed time steps. Specifically, as σ increases, the systematic errors increase significantly to peak at $\sigma = 1$, and then begin to decrease slightly. In contrast, when the boundary tests are performed, these methods produce systematic errors that are approximately independent of the choice of noise σ, in particular for small values of $\Delta t = \frac{1}{\lambda}$, although the range of σ varies from a small value, $\sigma = 0.25$ to a large one, $\sigma = 10$.

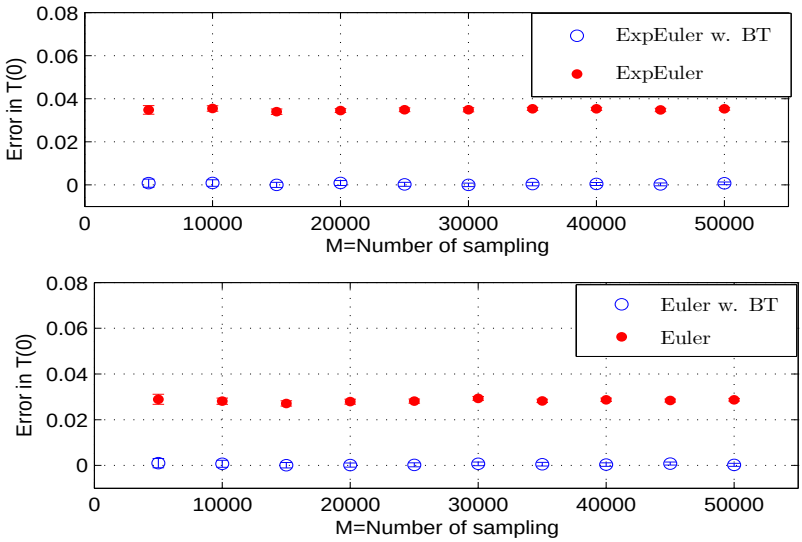

Figure 3.1: Error in mean exit time of the FHN system against the sampling M. The results obtained by the fixed and exponential time-stepping Euler methods with boundary tests are shown as empty circles with error bars, and shaded circles with error bars represent the results obtained using the corresponding methods without boundary tests. Statistical errors are indicated by error bars.

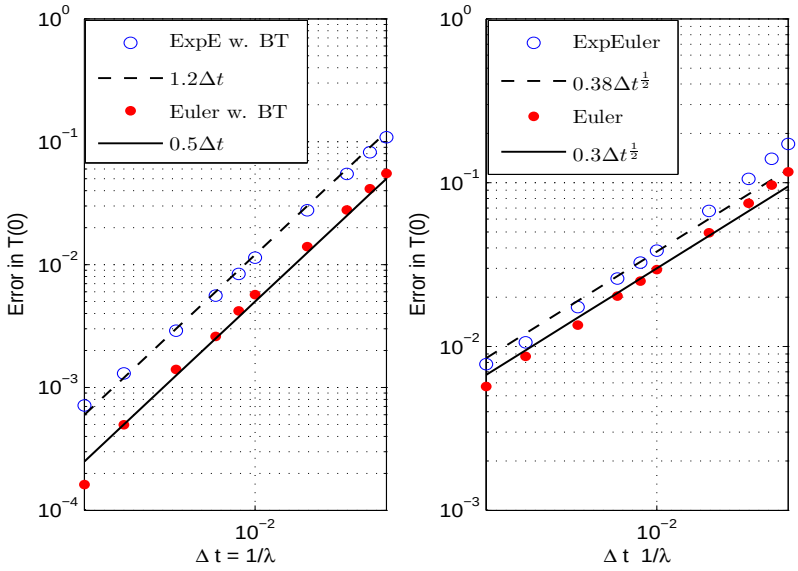

Figure 3.2: Error in mean exit time of the FHN system against $\Delta t = \frac{1}{\lambda}$. The results obtained by the exponential time-stepping Euler method are shown as empty circles, and shaded circles represent the results obtained using the fixed time-stepping Euler method. The noise $\sigma = 0.25$.

3.4.2 Ornstein Uhlenbeck model

The simplest stochastic leaky integrate and fire (LIF) model for describing the behavior of nerve membrane is the Ornstein Uhlenbeck (OU) process [51]. It is used to approximate the subthreshold membrane potential of a nerve cell receiving random synaptic inputs and is given by the Itô-type SDE [4]

$$\begin{aligned} dX(t) &= (-\alpha X(t) + \eta)dt + \sigma dw(t), \\ X(0) &= x, \end{aligned} \tag{3.78}$$

where "the constants η and σ reflect the input signal and its variability, resulting from the stochastic dendritic currents that are caused by the action potential of other neurons or by external stimulation in sensory neurons" [53, 54]. $\frac{1}{\alpha} = CR > 0$ is the time membrane constant governing the spontaneous decay of the membrane potential to its resting state, where R and C are the membrane resistance and its capacitance respectively [51]. This comes from the deterministic version of the model, which is

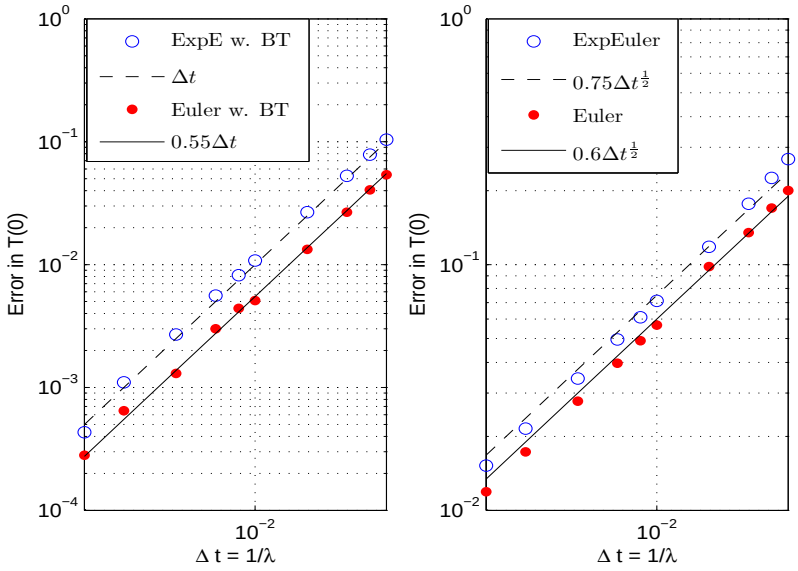

Figure 3.3: Error in mean exit time of the FHN system against $\Delta t = \frac{1}{\lambda}$. The noise parameter σ is chosen as 0.5

known as an RC-circuit with a generator, a resistor and a capacitor in parallel [55].

In the OU model, the neuron emits a spike whenever the firing threshold ($b > x$) is reached, and then the membrane potential is reset to its equilibrium potential, which is conveniently set to zero [16]. Unlike more complex models such as the HH model and the FHN model, the action potential is not a part of the OU model; only its time generation is considered and so we have to impose the threshold condition [53, 54].

The action potential $X(t)$ given by the OU model is a Gaussian random variable with mean

$$E[X(t)] = \frac{\eta}{\alpha} + (x - \frac{\eta}{\alpha})e^{-t\alpha}$$

and variance

$$Var[X(t)] = \frac{\sigma^2}{2\alpha}(1 - e^{-2t\alpha}),$$

and hence, the behavior of $X(t)$ is described completely by these moments [54]. For $t \to \infty$, the asymptotic mean depolarization is $\frac{\eta}{\alpha}$ and thus we have two firing regimes for the OU model. The first is called suprathreshold firing and occurs when

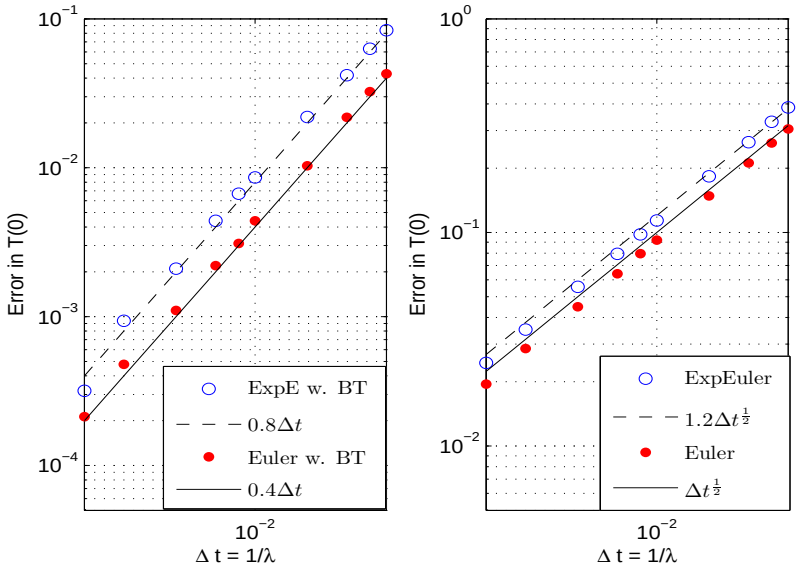

Figure 3.4: Error in mean exit time of the FHN system against $\Delta t = \frac{1}{\lambda}$. $\sigma = 1$ is the noise parameter.

$\frac{\eta}{\alpha} > b$ and the neuron produces spikes even in the absence of noise. The other is called subthreshold firing and is caused only by the random fluctuations of the depolarization when $\frac{\eta}{\alpha} < b$ [51]. The neuron, therefore, never fires when $\sigma = 0$. We are interested here in exploring the effect of noise on the spiking activity of the OU model and so we limit ourselves to the second regime, in particular when there is an absence of input ($\eta = 0$). The spiking activity of the OU model is identified by the first exit time (FET) of the membrane potential through constant boundary b:

$$H_b(x) = \inf\{t \geq 0 : X(t) \geq b | X(0) = x < b\},$$

which is described completely by its density probability function

$$g(t) = \frac{d}{dt}\mathbf{P}(H_b \leq t).$$

Unfortunately, no closed form solution, in general, can be obtained for $g(t)$ and so numerical techniques and simulation procedures are needed [54]. It is also of interest to evaluate the moments of the FET of the model, in particular the first moment or

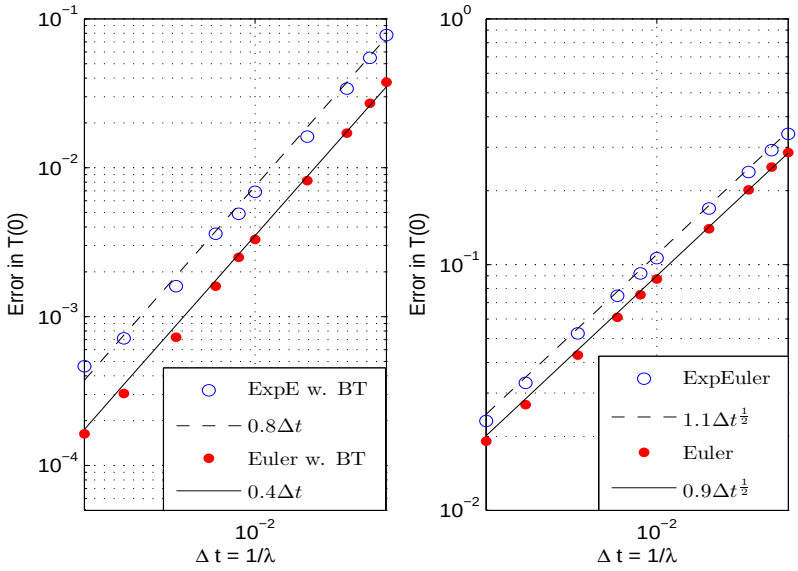

Figure 3.5: Error in mean exit time of the FHN system against $\Delta t = \frac{1}{\lambda}$. The noise parameter $\sigma = 3$.

the mean FET (MFET)

$$T(x) = E_x[H_b]$$

which, by (3.23), satisfies the differential equation

$$\frac{\sigma^2}{2}\frac{d^2T(x)}{dx^2} - \alpha x \frac{dT(x)}{dx} = -1, \quad T(-\infty) = T(b) = 0. \tag{3.79}$$

Using Siegert theory [81], the MFET can be given as

$$T(x) = \sqrt{\frac{\pi}{\alpha\sigma^2}} \int_x^b (1 + \text{erf}(\frac{z\sqrt{\alpha}}{\sigma})) \exp(\frac{z\alpha}{\sigma^2}) dz, \tag{3.80}$$

where $\text{erf}(x) = \frac{2}{\sqrt{\pi}} \int_0^x e^{-t^2} dt$, is the error function. However, in addition to the Siegert formula (3.80), several numerical and simulation techniques for obtaining the distributions of the FET of the OU model and its moments have been discussed in the literature. See for example [52, 11, 30, 31, 74] and the references quoted therein.

Here, we simulate the MFET of the OU process through constant boundary b using the same algorithms considered for the FHN equation in the previous section, and

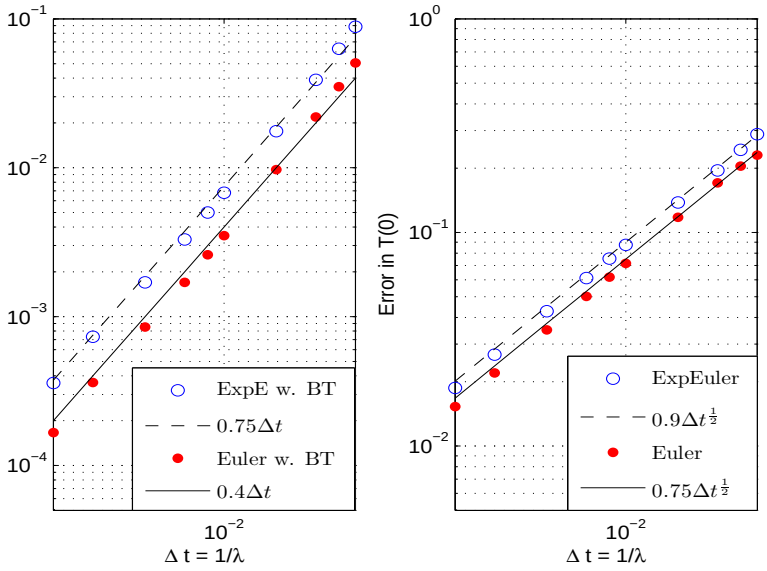

Figure 3.6: Error in mean exit time of the FHN system against $\Delta t = \frac{1}{\lambda}$ and $\sigma = 5$.

compare the results with the theoretical values obtained using the Siegert formula (3.80). We thus consider two cases of the OU process that were studied in [52], with parameters $\alpha = 1, b = 2, \sigma = \sqrt{2}$ in the first case and $\alpha = 0.2, b = 30, \sigma = 20$ in the second. Furthermore, the effect of noise on the spiking activity of the OU process is investigated by taking different levels of the noise parameter σ. The results of these experiments are summarized in the following.

To study the effects of noise on the systematic errors produced by the simulation algorithms, both the standard Euler method with boundary correction and the exponential time-stepping algorithm with boundary test are performed. Different levels of noise parameter σ are taken, and in order to avoid any influence from statistical errors, M and N are chosen as 50000 and 500 respectively. For the OU process with parameters $\alpha = 1, b = 2$ (case I), the noise parameter σ is chosen to take values between $\sqrt{2}$ and 10, whereas for the OU process modeled with parameters $\alpha = 0.2, b = 30$ (case II), σ takes values between 20 and 100. Figures 3.10 and 3.11 illustrate that, for σ close to the threshold b, the systematic error decreases steeply in case I and gradually in case II, in particular for the methods without boundary

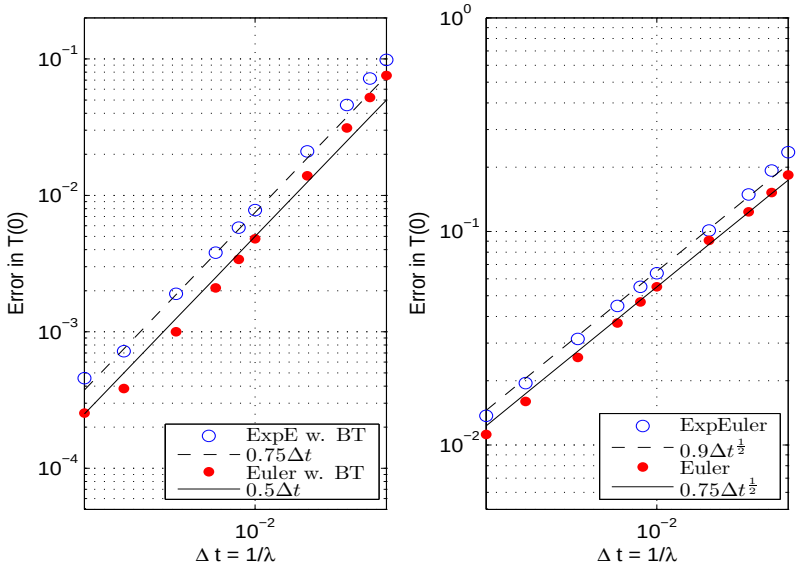

Figure 3.7: Error in mean exit time of the FHN system against $\Delta t = \frac{1}{\lambda}$ where $\sigma = 10$.

correction. When the noise increases further, the MFET becomes smaller, and so the systematic error begins to stabilize. For both cases of the OU process, as shown in Figures 3.12, 3.13, 3.14 and 3.15, the systematic errors in mean exit time using the underlying simulation algorithms are increasing functions of $\Delta t = 1/\lambda$. Moreover, we find that the systematic errors are proportional to $\Delta t^{\frac{1}{2}}$ when the Euler methods without boundary tests are used. In contrast, the systematic errors of the Euler methods with boundary tests are reduced to being proportional to $\Delta t = 1/\lambda$. However, as can be observed from these figures, the fixed time-stepping algorithm seems to be more accurate than the exponential time-stepping method, although the two algorithms have the same rate of convergence. All of these observations coincide with the results obtained for the FHN equation discussed in the previous section.

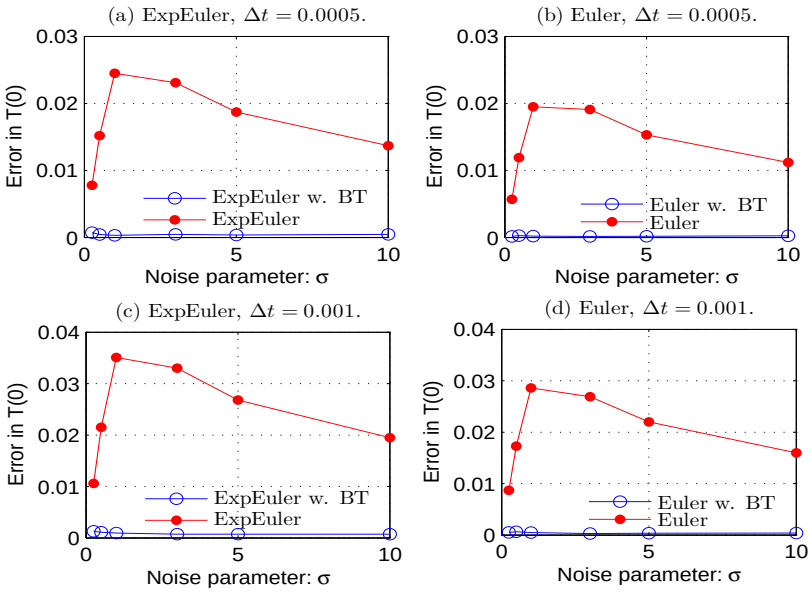

Figure 3.8: Error in mean exit time of the FHN system against the noise parameter σ.

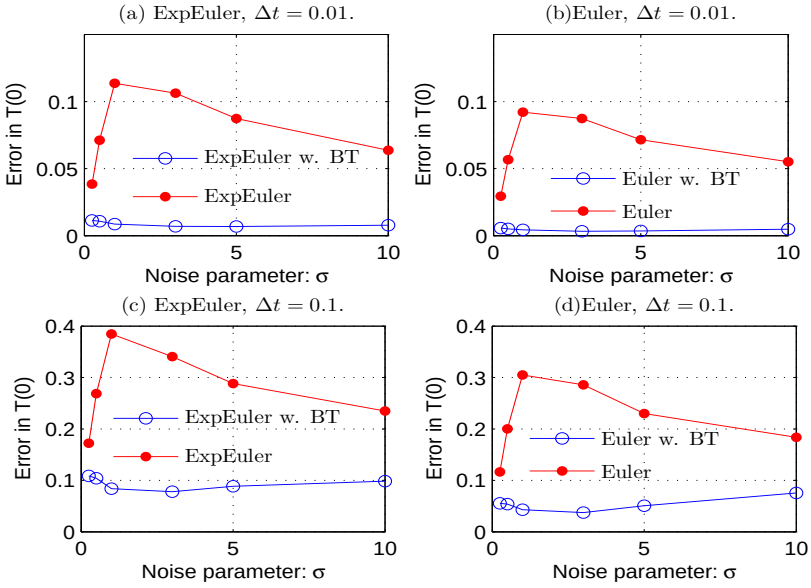

Figure 3.9: Error in mean exit time of the FHN system against the noise parameter σ.

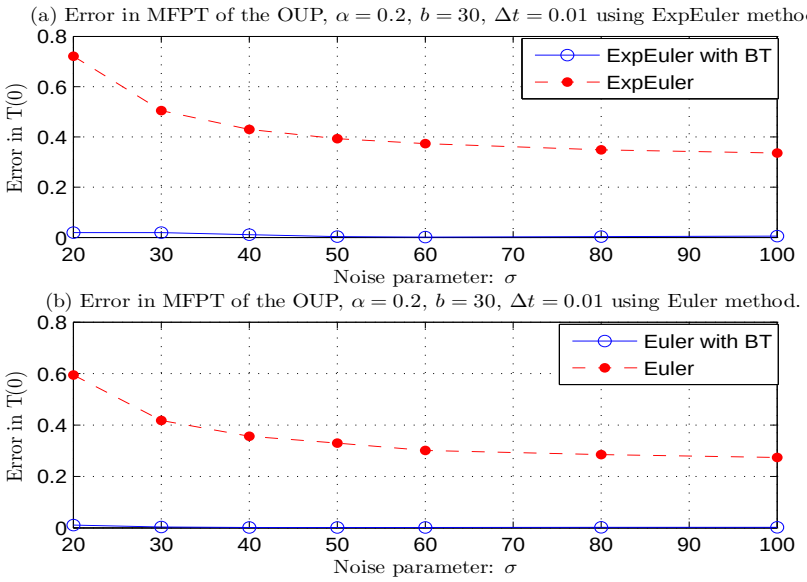

Figure 3.10: Error in mean exit time of the OU process against the noise parameter σ.

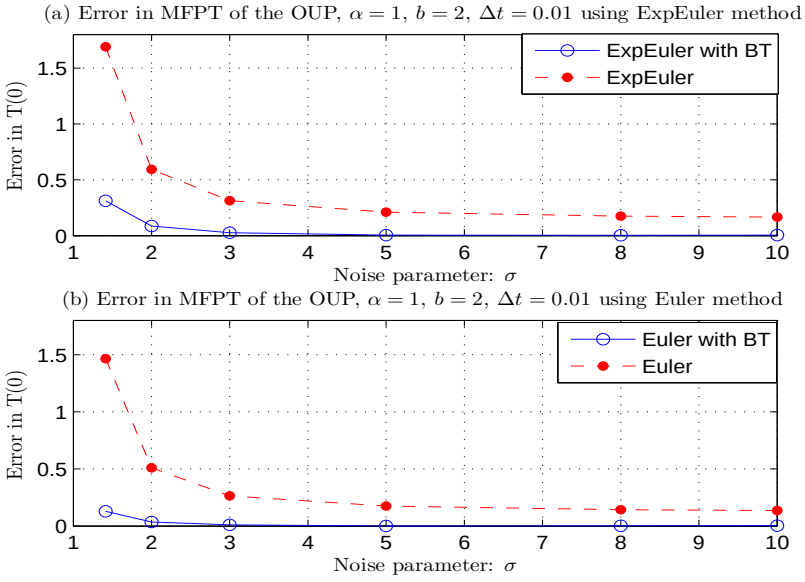

Figure 3.11: Error in mean exit time of the OU process against the noise parameter σ.

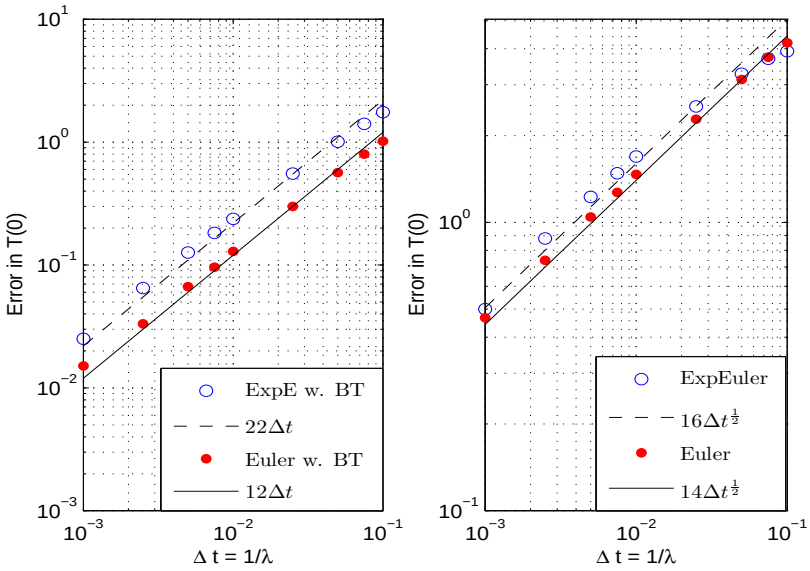

Figure 3.12: Error in mean exit time of the OU process against $\Delta t = \frac{1}{\lambda}$ where $\alpha = 1$, $b = 2$ and $\sigma = \sqrt{2}$.

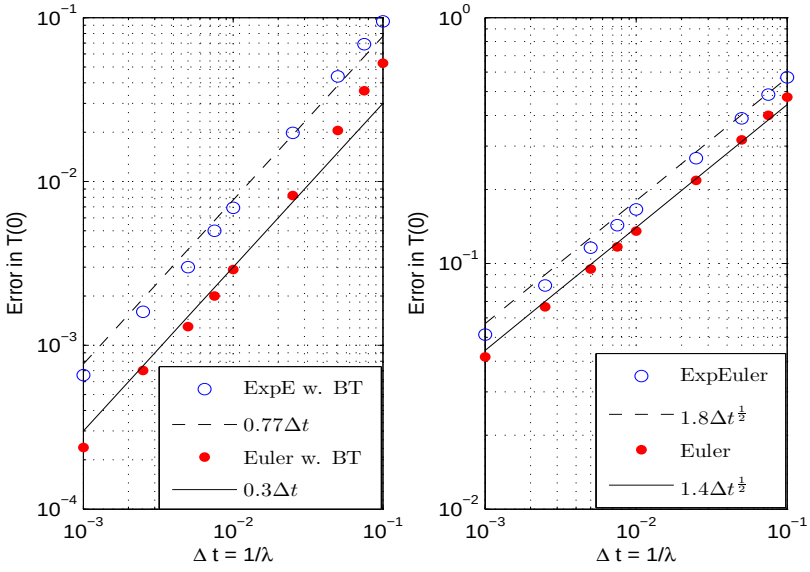

Figure 3.13: Error in mean exit time of the OU process against $\Delta t = \frac{1}{\lambda}$ where $\alpha = 1$, $b = 2$ and $\sigma = 10$.

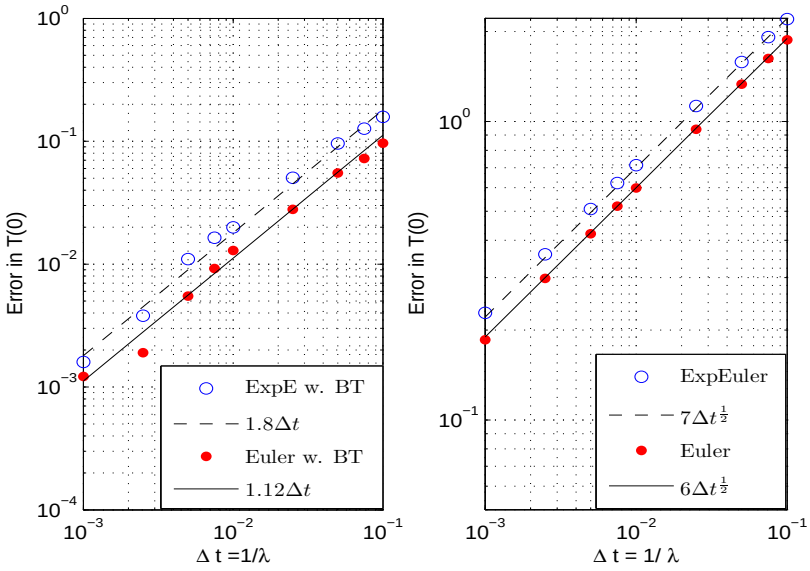

Figure 3.14: Error in mean exit time of the OU process against $\Delta t = \frac{1}{\lambda}$ where $\alpha = 0.2$, $b = 30$ and $\sigma = 20$.

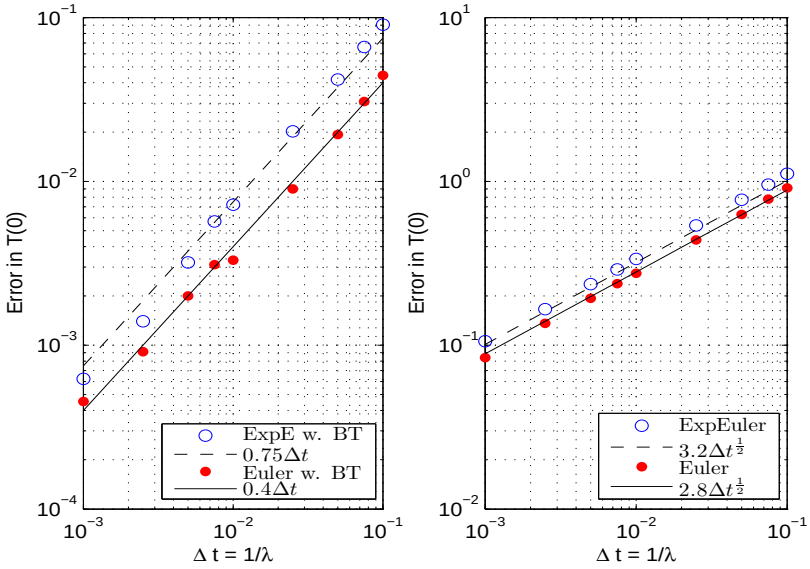

Figure 3.15: Error in mean exit time of the OU against $\Delta t = \frac{1}{\lambda}$ where $\alpha = 0.2$, $b = 30$ and $\sigma = 100$.

Chapter 4

Simulation of first exit time problems of spatially extended excitable models

The phenomenon of waves in excitable media, such as traveling pulses and spiral waves, has received a significant amount of attention due to their occurrence in a wide range of natural systems [92, 61]. The propagation of traveling waves along nerve fibre [80, 95], and a chemically-active medium with the Belousov-Zhabotinsky reaction [93], are typical examples; see [66, 95] for further examples of excitable media. An excitable medium is a non-linear, spatially-extended system, characterized by three states: rest state, excited state and refractory or recovery state [95]. To be precise, under a sufficiently strong stimulus, the excitable system switches from the rest state to the excited state and then falls into the refractory state after a short time, before returning to the rest state. Subsequent excitation cannot be generated until a suitable amount of time, known as refractory time, has passed. Thus, in an excitable system, it is possible for waves to be produced, through strong changes to the rest state, caused by local non-linearity and diffusion [61, 95]. Therefore, a generic excitable medium can be represented simply by a two-variable system of

reaction-diffusion equations, such as the Barkley model [2] or the FitzHugh Nagumo system [20, 68].

Adding noise to these systems increases the production of spatio-temporal patterns, such as spiral waves and traveling pulses [45, 44]. Noise, generally, can affect the excitable media in various ways; see [56] for an extensive review and the references given there. However, here we are concerned with the Barkley model influencing space-time additive noise: [82]

$$\begin{aligned} du &= (D\Delta u + f(u,v))dt + \sigma dw(t,x) \\ dv &= g(u,v)dt, \end{aligned} \tag{4.1}$$

with initial conditions $u(0,x) = u_0$, $v(0,x) = v_0$ and periodic boundary conditions on domain $[0, L]$. D is a diffusion coefficient and $\sigma > 0$ is a small noise parameter. $w(t,x)$ is the Wiener process, white in time and correlated in space. We assume the reaction terms take the form:

$$\begin{aligned} f(u,v) &= \frac{1}{\epsilon}u(1-u)(u - \frac{v+b}{a}), \\ g(u,v) &= u - v, \end{aligned}$$

for $a, b > 0$. Following [2], we set $a = 0.75$, and $b = 0.01$. The small parameter $0 < \epsilon \ll 1$ represents the time-scale separation of the fast variable u and the slow variable v. Our focus is studying the influence of the small additive noise on the formation and propagation of traveling Barkley waves in one-dimensional excitable media, with homogeneous initial states. In this subexcitable regime, the system can produce waves when appropriate amounts of noise are added, and consequently no structure can be nucleated under purely deterministic conditions [26].

Our study of the effects of a small amount of additive noise on the propagation of a traveling wave, under the Barkley model, is divided into two parts: the effects of the noise on the nucleation time of the wave and the effects on its mean lifetime. The effect of the time-scale parameter ϵ is also considered. The nucleation time of a traveling wave through an excitable medium can be defined as the first time the maximum value of the fast variable passes the threshold of excitability, which we treat as a first exit problem. The mean lifetime of such a wave is the average time between its nucleation and its annihilation. The nucleation and dynamics of solitary structures in spatially-extended systems have been studied extensively, in particular for the ϕ^4-equation associated with additive space-time white noise [7]. Such structures are known as kinks, in one-dimensional equations, and their nucleation, propagation and eventual annihilation are worth studying. A kink is defined here as a boundary with a region close to 0 to its left and a region close to 1 to its right; the opposite case is called an antikink [58]. In our work, the left(right) sides of front waves and the right(left) sides of back waves are examples of kink(antikink) structures, as illustrated in Figure 4.1. The kinks and antikinks are nucleated at random times and in random positions. They diffuse independently and are annihilated in collision [35].

Following these introductory remarks, the rest of this chapter is arranged as follows. In Section 4.1, we introduce the local dynamics of the Barkley model. Section 4.2 is devoted to approximating the Wiener process efficiently using the fast Fourier transform (FFT). FFT is a more efficient algorithm for computing the discrete Fourier transform, and is discussed in detail in Section 4.2.1. The noise is chosen to be white in time and correlated in space, with periodic boundary conditions; this is demonstrated in Section 4.2.2. In Section 4.3, the Laplacian is approximated effectively using a spectral method. In addition, the exponential Euler method is applied to preserve the eigenvalues of the Laplacian. Section 4.4 describes the numerical technique we use to simulate the Barkley model (4.1) efficiently. The purpose of the computer simulation is to compute the mean first exit time (nucleation time) of a traveling wave, as well as

the mean of its lifetime, accurately for the model. The formulation of these problems is discussed in Section 4.5.1. However, making the accurate calculations needed for the numerical simulation of (4.1) requires a large amount of computer time. Moreover, using this approach becomes computationally impractical in the case of interacting waves. For these reasons, we propose in Section 4.5.2, a simple, reduced model for the dynamics of the underlying SPDE that can deal with interacting waves adequately. Our results are summarized and discussed in Section 4.5.3. We also analyze the agreement between the results obtained by simulating the underlying SPDE and those obtained from the reduced model. Other applications of the reduced model, such as calculating the mean number of kinks at a specific time and the probability of a given part of the phase space of the Barkley system being excited, are also considered.

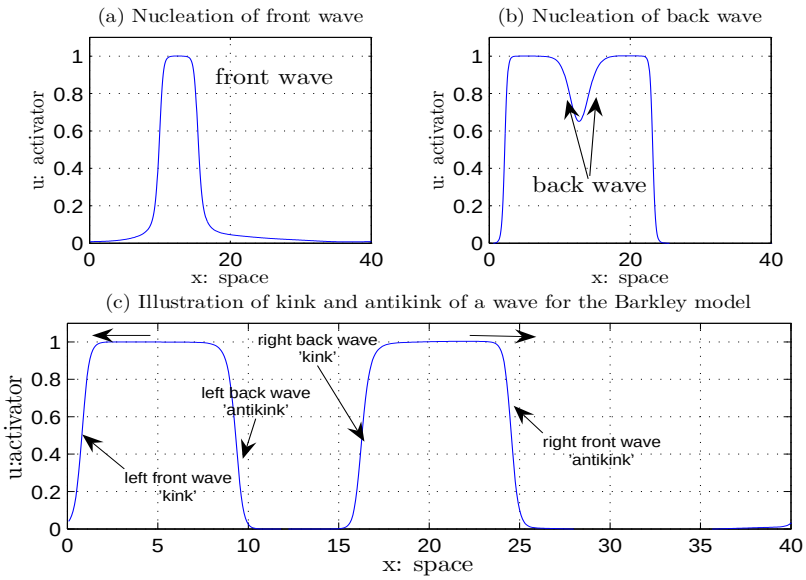

Figure 4.1: Nucleation of (a) front wave and (b) back wave for the Barkley model(4.1). (c) Illustration of the kinks and antikinks of the front and back waves of the Barkley system. The parameters used are $a = 0.75$, $b = 0.01$, $\epsilon = 0.02$, $D = 1$ and $L = 40$ with noise of correlation length $\xi = 2$ and intensity $\sigma = 0.09$. The resolution $N = 512$ grid points with time step $\Delta t = 0.01$.

4.1 Dynamics of the Barkley model

For the deterministic Barkley model, the dynamics of the reaction kinetics (or, in other words, the dynamics of the model in the absence of diffusion) is illustrated in Figure 4.2, with nullclines pictures of u and v. The u-nullclines ($f(u,v) = 0$) are represented by three straight lines: $u = 0, u = 1, u = \frac{v+b}{a}$, whereas v-nullclines ($g(u,v) = 0$) is the line $u = v$. Systems of excitable media are made up of excitation and recovery dynamical states. Thus, by setting a small boundary, say δ, bordering the line $u = 0$, a given point (u, v) is said to be excited if $u > \delta$ and recovering otherwise. The physical parameters ϵ, a and b specify the details of the local dynamics. ϵ is selected to be very small, so that the activator u is much faster than the inhibitor v within the excited region. However, $u \approx 0$ within the recovery region and therefore the exponential decay of the inhibitor v affects only the local dynamics [2]. Larger a would increase the duration of the excitation and a larger value of $\frac{b}{a}$ would raise the threshold of the excitation [10].

The intersection of all the nullclines yields the fixed points $(0,0)$ and $(1,1)$. The origin $(0,0)$ is the stable and excitable fixed point of the model, with excitation threshold $u_{th} = \frac{v+b}{a}$. To be precise, when the starting point is located to the left of the threshold u_{th} and close to the origin $(0,0)$, the solution to the ordinary differential equations (ODEs), $\frac{du}{dt} = 0$, $\frac{dv}{dt} = 0$, converges directly to the origin fixed point. In contrast, when the starting point is to the right of u_{th} , the solution moves away initially, before finally shrinking to $(0,0)$ [2]. However, when the initial data is outside the region $[0,1]$, the solution may diverge to infinity, see Figure 1 in [83].

Adding spatial diffusion to these reaction kinetics leads to the propagation of waves for certain initial data. Under additive small noise, waves can be nucleated even for zero homogeneous initial conditions. However, when simulating the model numerically, care must be taken with the reaction terms to prevent the fast variable u

from overshooting the stable branches of the u-nullclines and stimulating divergent behavior. To this end, one can modify the reaction terms f and g as [83]

$$\tilde{f}(u,v) = \begin{cases} f(u,v), & u \leq 1, \\ -|f(u,v)|, & u \geq 1, \end{cases}$$

and

$$\tilde{g}(u,v) = \begin{cases} g(u,v), & v \geq 0, \\ |g(u,v)|, & v < 0. \end{cases}$$

In this situation, the model remains well behaved and the desired dynamics are unchanged [83]. These modified reaction terms will be used in our numerical simulation of the SPDEs (4.1).

However, our objective is to simulate the SPDEs (4.1) numerically, using an efficient numerical approach, in order to rigorously explore the dynamic behavior of the Barkley system (4.1). To this end, it will be necessary first to find efficient approximations to the Laplacian and to the Wiener process $w(t,x)$.

Due to properties of the rapid decay of the Fourier coefficient of the noise that we will later define in (4.6), it will be appropriate to simulate the Wiener process using the FFT as demonstrated in the following section.

4.2 Approximation of the Wiener process

4.2.1 Fast Fourier Transform

The Fast Fourier Transform (FFT) is a more efficient algorithm for computing the Discrete Fourier Transform (DFT). The DFT of a set of complex inputs to a vector

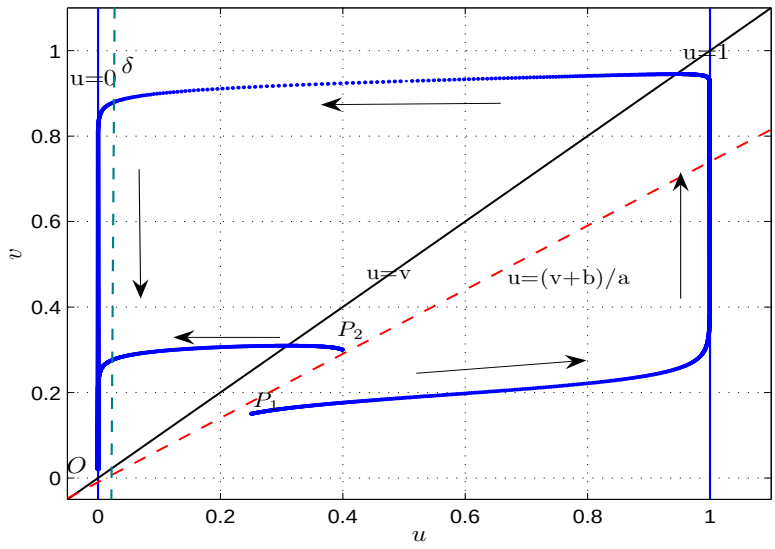

Figure 4.2: Illustration of local dynamics of deterministic Barkley model in absence of diffusion ($D = 0$). The systems parameters are chosen as $a = 0.75$, $b = 0.01$, $\epsilon = 0.02$ with time step $\Delta t = 0.01$. u and v nullclines are shown, and see Section 4.1 for more details. Intersection of these nullclines yields a stable fixed point $O = (0, 0)$ with excitation threshold $u = \frac{v+b}{a}$. For initial conditions near O and to the left of the threshold $u = \frac{v+b}{a}$, the system decays directly to the fixed point O as shown for $P_2 = (0.4, 0.3)$. However, for the initial conditions located to the right of the excitation threshold such as $P_1 = (0.25, 0.15)$, the system undergos a large excursion before returning to the fixed point O. The small boundary layer δ is plotted as well.

of length N is defined as [13, 85, 17, 64, 21]

$$Y_k = \sum_{j=0}^{N-1} X_j \omega_N^{jk}, \tag{4.2}$$

where $k = 0, 1, \cdots, N-1$, $\omega_N = e^{\frac{-2\pi i}{N}}$ is the root of unity and $i = \sqrt{-1}$. The inverse DFT is then given by

$$X_j = \frac{1}{N} \sum_{k=0}^{N-1} Y_k \omega_N^{-jk}. \tag{4.3}$$

Calculating the DFT (4.2) directly would require $2N^2$ operations: N multiplications and N additions for each of the N components of Y. However, when FFT is applied, the overall runtime is reduced to $O(NlogN)$ [13].

The most common FFT is the Cooly-Tukey algorithm [13]. It re-expresses a DFT whose its size N can be factored into $N = N_1 N_2$. By a change of variables, one can then turn the one-dimensional sum in (4.2) in j into a two-dimensional sum in j_1 and j_2 with N_1 rows and N_2 columns: [13, 17, 21]

$$j = j_2 N_1 + j_1, \quad j_1 = 0, 1, \cdots, N_1 - 1, \quad j_2 = 0, 1, \cdots, N_2 - 1,$$

and

$$k = k_1 N_2 + k_2, \quad k_1 = 0, 1, \cdots, N_1 - 1, \quad k_2 = 0, 1, \cdots, N_2 - 1.$$

(4.2) is rewritten then as

$$\begin{aligned} Y_k &= \sum_{j_1=0}^{N_1-1} \sum_{j_2=0}^{N_2-1} X_{j_2 N_1 + j_1} \omega_N^{(j_2 N_1 + j_1)(k_1 N_2 + k_2)}, \\ &= \sum_{j_1=0}^{N_1-1} \sum_{j_2=0}^{N_2-1} X_{j_2 N_1 + j_1} \omega_N^{j_1 (k_1 N_2 + k_2)} \omega_N^{j_2 N_1 (k_1 N_2 + k_2)}. \end{aligned}$$

Since $\omega_N^{j_2 N_1 k_1 N_2} = 1$, $\omega_N^{j_2 k_2 N_1} = \omega_{N_2}^{j_2 k_2}$ and $\omega_N^{j_1 k_1 N_2} = \omega_{N_1}^{j_1 k_1}$, we get

$$Y_k = \sum_{j_1=0}^{N_1-1} \omega_N^{j_1 k_2} \Big(\sum_{j_2=0}^{N_2-1} (X_{j_2 N_1 + j_1}) \omega_{N_2}^{j_2 k_2} \Big) \omega_{N_1}^{j_1 k_1}. \tag{4.4}$$

Roughly speaking, the Cooly-Tukey algorithm is performed in three steps: [17]

1. Compute, for each j_2, the inner sum:

$$\tilde{X}_{j_1, k_2} = \sum_{j_2=0}^{N_2-1} (X_{j_2 N_1 + j_1}) \omega_{N_2}^{j_2 k_2},$$

   which is a DFT of size N_2.

2. Multiply $\tilde{X}_{j_1, k_2}$ by the twiddle factors (the roots of unity $\omega_N^{j_1 k_2}$) as

$$\hat{Y}_{j_1, k_2} = \omega_N^{j_1 k_2} \tilde{X}_{j_1, k_2}.$$

3. Compute N_2 DFTs of length N_1:

$$Y_k = \sum_{j_1=0}^{N_1-1} \hat{Y}_{j_1,k_2} \omega_{N_1}^{j_1 k_1}.$$

A fairly popular form of Cooly-Tukey FFT is a Radix-2 decimation-in-time (DIT) algorithm which is suitable for a length equal to a power of 2, $(2^p, p \in \mathbb{N})$. To derive the algorithm, assume first that $N = 2^p$ and then, by setting $N_1 = 2$ and $N_2 = 2^{p-1} = \frac{N}{2}$ in (4.4), we have

$$Y_{k_1 \frac{N}{2}+k_2} = \sum_{j_2=0}^{\frac{N}{2}-1} X_{2j_2} \omega_{\frac{N}{2}}^{j_2 k_2} + \omega_N^{k_2} (\sum_{j_2=0}^{\frac{N}{2}-1} X_{2j_2+1} \omega_{\frac{N}{2}}^{j_2 k_2}) \omega_2^{k_1}.$$

Since $k_1 = 0, 1$, we get $\omega_2^0 = 1$ and $\omega_2^1 = -1$ which leads to a two DTFs of length $\frac{N}{2}$ for the even and odd index terms: [17, 21]

$$\begin{aligned} Y_{k_2} &= \sum_{j_2=0}^{\frac{N}{2}-1} X_{2j_2} \omega_{\frac{N}{2}}^{j_2 k_2} + \omega_N^{k_2} (\sum_{j_2=0}^{\frac{N}{2}-1} X_{2j_2+1} \omega_{\frac{N}{2}}^{j_2 k_2}), \\ Y_{\frac{N}{2}+k_2} &= \sum_{j_2=0}^{\frac{N}{2}-1} X_{2j_2} \omega_{\frac{N}{2}}^{j_2 k_2} - \omega_N^{k_2} (\sum_{j_2=0}^{\frac{N}{2}-1} X_{2j_2+1} \omega_{\frac{N}{2}}^{j_2 k_2}) \end{aligned} \tag{4.5}$$

This process can then be repeated multiple times to reduce the overall runtime to $O(Nlog_2 N)$. Thus, under the Radix-2 algorithm, the DFT of length N is divided into two transforms of size $\frac{N}{2}$, then four transforms of length $\frac{N}{4}$, then eight of length $\frac{N}{8}$ and so on until N transforms of length 1 are obtained. the algorithm is performed $p = \log_2 N$ times and requires N multiplications at each step, which leads to the following level of computational complexity in the underlying algorithm: [13, 64]

$$O(Np) = O(Nlog_2 N).$$

The original algorithm, introduced by Cooly and Tukey in 1965 [13], is considered the basic groundwork for FFT algorithms. Many improvements and extensions have

been made since, increasing, among other things, its efficiency and applicability [17]. As a results of these changes, various new FFT algorithms were created, such as the prime factor algorithm, the split-radix algorithm and the Winograd FFT. For more details of how to use these approaches, see for instance [17] and the further references cited in that paper.

Here, we use the built-in Matlab functions, fft and ifft, in order to calculate efficiently the DFT and its inverse, respectively. fft is based on the Fastest Fourier Transform in the West (FFTW), released by Matteo Frigo and Steven Johnson [21]. The FFTW library is a collection of fast C codes which can be used to compute DFTs of any length and for one or more dimensions. Through the special-purpose compiler genfft, the fastest code is generated automatically in FFTW. For example, genfft uses a Cooly-Tukey algorithm when $N = N_1 N_2$ and $N_i \neq 1$, whereas a prime factor algorithm is used when $N = N_1 N_2$ and N_1 and N_2 are relatively prime, as is illustrated in detail in [21, 22].

4.2.2 Simulation of the Wiener process using FFT

We consider the Wiener process $w(t, x)$ that is white in time and correlated in space, with exponential decay in the spatial correlation, given by [83, 25]

$$E(w(t,x)w(s,y)) = \min\{t,s\}C(x-y), \quad C(x-y) = \frac{1}{2\xi}\exp(\frac{-\pi(x-y)^2}{4\xi^2}), \quad (4.6)$$

where C, a function of $x - y$, is the covariance of $w(t, x)$, which describes the spatial correlation, the parameter ξ controls the length of the spatial correlation and E denotes mathematical expectation. This type of covariance is known as the squared exponential covariance function, and is stationary and thus invariant to translations [72]. Moreover, it is infinitely differentiable and therefore the Wiener process defined by such covariance has smooth spatial sample functions [72]. The degree of such smoothness and the correlation between nearby points is controlled by the parameter ξ. A

large value of ξ extends the range of similarity between the distinct points and the noise $w(t,x)$ thus becomes an approximately constant function of the spatial input $0 \leq x \leq L$, where L is the length of the spatial domain [72]. In contrast, as ξ decreases, the degree of rapid variations in $w(t,x)$ along the space increases, and thus the correlation between the nearby points begins to decay [72]. As ξ tends to zero, $w(t,x)$ tends to white noise with no correlation between the distinct points [83]. However, we should choose small but non-zero values of $\xi << L$ since, in the case of white noise, it is hard to keep the existing deterministic dynamics of the underlying SPDE [83].

Assume $w(t,x)$ has the expansion [83, 82]

$$w(t,x) = \sum_{j=0}^{\infty} \alpha_j [e_j(x) + \tilde{e}_j(x)]\beta_j(t), \tag{4.7}$$

for independent standard Wiener processes $\beta_j(t)$.

$$e_j(x) = \sqrt{\frac{2}{L}} \cos(\frac{2\pi j x}{L}), \quad j = 1, 2, 3, \cdots, \quad e_0(x) = \sqrt{\frac{1}{L}},$$

and

$$\tilde{e}_j(x) = \sqrt{\frac{2}{L}} \sin(\frac{2\pi j x}{L}), \quad j = 0, 1, 2, 3, \cdots$$

are orthonormal eigenfunctions of the Laplacian on $[0, L]$ with periodic boundary conditions. The coefficients α_j are determined as [83]

$$\alpha_j = \frac{1}{2} \exp(\frac{-\lambda_j \xi^2}{2\pi}), \quad j = 1, 2, 3, \cdots, \quad \text{for} \quad \lambda_j = (\frac{2\pi j}{L})^2 \quad \text{and} \quad \alpha_0 = 1 \quad \text{for} \quad \lambda_0 = 0.$$

It follows that

$$w(t,x) = \alpha_0 \sqrt{\frac{1}{L}} \beta_0(t) + \sqrt{\frac{2}{L}} \sum_{j=1}^{\infty} \alpha_j [\cos(\frac{2\pi j x}{L}) + \sin(\frac{2\pi j x}{L})]\beta_j(t). \tag{4.8}$$

For numerical purposes, we need to calculate the approximation $w_k^n = w(t_{n+1}, x_k) - w(t_n, x_k)$ at $t_n = n\Delta t$, where Δt is the time step, and at $x_k = \frac{kL}{N}$, where x_k is the spatial grid, and $k = 0, 1, 2, \cdots, N-1$. By substituting x_k for x in (4.8) and truncating the series, σw_k^n is given by [49]

$$\sigma w_k^n = \alpha_0 \eta_0^n + \sqrt{2} \sum_{j=1}^{\frac{N}{2}} \alpha_j [\cos(\frac{2\pi jk}{N}) \eta_{j,1}^n + \sin(\frac{2\pi jk}{N}) \eta_{j,2}^n], \tag{4.9}$$

where $k = 0, 1, 2, \cdots, N-1$, σ is the noise intensity, and $\eta_0^n, \eta_{j,1}^n, \eta_{j,2}^n \sim N(0, \frac{\sigma^2 \Delta t}{L})$ are identical and independent normally distributed random variables. The exponential decay in spatial correlation provides very rapid decay in the Fourier coefficient in expansion (4.7) and therefore the Wiener process can be generated efficiently using FFTs[83]. Expressed in terms of complex exponentials: [83]

$$\cos(\frac{2\pi jk}{N}) \eta_{j,1}^n + \sin(\frac{2\pi jk}{N}) \eta_{j,2}^n = \frac{1}{2} [z_j^n e^{\frac{2i\pi jk}{N}} + \bar{z}_j^n e^{\frac{-2i\pi jk}{N}}], \tag{4.10}$$

where $z_j^n = \eta_{j,1}^n - i\eta_{j,2}^n$, $\bar{z}_j^n = \eta_{j,1}^n + i\eta_{j,2}^n$ and $i = \sqrt{-1}$.
To verify this:

$$\begin{aligned}
RHS &= \frac{1}{2} [z_j^n e^{\frac{2i\pi jk}{N}} + \bar{z}_j^n e^{\frac{-2i\pi jk}{N}}] \\
&= \frac{1}{2} [(\eta_{j,1}^n - i\eta_{j,2}^n)(\cos(\frac{2\pi jk}{N}) + i \sin(\frac{2\pi jk}{N}))] \\
&+ \frac{1}{2} [(\eta_{j,1}^n + i\eta_{j,2}^n)(\cos(\frac{2\pi jk}{N}) - i \sin(\frac{2\pi jk}{N}))] \\
&= \frac{1}{2} \cos(\frac{2\pi jk}{N}) \eta_{j,1}^n - \frac{1}{2} i \cos(\frac{2\pi jk}{N}) \eta_{j,2}^n + \frac{1}{2} i \sin(\frac{2\pi jk}{N}) \eta_{j,1}^n + \frac{1}{2} \sin(\frac{2\pi jk}{N}) \eta_{j,2}^n \\
&+ \frac{1}{2} \cos(\frac{2\pi jk}{N}) \eta_{j,1}^n + \frac{1}{2} i \cos(\frac{2\pi jk}{N}) \eta_{j,2}^n - \frac{1}{2} isin(\frac{2\pi jk}{N}) \eta_{j,1}^n + \frac{1}{2} \sin(\frac{2\pi jk}{N}) \eta_{j,2}^n \\
&= \cos(\frac{2\pi jk}{N}) \eta_{j,1}^n + \sin(\frac{2\pi jk}{N}) \eta_{j,2}^n \\
&= LHS.
\end{aligned}$$

Now (4.9) becomes

$$\sigma w_k^n = \alpha_0 \eta_0^n + \frac{\sqrt{2}}{2} \sum_{j=1}^{\frac{N}{2}} \alpha_j [z_j^n e^{\frac{2i\pi jk}{N}} + \bar{z}_j^n e^{\frac{-2i\pi jk}{N}}]. \tag{4.11}$$

In order to solve (4.11) using the FFT algorithm discussed above in Section 4.2.1, (4.11) can be rewritten as [83]

$$\sigma w_k^n = \sum_{j=0}^{N-1} \hat{\alpha}_j Z_j^n e^{\frac{2i\pi jk}{N}}, \tag{4.12}$$

where $\hat{\alpha_0} = 1$, $\hat{\alpha_j} = \hat{\alpha}_{N-j} = \frac{1}{\sqrt{2}}\alpha_j$ for $j = 1, 2, \cdots, N/2$, $Z_0^n = \eta_0^n$ and

$$Z_j^n = \begin{cases} z_j^n, & j = 1, 2, \cdots, \frac{N}{2}, \\ \bar{z}_{N-j}^n, & j = \frac{N}{2}+1, \frac{N}{2}+2, \cdots, N-1. \end{cases}$$

4.3 Approximation of the Laplacian

The spectral method is used to approximate the Laplacian, and the geometric integrator is applied in order to preserve its eigenvalues. First, look at the one-dimensional diffusion equation:

$$\frac{\partial u}{\partial t} = D\frac{\partial^2 u}{\partial x^2}, \quad u(0, x) = f(x), \tag{4.13}$$

on the interval $[0, L]$ with boundary conditions $u(t, 0) = u(t, L)$, where $t \geq 0$ and the assumption that $f(x) \in L^2[0, L]$. For the Fourier expansion, an approximation of $u(t, x)$ can be obtained as [14]

$$u_N(t, x) = \sum_{k=0}^{N-1} \tilde{u}_k(t) e^{\frac{-2\pi ikx}{L}}. \tag{4.14}$$

Since

$$\frac{\partial u_N}{\partial t} = \sum_{k=0}^{N-1} \frac{d\tilde{u}_k}{dt} e^{\frac{-2\pi ikx}{L}},$$

and

$$\frac{\partial^2 u_N}{\partial x^2} = \sum_{k=0}^{N-1} (\frac{-4\pi^2 k^2}{L^2}) \tilde{u}_k(t) e^{\frac{-2\pi i k x}{L}},$$

we have

$$\sum_{k=0}^{N-1} \frac{d\tilde{u}_k}{dt} e^{\frac{-2\pi i k x}{L}} = \sum_{k=0}^{N-1} D(\frac{-4\pi^2 k^2}{L^2}) \tilde{u}_k(t) e^{\frac{-2\pi i k x}{L}}, \tag{4.15}$$

which leads to the system of ODE's:

$$\frac{d\tilde{u}_k}{dt} = -D(\frac{4\pi^2 k^2}{L^2}) \tilde{u}_k(t), \quad \tilde{u}_k(0) = B_k, \quad k = 0, 1, 2, \cdots, N-1, \tag{4.16}$$

where $B_k = \frac{1}{L} \int_0^L f(x) e^{\frac{2\pi i k x}{L}} dx$ are the Fourier coefficients of the initial function $f(x)$. Setting $\lambda_k = (\frac{4\pi^2 k^2}{L^2})$, yields

$$\frac{d\tilde{u}_k}{dt} = -D\lambda_k \tilde{u}_k(t), \quad \tilde{u}_k(0) = B_k, \quad k = 0, 1, 2, \cdots, N-1. \tag{4.17}$$

The exact solution of this system is given by

$$\tilde{u}_k(t) = B_k e^{-D\lambda_k t}, \quad t \geq 0, \quad k = 0, 1, 2, \cdots, N-1. \tag{4.18}$$

Numerically, one can use the semi-implicit Euler method, which produces approximations $\tilde{u}_k^n$ to $\tilde{u}_k(t_n)$, for $t_n = n\Delta t$, where $n = 0, 1, 2, \cdots$ and Δt is the time step, using the following iterated formula

$$\tilde{u}_k^{n+1} = (1 + D\lambda_k \Delta t)^{-1} \tilde{u}_k^n, \quad \tilde{u}_k^0 = B_k, \quad k = 0, 1, 2, \cdots, N-1, \quad n = 0, 1, 2, \cdots. \tag{4.19}$$

However, to preserve the eigenvalues of the Laplacian, one can use the the exponential Euler method

$$\tilde{u}_k^{n+1} = e^{-D\lambda_k \Delta t} \tilde{u}_k^n, \quad \tilde{u}_k^0 = B_k, \quad k = 0, 1, 2, \cdots, N-1, \quad n = 0, 1, 2, \cdots \tag{4.20}$$

which gives the exact solutions to the linear system (4.17) at mesh points t_n(i.e. $\tilde{u}_k(t_n) = \tilde{u}_k^n$) and is thus considered a linearization-preserving (geometric) integrator. Such integrators are numerical integrators of a system of differential equations that preserve exactly one or more of its properties, such as fixed points, eigenvalues or many other geometric or physical properties [60]. For more details of exponential integrators, see for instance [62], or for more on linearization-preserving methods, see [60] and the further references given there.

4.4 Numerical technique

The task is to find efficient approximations u_k^n, v_k^n for $k = 0, 1, 2, \cdots, N-1$ at time $n\Delta t$, $n = 1, 2, \cdots$, to $u(x_k)$, $v(x_k)$ where $x_k = \frac{kL}{N}$ is the spatial grid and L is the length of the spatial domain. To that end, we consider the algorithm constructed by [83] as follows:

- Calculate the Fourier coefficient $\hat{u}_k^n$, where $u_k^n = \sum_{j=0}^{N-1} \hat{u}_j^n[e_j(x_k) + \tilde{e}_j(x_k)]$ and $k = 0, 1, \cdots, N-1$ using the fft algorithm discussed in Section 4.2.1.
- $\hat{u}_k^{n+\frac{1}{2}} = e^{-D\lambda_k \Delta t}\hat{u}_k^n + \hat{\alpha_k} Z_k^n$, where $\hat{\alpha_k}$ and Z_k^n are as defined in (4.12).
- $u_k^{n+\frac{1}{2}} = \text{ifft}(\hat{u}_k^{n+\frac{1}{2}})$ where ifft is the inverse FFT.
- Apply the modified reaction terms:

$$\begin{aligned} u_k^{n+1} &= u_k^{n+\frac{1}{2}} + \Delta t \tilde{f}(u_k^{n+\frac{1}{2}}, v_k^n) \\ v_k^{n+1} &= v_k^n + \Delta t \tilde{g}(u_k^{n+\frac{1}{2}}, v_k^n). \end{aligned}$$

Using this numerical approach, we will calculate the mean first exit time or the mean of nucleation time of a traveling wave and its mean lifetime, for the Barkley system (4.1). This is described in the following sections.

4.5 First exit time and mean lifetime

As illustrated in Figure 4.3, the system (4.21) with $u_0 = v_0 = 0$ initially lies in its stable zero state, ($u \approx 0$ and $v \approx 0$). When forcing the model with suitable amounts of small additive noise, the nucleation of the front wave occurs and the system becomes excited, $u \approx 1$. Afterwards, the system moves to its refractory state, in which $v \approx 1$, causing the nucleation of the back wave. The left and right sides of the front wave are eventually annihilated on collision as are the left and right sides of the back wave. However, we are interested in the nucleation of a traveling wave for the Barkley model and thus formulate this event as an exit time problem.

4.5.1 Formulation of the problem

We use the infinity norm to formulate the problem of the first exit time by determining a threshold θ so that the nucleation of a wave occurs when the infinity norm, or precisely, the maximum value, of the activator variable u over x as a function of time, exceeds θ. As in the case illustrated in Figure 4.6, the threshold level is assumed as $\theta = 0.275$. The nucleation time of a wave is, therefore, the first time the threshold level is exceeded. The first exit time is a random variable and therefore its mean is of great interest.

We use the maximum value of u, denoted by u_m, to determine the mean lifetime of the wave under the Barkley model. Thus, the wave is nucleated when u_m goes above θ for the first time and then is annihilated when u_m becomes smaller than the small boundary layer $\delta = 0.008$. The lifetime is then the difference between the time of nucleation and the time of annihilation. The mean lifetime is simply calculated as the average over a sample of random lifetimes produced using the SPDE (4.1) over the spatial interval $[0, L]$. This technique can be applied when L is small and consequently a single wave is nucleated at time T as shown in Figure 4.3. However,

in the case of large L and when many waves are nucleated at almost the same time, this approach becomes computationally impracticable. To overcome this drawback, we produce, in the next section, a simple model of the dynamics of the underlying SPDE (4.1), which allows us to compute the mean lifetime of the generated waves, even for a large domain.

4.5.2 The reduced model

We aim to simulate the dynamic behavior of the traveling waves under the Barkley model (4.1) in order to compute their mean lifetime efficiently. For this purpose, we first calculate their constant speed and their width. Unlike under multiplicative noise, the characteristics of propagated waves are not affected, generally, by additive noise [25, 24], see Figures 4.4 and 4.5. In Figures 4.4 and 4.5, the wave speed and width obtained from simulating the SPDEs (4.1) are plotted as functions of the noise parameter σ, for $\epsilon = 0.02$. The results indicate that both remain approximately constant over different values of σ. Since we are looking at additive noise in our work, we only need to evaluate the speed and width via the deterministic version of the Barkley system:

$$\begin{aligned} \frac{\partial u}{\partial t} &= D\Delta u + \frac{1}{\epsilon}u(1-u)(u - \frac{v+b}{a}) \\ \frac{\partial v}{\partial t} &= u - v. \end{aligned} \tag{4.21}$$

To this end, we set $z = x - ct$, and so $u(t,x) = U(x-ct) = U(z)$ and $v(t,x) = V(x-ct) = V(z)$. Consequently, we get

$$u_t = -c\frac{dU}{dz} = -cU' \quad , \quad u_{xx} = \frac{d^2U}{dz^2} = U'' \quad \text{and} \quad v_t = -cV'.$$

Substituting these into (4.21) and setting $D = 1$, yields

$$\begin{aligned} U'' + cU' + \frac{1}{\epsilon}U(1-U)(U - \frac{V+b}{a}) &= 0, \\ cV' - V + U &= 0, \end{aligned}$$

with boundary conditions $U \to 0$, $U' \to 0$ and $V \to 0$ as $|z| \to \infty$. Now, supposing $\epsilon \to 0$, which implies $\frac{\partial v}{\partial t} \to 0$, and consequently, $V \approx const = 0$, we obtain

$$L(U) = U'' + cU' + \frac{1}{\epsilon}U(1-U)(U - \frac{b}{a}) = 0. \tag{4.22}$$

Let us suppose that $U' = AU(U-1)$, where A is a constant that needs to be determined [90]. It follows that

$$U'' = A^2U(U-1)(2U-1).$$

Substituting these expressions for U' and U''into (4.22) gives [66]

$$\begin{aligned} L(U) = A^2U(U-1)(2U-1) + cAU(U-1) + \frac{1}{\epsilon}U(1-U)(U-\frac{b}{a}) &= 0 \\ U(1-U)[A^2(1-2U) - cA + \frac{1}{\epsilon}(U - \frac{b}{a})] &= 0 \\ U(1-U)[(-2A^2 + \frac{1}{\epsilon})U - cA + A^2 - \frac{b}{a\epsilon}] &= 0. \end{aligned}$$

Now, setting $-2A^2 + \frac{1}{\epsilon} = 0$ and $-cA + A^2 - \frac{b}{a\epsilon} = 0$ yields $L(U) = 0$. This gives $A = \frac{1}{\sqrt{2\epsilon}}$ and $cA = A^2 - \frac{b}{a\epsilon}$. The wave speed can then be approximated as

$$c = \frac{1}{\sqrt{2\epsilon}}(1 - \frac{2b}{a}). \tag{4.23}$$

According to [24], the width $W = cT_{ther}$, where T_{ther} is the time the system (4.21) in the excited level and c is the wave speed. As $\epsilon \to 0$, we have [24]

$$T_{ther} = \int_0^{v_m} \frac{dv}{g(1,v)} = \int_0^{v_m} \frac{dv}{1-v}, \tag{4.24}$$

where v_m represents the maximum value that the inhibitor v over x reaches before the activator u leaves the excited level [24]. Consequently, we have

$$T_{ther} = \int_0^{v_m} \frac{dv}{(1-v)} = [-\ln(1-v)]_0^{v_m} = -\ln(1-v_m) = \ln(\frac{1}{1-v_m}).$$

Hence, the width can be written as [24]

$$W = c\ln(\frac{1}{1-v_m}). \tag{4.25}$$

Moreover, according to Figures 4.4 and 4.5, such theoretical values of wave speed and width can be considered good approximations to the corresponding quantities obtained in the simulation of the SPDEs (4.1), in particular for high resolution N and small time step Δt.

In order to construct the algorithm for the reduced model, it is necessary to simulate the wave nucleation positions and times under the Barkley model(4.1). The Wiener process $w(t,x)$, with covariance given by (4.6) is a spatially stationary Gaussian process, since the covariance is a function of the increment $x-y$ not of a specific value x or y, where $0 \leq x < y \leq L$. The process is thus invariant to shifts in space and, therefore, the nucleation events, which are caused by the input noise, are independent of the position x. As a result, the nucleation positions, say $x_i, i = 1$ to N_1 where N_1 is the number of nucleated front waves (it is also the number of back waves), are uniformly distributed on $[0, L]$.

Furthermore, no wave can be nucleated within the boundaries of another wave, as is observed from the dynamic behavior of the SPDE (4.1). Mathematically, for any nucleation positions x_i and x_j, where $i, j = 1$ to N_1, $i \neq j$, we have $|x_i - x_j| > W$ where W is the constant wave width.

We now proceed to simulate the nucleation times of the front and back waves under the Barkley model. Suppose $T_i, i = 1$ to N_1 are the nucleation times of front waves. Since the nucleation events occur with a constant probability per unit of time, the exponential distribution with rate λ is appropriate for modeling the nucleation times. The rate of nucleation, λ, is calculated simply as the inverse of the mean first exit time, $\lambda = \frac{1}{T_m}$, obtained from the simulation of the SPDE (4.1). The nucleation times of the back waves, $\bar{T}_i$ say, are computed as:

$$\bar{T}_i = T_i + T_{diff},$$

where T_{diff} is the average difference between the nucleation time of the front wave and that of the back wave, obtained from SPDE (4.1) by observation. To be precise, according to the dynamics of the Barkley model shown in Figure 4.2, the maximum value of inhibitor v can be used to determine the threshold of nucleation of the back wave, say θ_b, as shown in Figure 4.9 and Figure 4.10, and $\bar{T}_i$ is therefore the first time that the maximum value of v exceeds $\theta_b = v_m$, where v_m is as in (4.24). Furthermore, the theoretical value T_{ther} of T_{diff} is also given by (4.24).

We are now in a position to simulate the spatio-temporal behavior of the front and back waves under the Barkley model (4.1). To this end, suppose Y_L and Y_R represent the position of front waves towards the left and right, respectively as shown in Figure 4.11. Thus,

$$\begin{aligned} Y_L(t) &= x_i - c(t - T_i), \quad t \geq T_i, \\ Y_R(t) &= x_i + c(t - T_i), \end{aligned} \tag{4.26}$$

where x_i is the nucleation position of the front wave, T_i is its nucleation time, c is the constant wave speed and $t > 0$ is the time variable. Similarly,

$$\begin{aligned} \bar{Y}_L(t) &= x_i - c(t - \bar{T}_i), \quad t \geq \bar{T}_i, \\ \bar{Y}_R(t) &= x_i + c(t - \bar{T}_i), \end{aligned}$$

are the corresponding expressions for the back waves.

As observed from the numerical simulation of the SPDE (4.1), a kink (antikink) at the spatial position, i say, will keep moving until it meets an antikink (kink) at position, j say, usually from a different nucleation process. Both the kink and the antikink then annihilate on collision. To simulate such an annihilation event using the reduced model, we first solve the equations for the front waves (4.26) (a similar process is then used for the back waves), in order to find all the crossing points (xc_{ij}, tc_{ij}) for i moving right and j moving left, where $i \neq j$ and, $i, j = 1, 2, \cdots, N_1$. We then set the minimum value of tc_{ij}, $Tn_{i_1 j_1}$ say, to be the annihilation time, and the corresponding value of xc_{ij}, $xn_{i_1 j_1}$ say, to be the annihilation position of i_1 moving to the right and j_1 moving to the left. We then continue in this fashion to compute all the annihilation points of other i right waves and j left waves, where $i \neq i_1$ and $j \neq j_1$. However, as a result of the chosen finite time interval in the simulation, a few so-called survivor particles (kinks or antikinks) will still be alive. A survivor particle with nucleation position x_k and nucleation time T_k will never meet another particle during the finite time interval of the simulation. The particle then will move according to (4.26) as

$$\begin{aligned} Y_L(t) &= x_k - c(t - T_k) \quad t \geq T_k, \\ Y_R(t) &= x_k + c(t - T_k), \end{aligned}$$

with the possibility that t can take the value infinity. However, for the purposes of plotting the values, we assume that the particle will be killed at time $T_k + T_{extra}$ where T_{extra} is chosen to be a large value. The corresponding surviving back wave can be treated in a similar way.

It remains only to include the periodic boundary conditions of the Barkley system in order to complete the reduced model algorithm. To do this, we duplicate the spatio-temporal dynamic behavior of the underlying SPDE on $[-L, 0]$ and $[L, 2L]$ as reflections of its dynamics on $[0, L]$. This simple technique guarantees that the periodic boundary conditions, as illustrated in Figures 4.14 and 4.15 are fulfilled. For full details of the algorithm used for the reduced model, see codes $C.3.2$ and $C.3.2.1$ in Appendix C. Figure 4.11 describes the nucleation and annihilation events for the traveling wave under the reduced model.

4.5.3 Numerical results: analysis and discussion

The maximum value of the activator u over x is used to determine the first exit time as demonstrated in Figure 4.6. The first exit time, here, is defined as the nucleation time of a wave under the Barkley model (4.1) or the first time that the maximum value of u over x exceeds $\theta = 0.0275$. To analyze the mean first exit time (MFET) of the underlying SPDE, two numerical experiments are carried out using the numerical technique presented in Section 4.4. We first plot the MFET, denoted by T_m, as a function of the time step Δt (Figure 4.7(a)) and as a function of the resolution N, where the values of N are powers of 2: 128, 256, 512 and 1024, as shown in Figure 4.7(b). The parameters used are $a = 0.75$,$b = 0.01$,$\epsilon = 0.02$, $D = 1$, and the averages are taken over $M = 10000$ realizations. The noise has a spatial correlation of length $\xi = 2$ and with intensity $\sigma = 0.09$ over the domain $[0, L]$, where $L = 40$. In Figure 4.7(a), the resolution is $N = 512$ and in Figure 4.7(b), the time step Δt is 0.01. The results reveal that the MFET T_m is approximately independent of the

value of Δt and of the value of $\Delta x = \frac{L}{N}$, and therefore, approximately constant values of T_m are obtained in both cases. In the second case, T_m is plotted against the small parameter ϵ, in Figure 4.8(a), and the spatial correlation length ξ, that is, the range of similarity between nearby points, in Figure 4.8(b), with other parameters as for Figure 4.7. Figure 4.8(a) shows that just a slight increase in ϵ produces a dramatic increase in the MFET. In Figure 4.8(b), meanwhile, we observe that the MFET grows as ξ increases.

However, when the spatial domain becomes much larger, one may expect that the MFET will be reduced considerably. To investigate this, we raise L to 400, and set $N = 1024$, with other parameters remaining as they were for Figure 4.7(a). For $L = 40$, the MFET is $T_{m1} = 22.7521$, while for $L = 400$, it is $T_{m2} = 17.7819$. Although the length of the spatial domain in the second case ($L = 400$) is ten times that of the first ($L = 40$), the ratio $\tau = \frac{T_{m1}}{T_{m2}}$ between the corresponding values of MFET is only $\tau = 1.2795$. One possible key reason for this unexpected result is due to the effect of spatial correlation length ξ, which is chosen as $\xi = 2$ in both cases. In order to examine the effect of ξ, we calculate the ratio $\tau = \frac{T_{m1}}{T_{m2}}$ for both cases ($L = 40$ and $L = 400$), for $\xi = 1, 1.5, 2$. To be more precise, it increases from $\tau = 1.2795$ for $\xi = 2$ to $\tau = 2.1574$ for 1.5 to $\tau = 2.8020$ for $\xi = 1$.

Two main cases are considered here in studying the mean lifetime of a wave under the Barkley model: the mean lifetime of a single wave and the mean lifetime of interacting waves. For a single wave, the maximum value u_m over x is used to calculate its mean lifetime. Figure 4.3 shows the propagation of a single wave, beginning with the nucleation of its front wave and ending with the annihilation of its back wave, with the parameters $a = 0.75$,$b = 0.01$,$\epsilon = 0.02$, $D = 1$, $\sigma = 0.09$, $\xi = 2$, $N = 512$ and $L = 40$. The lifetime of a single wave is then computed as the difference between the time of nucleation of its front wave and the time of annihilation of its back wave. The average over the lifetimes of a random sample of such waves yields the mean

lifetime.

Figure 4.12 displays the mean lifetime of a wave, using the simulation of the SPDE (4.1) and the reduced model discussed in Section 4.5.2, as a function of the small noise parameter σ, for (a) $\epsilon = 0.02$ and (b) $\epsilon = 0.025$. The results obtained from the simulation of the SPDE (4.1), represented by stars symbols, with parameters as used for Figure 4.3 and using $M = 200$ simulations, indicate that the additive noise does not affect the mean lifetime of the Barkley wave, and this should be taken into account when we design the corresponding reduced model. However, a comparison of the results from the reduced model, represented as solid lines, with those obtained from the simulation of the SPDE, shows excellent agreement, in particular for smaller ϵ. This is due to the asymptotic constant speed c used for the reduced model, as $\epsilon \to 0$.

Applications of the reduced model

To apply the reduced model, we first need to determine two quantities: the rate of nucleation times λ and the difference in nucleation times T_{diff}. The rate λ is calculated as the inverse of the mean first exit time, obtained from the simulation of the underlying SPDE, as shown in Figure 4.7. T_{diff} is defined as the average difference between the nucleation time of the front wave and the nucleation time of the back wave, again obtained from the simulation. For example, T_{diff} is estimated as 1.44, with $\theta_b = v_m \approx 0.75$, for $\epsilon = 0.02$ as illustrated in Figure 4.9. The corresponding value for $\epsilon = 0.025$ is 1.7, with $\theta_b = v_m \approx 0.825$, as shown in Figure 4.10. These values are close to the analytical values of T_{diff} given by (4.24), where $T_{ther} = 1.38629$ for $\epsilon = 0.02$ and $T_{ther} = 1.74297$ for $\epsilon = 0.025$.

In Figure 4.13, we plot the mean lifetime of a wave versus the small parameter ϵ for (a) $\sigma = 0.0825$ and (b) $\sigma = 0.09$, where the shaded circles and red stars represent the results obtained with the reduced model and simulation of the SPDE (4.1), respectively. Both graphs indicate that the mean lifetime increases as ϵ increases, and

there is close agreement between the two methods.

The second aim of the present work is to study the mean lifetime of the interacting waves. Waves interact when a large domain is used and, as a result, many waves are nucleated at almost the same time, as shown in Figure 4.15. The parameters used are $a = 0.75$, $b = 0.01$, $\epsilon = 0.02$, $D = 1$, $L = 400$ and $\lambda = \frac{1}{T_m} = \frac{1}{17.78}$, where λ is the rate of nucleation time and T_m is the mean first exit time obtained by simulating the SPDE (4.1). The nucleation points and corresponding annihilation points are represented by shaded circles and stars, respectively. However, the harmony shown in Figures 4.12, 4.13 and 4.14 between the two approaches, led us to decide to use the reduced model to study the mean lifetime of the interacting waves, since applying the simulation of the underlying SPDE directly becomes computationally impractical in this case.

Due to the interaction of the waves with each other, we need to calculate the mean lifetime of each kink and antikink, individually, as demonstrated in Figure 4.16. To be precise, Figure 4.16 shows the mean lifetime, computed using the reduced model, of (a) the first 10 front waves and (b) the first 10 back waves, with number of trials $M = 5000$, $\epsilon = 0.02$ and a total of $N_1 = 30$ front waves nucleated during the overall period of simulation on the space domain $[0, 400]$, with the same number of corresponding back waves. There are thus $2N_1 = 60$ kinks and 60 antikinks. In the Figure 4.16, right-moving waves are represented by circles and left-moving waves by stars. The results reveal that each kink has approximately the same mean lifetime as its corresponding antikink, for a large number of trials M. Furthermore, the first kink and antikink have the longest mean lifetimes. The lifetime falls sharply but then remains fairly constant for the rest of the particles.

The simplicity of the reduced model encourages us to explore more about the dynamics of kinks and antikinks under the Barkley model (4.1). For instance, the

average number of kinks and antikinks that are still alive at a specific time, t, can be computed easily using the reduced model, as shown in Figure 4.17(a). The figure describes the mean number of kinks at time t, denoted by N_k, using the same parameters as used for Figure 4.16, except for the number of trials, which is $M = 1000$. Firstly, we observe that no particles are nucleated at $t = 0$. The mean number of kinks (antikinks) at time t then increases as t increases, until $t = 30$. At this time, the mean number of kinks begins to level off, with the maximum being just above 2.3.

Our calculations of the mean number of kinks at time t can be used to obtain the probability of a part of the phase space of the Barkley model being excited at (t, x), where $t > 0$ and $0 \leq x \leq L$. Precisely, this is calculated simply by multiplying the mean number of kinks by the constant width W given in (4.25) and dividing the result by the length of the domain L. Thus

$$\mathbb{P}(\text{a part of the phase space being excited at}(t, x)) = \frac{N_K \times W}{L}. \tag{4.27}$$

These calculations are demonstrated as shaded circles in Figure 4.17(b). The results provide important information about the excitability of the Barkley system (4.1). For instance, there is an approximately 4% chance of the phase space of the system (4.1) being excited at $t = 50$, whereas the chance is only around 0.8% at time $t = 5$. To check the validity of our calculations, we also compute the probabilities using the simulation of the SPDE(4.1), with parameters $L = 400$, $\Delta t = 0.01$, $N = 1024$, $\epsilon = 0.02$, $\sigma = 0.09$ and $M = 2000$. The results are represented by the squares in Figure 4.17(b), and exhibit similar behaviour to those obtained with the reduced model shown in Figure 4.17(b). The probability obtained from the simulation of the SPDE increases gradually until $t = 30$ when it begins to become stable at around 0.03. In spite of this similarity, there are slight differences between the results. Besides the effects of statistical errors and other errors which can arise due to the use of numerical

approximations, the wave speed c also affects the results. The wave speed used in the reduced model is a symptomatic value, derived for $\epsilon \to 0$, whereas the corresponding wave speed for the underlying SPDE is simulated for $\epsilon = 0.02$.

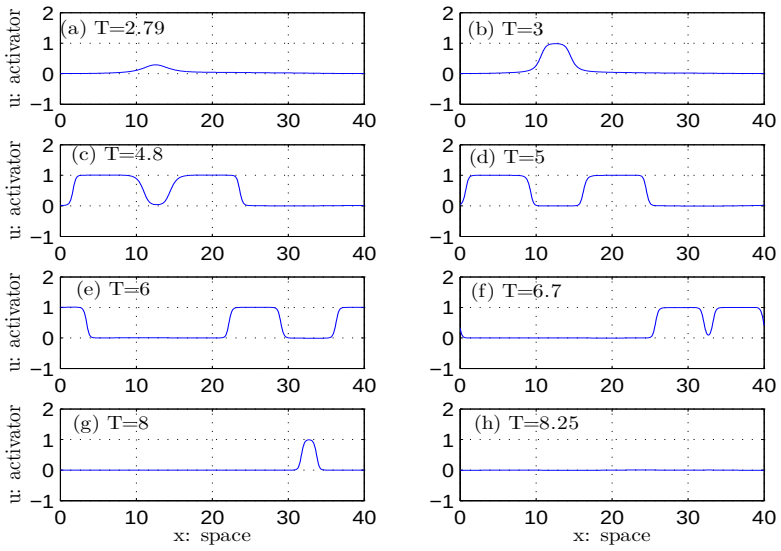

Figure 4.3: Plots of the nucleation and annihilation of a wave for the Barkley model(4.1). The parameters of the system are $a = 0.75$, $b = 0.01$, $\epsilon = 0.02$, $D = 1$ and $L = 40$ with noise of correlation length $\xi = 2$ and intensity $\sigma = 0.09$. The resolution $N = 512$ grid points with time step $\Delta t = 0.01$.

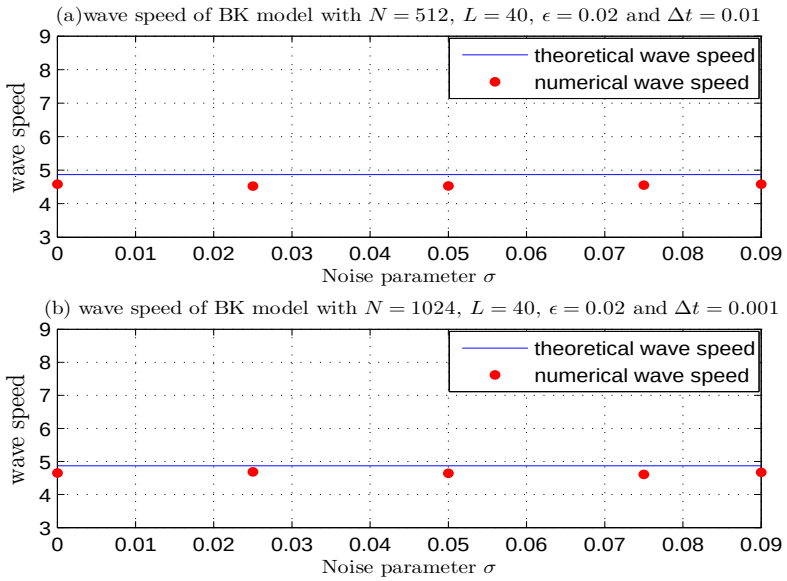

Figure 4.4: Plotting of the wave speed as a function of the noise parameter σ with initial condition $u_0 = 0$ except $u_0(1:5) = 1$ and $v_0 = 0$. The parameters used are $\epsilon = 0.02$, $L = 40$, (a) $N = 512$, $\Delta t = 0.01$ and (b) $N = 1024$, $\Delta t = 0.001$.

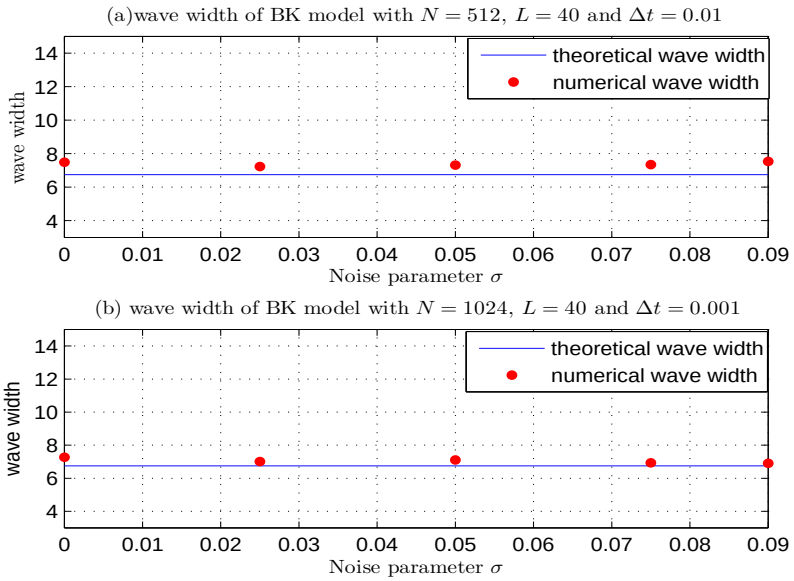

Figure 4.5: Plotting of the wave width as a function of the noise parameter σ with initial condition $u_0 = 0$ except $u_0(1:5) = 1$ and $v_0 = 0$. The parameters used are $\epsilon = 0.02$, $L = 40$, (a) $N = 512$, $\Delta t = 0.01$ and (b) $N = 1024$, $\Delta t = 0.001$.

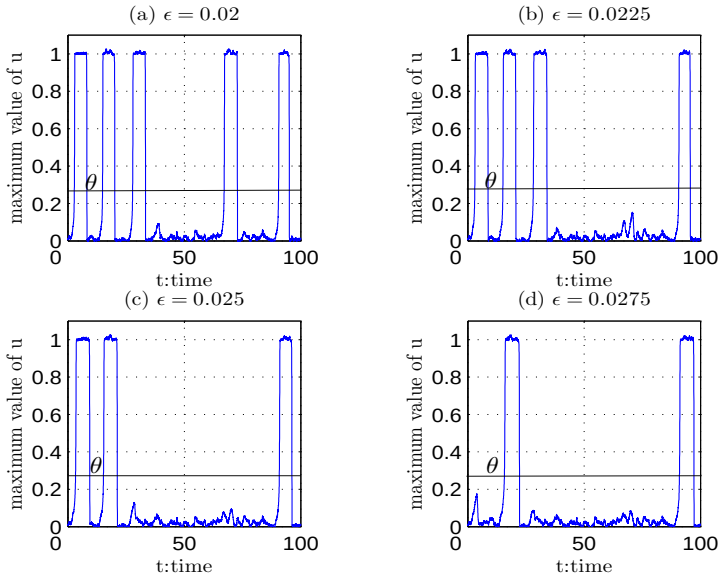

Figure 4.6: Illustration of the threshold of nucleation of waves for the Barkley model using maximum value of activator u over x. The parameters used are as in Figure 4.3 except for ϵ.

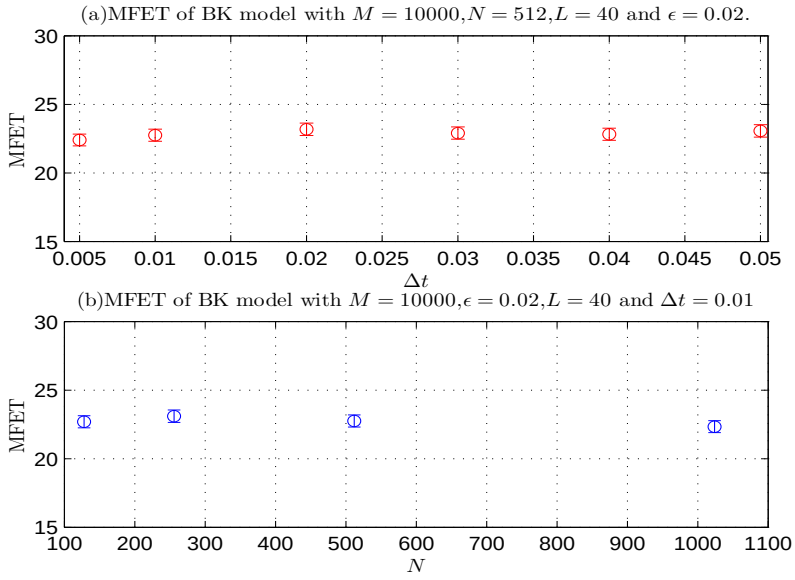

Figure 4.7: Showing of the mean first exit time (MFET) as a function of (a) Δt and (b) N, with parameters used are as in Figure 4.3.

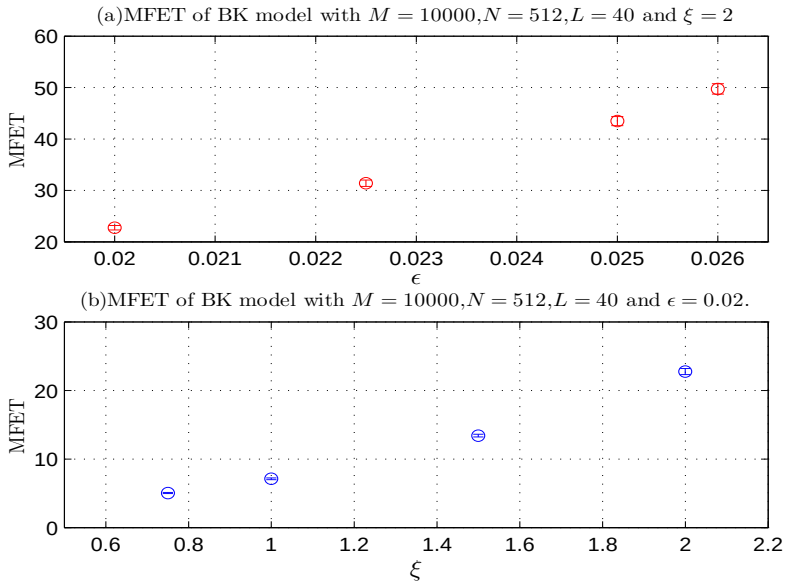

Figure 4.8: Showing of the mean first exit time (MFET) as a function of (a) ϵ and (b) ξ, with parameters used are as in Figure 4.3.

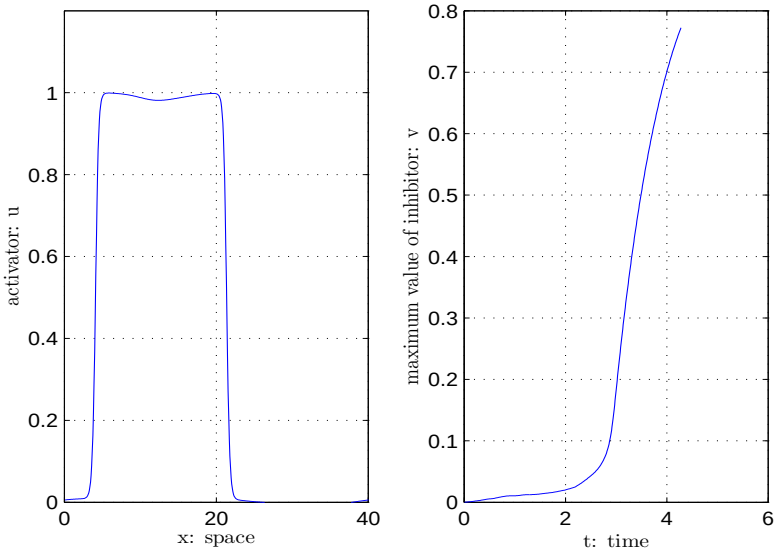

Figure 4.9: Nucleation of back wave for the Barkley model is illustrated in the left plot with the same parameters of Figure 4.3. In the right one, maximum value of inhibitor v over x is plotted against the time t in order to calculate the threshold θ_b of wave back nucleation.

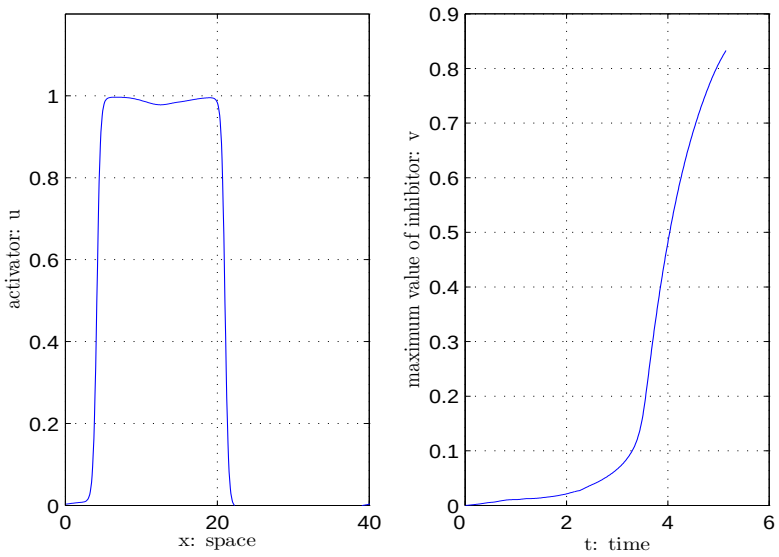

Figure 4.10: Nucleation of back wave for the Barkley model is shown in the left plot with the same parameters of Figure 4.3 except for $\epsilon = 0.025$. In the right, maximum value of inhibitor v over x is plotted versus the time t for determining the threshold θ_b of back wave nucleation.

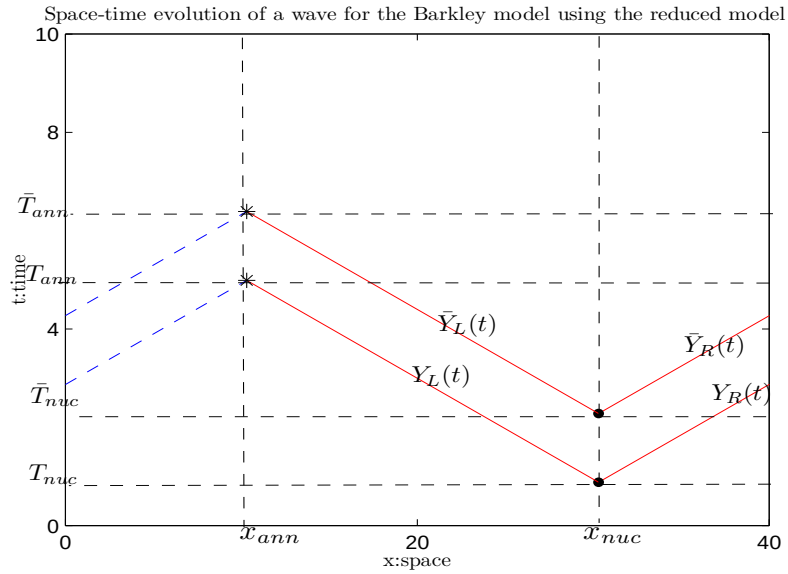

Figure 4.11: Plots of the nucleation and annihilation of a wave for the Barkley model (4.1) with $\epsilon = 0.02$ and using the reduced model.

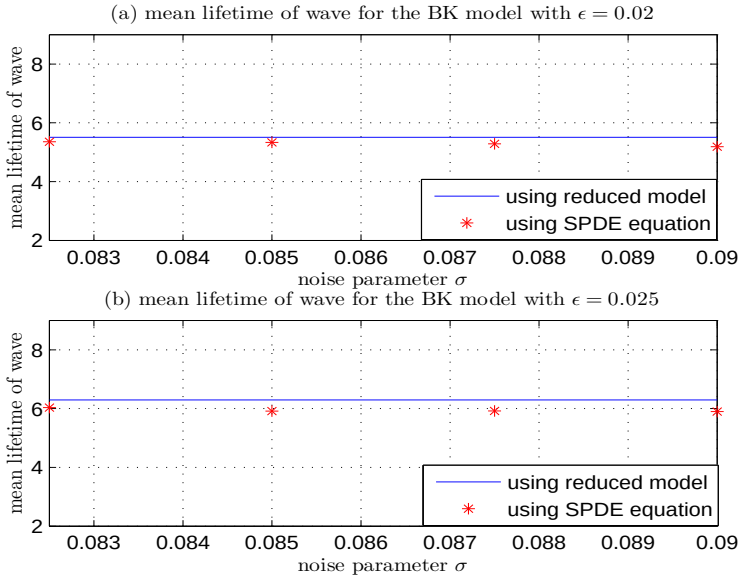

Figure 4.12: Mean lifetime of a wave for the Barkley model as a function of noise parameter σ is shown for $(a)\epsilon = 0.02$ and $(b)\epsilon = 0.025$. The results obtained by simulation of SPDE (4.1) are represented by stars symbols and solid lines represent the results obtained by the reduced model. Figures show the good agreement between these results, in particular for $\epsilon = 0.02$.

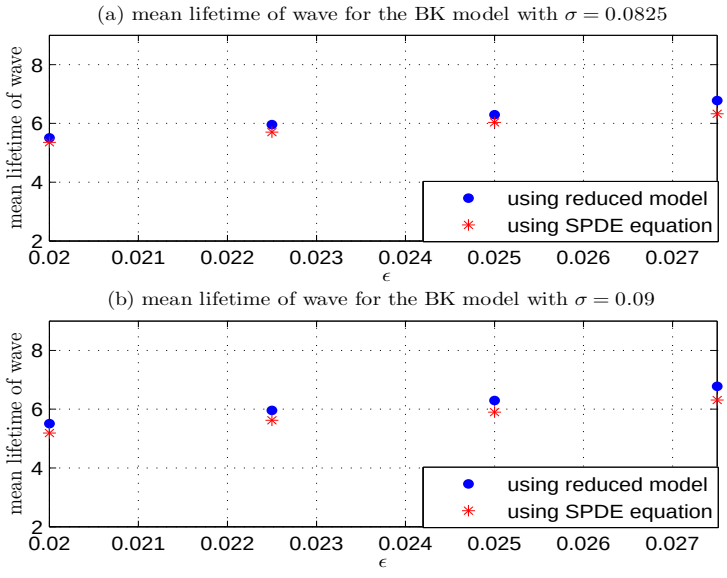

Figure 4.13: Mean lifetime of a wave for the Barkley model is plotted versus a small parameter ϵ for (a) $\sigma = 0.0825$ and (b) $\sigma = 0.09$. The results from simulation of the underlying SPDE represented by stars symbols are compared to those obtained by the reduced model, (shaded circles).

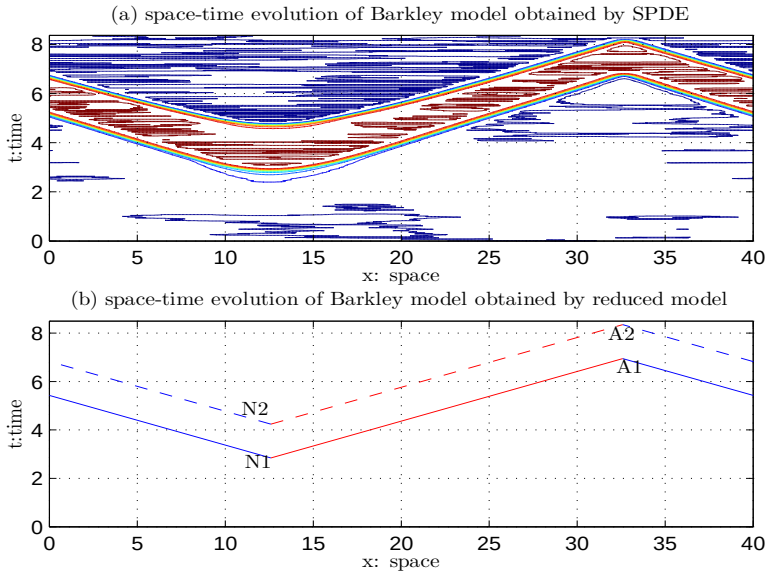

Figure 4.14: (a) Space-time contour plot of dynamical behaviour of the Barkley model (4.1) with parameters values used in Figure 4.3. (b) Simulation of the dynamical behaviour of the Barkley model using the reduced model. N_1 and N_2 are nucleation points of the front and back waves, respectively. A_1 and A_2 are corresponding points of annihilation.

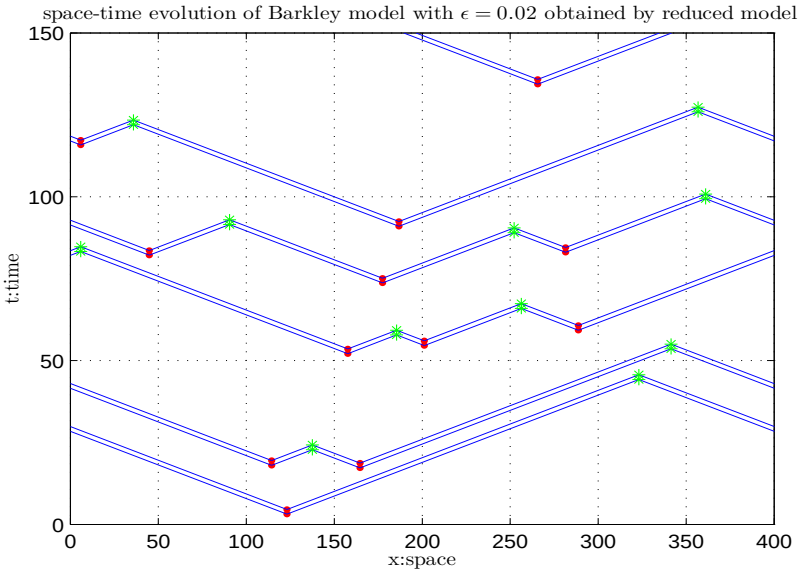

Figure 4.15: Simulation of dynamical behaviour of the Barkley model using the reduced model when L is large and many waves are nucleated at almost the same time. The parameters values are $a = 0.75$, $b = 0.01$, $\epsilon = 0.02$, $D = 1$ and $L = 400$.

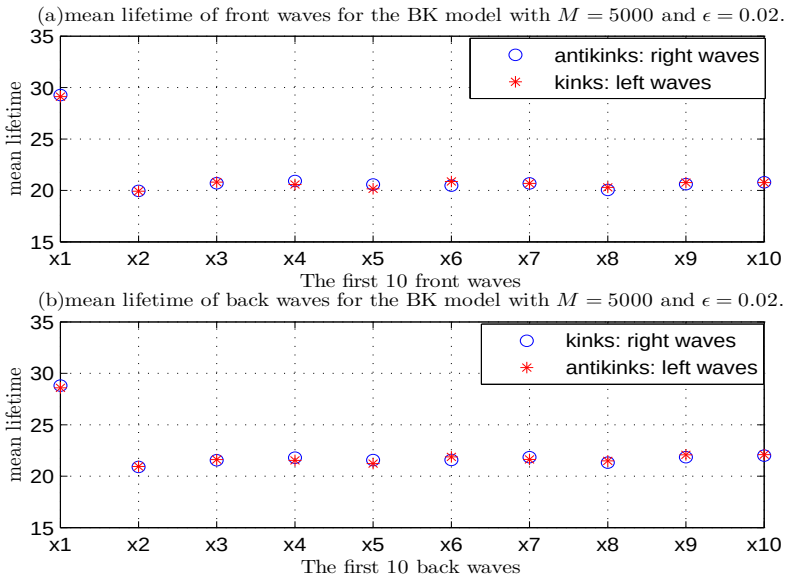

Figure 4.16: Shown of the mean lifetime of (a)the first 10 front waves and (b)the first 10 back waves. The parameters of the system are $a = 0.75$,$b = 0.01$,$\epsilon = 0.02$, $D = 1$ and $L = 400$.

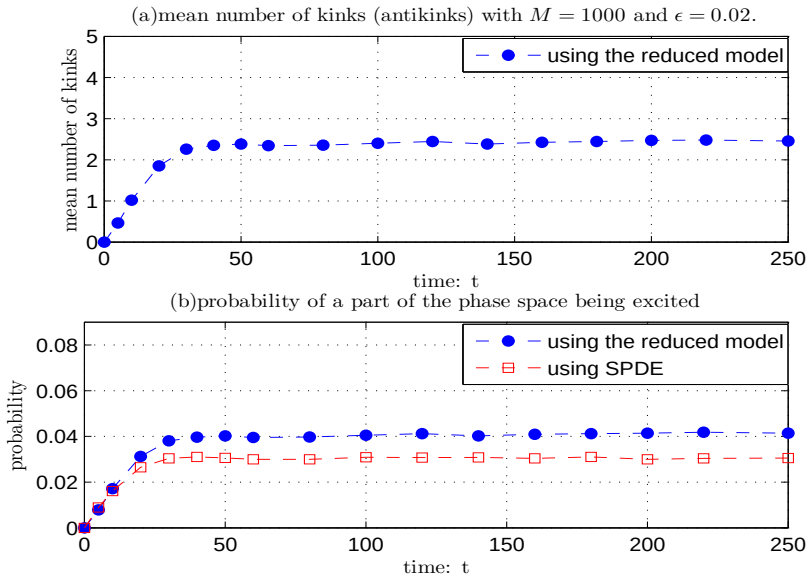

Figure 4.17: (a) Shown of the mean number of kinks (antikinks) at time t on space domain $[0, 400]$ with $\epsilon = 0.02$, $N_1 = 30$ and $M = 1000$. (b) Illustration of the probability that a part of the phase space is excited at (x, t) .

Chapter 5

Conclusion and future work

5.1 Conclusion

Using SDELab, a mathematical software for solving SDEs within MATLAB, we studied the firing properties of the space-clamped HH model, in response to the application of a suprathreshold, constant current. Moreover, we examined the influence of additive white noise on the output spike trains. We found that a suitable amount of additive noise can enhance the regularity of the repetitive spiking of the model. Furthermore, the SDELab package was used to simulate a system of SPDEs, represented by the spatially-extended FHN system with additive space-time white noise. Again, we evaluated the effects of additive noise on the regularity of the output spikes. We found that this type of model is sensitive to noise and therefore very small values of noise should be chosen, in order to produce regular spikes.

We further examined the effects of an additive noise on the FET for the one-dimensional diffusion neural models represented by the stochastic space-clamped FHN system and by the OU model, using the fixed time-stepping Euler method with boundary correction and the exponential time-stepping Euler algorithm with boundary test. We provide a detailed exposition of the strategies employed in these

numerical techniques and the analytical frameworks for relevant functionals of the FETs of the diffusion processes. We studied the effects of additive noise on the systematic errors in the MFET, produced by these simulation techniques, for the FHN and OU models. We found that, for different values of noise, combining the boundary tests with these numerical methods can improve the rate of convergence of the MFET from the order of one half to first order convergence, which coincides with previous studies [43, 59, 32, 8].

The nucleation and dynamics of traveling waves under the stochastic Barkley model were also studied. The left (right) sides of front waves and the right (left) sides of back waves are known as kinks (antikinks) and their nucleation, propagation and eventual annihilation are of great interest. We studied the effect of a small additive noise and that of the time scale of separation, on the nucleation times of such structures and on their mean lifetimes, using an efficient numerical simulation of the Barkley model with additive noise that is white in time and correlated in space. However, that technique becomes computationally impractical in the case of interacting waves or when the domain is large. We therefore introduced a simple model of the dynamics of the underlying model, in order to calculate the mean lifetimes of the kinks and antikinks efficiently. Moreover, the ease of use of the reduced model motivated us to explore the full dynamics of the kinks and antikinks, in particular over long periods. One application of the reduced model is to calculate the mean number of kinks at a specific time t and use this to obtain the probability that the system is excitable at time t and position x, in the given space domain.

5.2 Future work

In this section, we propose some interesting topics for future work, which have arisen as a result of the research carried out for this thesis. **In Chapter 2**, the neural models we deal with are forced by additive noise, where the noise is used to

model the external fluctuations. However, as a further piece of work, we would like to use SDELab to explore the possible effects of the other type of noise, so-called multiplicative noise, on the firing properties and the output spike trains of these systems. Multiplicative noise depends on the voltage variable and so the activity of the neuron has a strong relationship with the amount of noise. The randomness of the opening and closing of ionic channels is the most important source of this type of noise, and therefore one interesting investigation would be to look at multiplicative noise in the conductance variables of the ionic channels of the HH model.

In the additive noise case, the Euler-Maruyama method converges strongly with order 1, which is reduced to order one half for the case of multiplicative noise [49]. To retrieve first-order strong convergence, the Milstein method can be used, in spite of the difficulty involved in estimating the second-order iterated integral that appears in the final term of the integrator [49]. SDELab provides Milstein methods for the Itô and Stratonovich SDEs, with efficient approximation of their second-order iterated integrals. In the case of additive noise, the Itô and Stratonovich SDEs have the same solutions, but this is not true when using multiplicative noise. One can move between the Itô and Stratonovich calculi using a simple transformation and hence, in the case of multiplicative noise, we can convert a Stratonovich SDE to the corresponding Itô equation or we can solve it directly using Stratonovich calculus [49, 47, 29]. SDELab, in fact, offers two strong solvers for the Stratonovich SDEs: the stochastic Heun method and the Stratonovich-Milstein algorithm, as illustrated in Chapter 2 (see [29] for more details). Briefly, we would like to exploit these benefits of the SDELab software in order to explore the effects of multiplicative noise on the spiking activity of the HH model and the FHN system, as a contribution to the field of computational neuroscience.

In Chapter 3, we used the fixed and exponential time-stepping Euler methods with boundary tests to examine the influence of additive noise on the systematic

errors in the MFETs for one-dimensional diffusion neural models, represented by the stochastic FHN system and the OU model. We found for the fixed time-stepping algorithm that using Mannella's boundary test improved the order of convergence in the MFETs from one half to one, which coincides with previous results, such as those in [43] and [8]. This result and the work done by Gobet [32] create a strong motivation for trying to find a simple proof for this rate of convergence of the MFET for the general case of a one-dimensional diffusion. Under the exponential time-stepping algorithm, Jansons and Lythe [43] obtained a similar improvement in the rate of convergence of the MFET for the additive noise problem with a double-well potential, and stated their expectation that this would also hold for the general case of one-dimensional diffusion. Indeed, our numerical results have confirmed this claim for the stochastic FHN system and the OU model, under different values of noise. Jansons and Lythe [43] also expected that further analysis of the solution of the (3.77) could lead to a simple general proof of this rate of convergence. This would be an interesting area to consider in our future work.

In Chapter 4, the dynamics of the traveling waves of the Barkley system under the influence of additive noise that is white in time and correlated in space, were studied using an efficient numerical technique. Moreover, we introduced a reduced model of these dynamics in order to efficiently calculate the mean lifetime of the traveling waves, particularly for interacting waves, where the mean lifetime of each kink and antikink of these waves need to be calculated individually. As a future piece of work, we plan to use our reduced model to further explore the dynamics of the kinks of the stochastic Barkley system. Beside numerical simulation, we would like to study these dynamics using theoretical approaches, as has been done extensively for the ϕ^4-equation with additive space-time white noise [7, 58, 35], for example.

On the other hand, it would be interesting to study the possible effects of multiplicative noise on the dynamics of the traveling waves of the Barkley system. For

a good introductory review of the different ways that multiplicative noise can influence the dynamics of the Barkley system and those of a generic excitable system, we recommend [56] and the references given there. We would aim, firstly, to restrict ourselves to investigating the randomness in the activator dynamics. The multiplicative noise in the activator equation of the Barkley system (4.1) will be assumed to be [24, 56]

$$\beta(u) = \frac{1}{a\epsilon}u(1-u)w(x,t),$$

where $w(t,x)$ is a wiener process that is white in time and correlated in space. The interesting point about this type of multiplicative noise is that it does not affect the system in the rest state ($u = 0$) or in the excited state ($u = 1$), since it vanishes at both these points, and in this behaviour it differs from the additive noise case we have studied in this thesis. We would like to develop our reduced model to deal with this case. In contrast to additive noise, multiplicative noise affects the speed and width of traveling waves [25, 24, 56], and this will need to be taken into account when we design the reduced model of the underlying dynamics under multiplicative noise.

We could also look at fluctuations in the inhibitor equation of the Barkley system, where sufficiently large fluctuations can lead to the backfiring phenomenon [24, 27]. This means that, for sufficiently large noise, in the middle of the wave, the transition can be induced from the excited state to the quiescent one, causing the wave to be broken into two halves, moving in opposite directions with the same speed.

In this section we have presented some ideas for further research, leading on from our current work. We hope that our work can be improved and extended by investigating and developing these ideas and we also hope that further reading on the subject will lead to new creative ideas.

Appendix A

Miscellaneous background from probability theory

Definition A.0.1. [49][**expectation,variance,covariance,Gaussian random variable**]

Let X be a continuous random variable, with integrable density function $f_X(x)$, on probability space $(\Omega, \mathcal{A}, P)$, then the *expected value* of X is given by

$$E[X] = \int_\Omega X dP = \int_{-\infty}^{\infty} x f_X(x) dx, \quad \forall x \in \mathbb{R},$$

and if $g(X)$ is a function of X, then the expected value of $g(X)$ is given by

$$E[g(X)] = \int_{-\infty}^{\infty} g(x) f_X(x) dx. \tag{A.1}$$

Furthermore, if h is a function of continuous real valued random variables X and Y defined on $(\Omega, \mathcal{A}, \mathbf{P})$ with joint density function f_{XY}, then the expectation of $h(X, Y)$ is defined by

$$E[h(X, Y)] = \int_{-\infty}^{\infty} \int_{-\infty}^{\infty} h(x, y) f_{XY}(x, y) dx dy. \tag{A.2}$$

The *variance* of the real valued random variable X with expected value $\mu = E[X]$ is given by

$$\sigma^2 = var(X) = E[X^2 - E[X]^2] = E[X^2] - \mu^2.$$

For two real valued random variables X and Y with mean values $E(X)$ and $E(Y)$, respectively, the *covariance* of X and Y is defined by

$$Cov(X, Y) = E[(X - E[X])(Y - E(Y))].$$

The continuous random variable X, with density function

$$f_X(x) = \frac{1}{\sqrt{2\pi}\sigma} \exp(\frac{-(x-\mu)^2}{2\sigma^2}),$$

is called a *Gaussian* or *normally distributed random variable* with mean μ and variance σ^2. Moreover, if $\mu = 0$ and $\sigma^2 = 1$, it is called a standard Gaussian random variable. For a random variable X with this distribution, we write $X \sim \mathcal{N}(\mu, \sigma^2)$. A Gaussian random variable is completely characterized by its expected value μ and variance σ^2, which are known as its first and second moments, respectively.

We now look at some properties of the expectation of a continuous random variable X with density function $f_X(x)$:

- Given the indicator function

$$1_{(-\infty,a]}(X) = \begin{cases} 1, & if X \leq a \\ 0, & \text{otherwise} \end{cases},$$

  where $a \in \mathbb{R}$, we would have

$$E[1_{(-\infty,a]}(X)] = \int_{-\infty}^{\infty} 1_{(-\infty,a]}(x) f_X(x) dx = \int_{-\infty}^{a} f_X(x) dx = \mathbf{P}(X \leq a). \quad \text{(A.3)}$$

- For any two random variables X and Y, with $E[X] < \infty$ and $E[Y] < \infty$, we

have

$$E[\alpha X + \beta Y] = \alpha E[X] + \beta E[Y], \quad \alpha, \beta \in \mathbb{R}, \tag{A.4}$$

and if X and Y are independent, then

$$E[XY] = E[X]E[Y]. \tag{A.5}$$

Definition A.0.2. [49][**mean-square convergence**]
The sequence of random variables $X_1, X_2, \cdots, X_n, \cdots$ is said to be strongly convergent to the random variable X in *mean-square* if

$$E(X^2) < \infty, \quad E(X_n^2) < \infty, \quad \text{for} \quad n = 1, 2, \cdots, \quad \text{and} \quad \lim_{n\to\infty} E(|X_n - X|^2) = 0.$$

Definition A.0.3. [49][**stochastic process, modification, continuous stochastic process, Gaussian process**]
Consider a time interval $[t_0, T]$ and a probability space $(\Omega, \mathcal{A}, P)$, then $X = \{X(t), t_0 \leq t \leq T\}$ is said to be a *stochastic process* if

$$X : [t_0, T] \times \Omega \to \mathbb{R}, \quad X(t) = X(t, .)$$

is a random variable for each $t \in [t_0, T]$.
Moreover, the stochastic process $Y = \{Y(t), t_0 \leq t \leq T\}$ is called a *modification* or a *version* of X if

$$P(\{\omega \in \Omega : X(t, \omega) \neq Y(t, \omega)\}) = 0, \quad \forall t \in [t_0, T].$$

The stochastic process X is *continuous* if its trajectories $X(., \omega)$ are continuous almost surely at any $t \in [t_0, T]$. Thus

$$P(\{\omega \in \Omega : \lim_{s\to t} |X(s, \omega) - X(t, \omega)| = 0\}) = 1.$$

The stochastic process $\{X(t), t_0 \leq t \leq T\}$ is called a *Gaussian process* if for any finite set $t_1, t_2, \cdots, t_n$ in $[t_0, T]$, the joint distribution of the collection of random variables $X(t_1), X(t_2), \cdots, X(t_n)$ is a multivariate Gaussian distribution. Thus, if every finite linear combination $\sum_{i=1}^{n} \alpha_i X(t_i)$, where $\alpha_i \in \mathbb{R}$, has a Gaussian distribution.

Definition A.0.4. [49][**filtration, adapted process**]
Consider a probability space $(\Omega, \mathcal{A}, P)$. A family $\{\mathcal{A}_t\}_{t\geq 0}$ of sub-σ-algebras of $\mathcal{A}$ is called a *filtration* if $\mathcal{A}_s \subseteq \mathcal{A}_t, \quad \forall s \leq t$. In addition, the stochastic process $X = \{X(t), t \geq 0\}$ defined on $(\Omega, \mathcal{A}, P)$ is said to be *adapted to the filtration* $\{\mathcal{A}_t\}_{t\geq 0}$ if $X(t)$ is $\mathcal{A}_t$-measurable for all $t \geq 0$.

Definition A.0.5. [**predictable process**]
Let $\{\mathcal{A}_t\}_{t\geq 0}$ be a filtration. Then a stochastic process $\{X(t), t \geq 0\}$ is called $\{\mathcal{A}_t\}_{t\geq 0}-$*predictable* if $X(t)$ is $\mathcal{A}_{t-}-$measurable for all $t \geq 0$ where
$\mathcal{A}_{t-} = \bigcup_{s<t} \mathcal{A}_s$. Therefore, if the process $\{X(t), t \geq 0\}$ is $\mathcal{A}_t$-adapted and left continuous, then it is predictable.

Definition A.0.6. [49][**conditional distribution, conditional density**]
Let X and Y be real-valued random variables defined on $(\Omega, \mathcal{F}, \mathbf{P})$. Then *the conditional distribution* of X given $\{Y = y\}$ is defined by

$$F_{X|Y}(x|y) = \mathbf{P}(X \leq x | Y = y) = \frac{\mathbf{P}(X \leq x, Y = y)}{\mathbf{P}(Y = y)}, \tag{A.6}$$

where $x, y \in \mathbb{R}$ and $\mathbf{P}(Y = y) > 0$. Moreover, if X and Y are continuous real-valued random variables with joint density function $f_{XY}(x, y)$ and with marginal densities $f_X(x)$ and $f_Y(y)$, where $f_Y(y) > 0$ for all $y \in \mathbb{R}$, then *the conditional density function* of X given $\{Y = y\}$ is given by

$$f_{X|Y}(x|y) = \frac{f_{XY}(x, y)}{f_Y(y)}. \tag{A.7}$$

Furthermore, if X and Y are independent, then

$$f_{X|Y}(x|y) = \frac{f_{XY}(x,y)}{f_Y(y)} = \frac{f_X(x)f_Y(y)}{f_Y(y)} = f_X(x), \tag{A.8}$$

and

$$f_{Y|X}(y|x) = f_Y(y). \tag{A.9}$$

However, the probability that $\{X < Y\}$ can be calculated as

$$\mathbf{P}(X < Y) = \int_{-\infty}^{\infty} \mathbf{P}(X < y|Y = y) f_Y(y) dy. \tag{A.10}$$

Further, given X and Y are independent yields

$$\mathbf{P}(X < Y) = \int_{-\infty}^{\infty} \mathbf{P}(X < y) f_Y(y) dy = \int_{-\infty}^{\infty} F_X(y) f_Y(y) dy. \tag{A.11}$$

Definition A.0.7. [49][**conditional expectation**]

The conditional expectation of X given $\{Y = y\}$ is defined as

$$E[X|Y = y] = \int_{-\infty}^{\infty} x f_{X|Y}(x|y) dx. \tag{A.12}$$

Consider a function g of X, then we have

$$E[g(X)|Y = y] = \int_{-\infty}^{\infty} g(x) f_{X|Y}(x|y) dx. \tag{A.13}$$

Lemma A.0.1. *Let X and Y be real-valued random variables defined on $(\Omega, \mathcal{F}, \mathbf{P})$ with joint density function $f_{XY}(x,y)$ and with marginal densities $f_X(x)$ and $f_Y(y)$, then*

$$E[X] = E[E[X|Y]]. \tag{A.14}$$

Proof. Obviously, $E[X|Y]$ is a function of random variable Y and therefore the distribution of Y will be used in calculating its expectation. Thus

$$\begin{aligned} E[E[X|Y]] &= \int_{-\infty}^{\infty} E[X|Y=y] f_Y(y) dy = \int_{-\infty}^{\infty}\int_{-\infty}^{\infty} x f_{XY}(x,y) dy dx \\ &= \int_{-\infty}^{\infty} x \int_{-\infty}^{\infty} f_{XY}(x,y) dy dx = \int_{-\infty}^{\infty} x f_X(x) dx = E[X]. \end{aligned}$$

□

Definition A.0.8. [49][**uniformly distributed random variable**]
A continuous real-valued random variable X is said to be *uniformly distributed* over (a,b), where $a,b \in \mathbb{R}$ if its density function is given by

$$f_X(x) = \begin{cases} \frac{1}{b-a}, & \text{for} \quad a < x < b \\ 0, & \text{otherwise.} \end{cases} \tag{A.15}$$

Consequently, its distribution function is

$$F_X(x) = \begin{cases} 0, & x \leq a \\ \frac{x-a}{b-a}, & a < x < b \\ 1, & x \geq b \end{cases}$$

Definition A.0.9. [49][**exponentially distributed random variable**]
A continuous real-valued random variable X with a density function given by

$$f_X(x) = \begin{cases} \lambda e^{-\lambda x}, & \text{for} \quad x \geq 0 \\ 0, & \text{otherwise,} \end{cases} \tag{A.16}$$

is called *exponentially distributed with parameter* λ, and its distribution function is given by

$$F_X(x) = \begin{cases} 1 - \lambda e^{-\lambda x}, & \text{for} \quad x \geq 0 \\ 0, & \text{otherwise,} \end{cases} \tag{A.17}$$

The exponential distribution plays an important role in exit time problems since it is used to model the time between random events. We therefore present some properties of this distribution as follows:

- An important property of the exponential distribution is that it is memoryless. Thus the conditional probability of an exponentially distributed random variable X satisfies

$$\mathbf{P}(X > x + y | X > y) = \mathbf{P}(X > x), \quad \forall x, y \geq 0. \tag{A.18}$$

  It is a simple matter to check this property as follows

$$\mathbf{P}(X > x + y | X > y) = \frac{\mathbf{P}(X > x + y, X > y)}{\mathbf{P}(X > y)} = \frac{\mathbf{P}(X > x + y)}{\mathbf{P}(X > y)},$$

  and consequently

$$\mathbf{P}(X > x + y | X > y) = \frac{e^{-\lambda(x+y)}}{e^{-\lambda y}} = e^{-\lambda x} = \mathbf{P}(X > x).$$

- The expectation of an exponentially distributed random variable X is equal to the inverse of its parameter λ. This is easily seen as follows

$$E[X] = \int_0^\infty x \lambda e^{-\lambda x} dx,$$

  and using integration by parts implies

$$E[X] = [-xe^{-\lambda x}]_0^\infty - \int_0^\infty -e^{-\lambda x} dx = \lim_{x \to \infty} -xe^{-\lambda x} - \frac{1}{\lambda}[e^{-\lambda x}]_0^\infty.$$

  Hence

$$E[X] = 0 - \frac{1}{\lambda}(-1) = \frac{1}{\lambda}. \tag{A.19}$$

- The uniform random generator can be used to generate an exponentially distributed random variable through the application of the inverse transform method:

  Theorem A.0.2. *(**Inverse Transform Method**) Let F_X be the distribution function of a real-valued random variable X and suppose F_X has an inverse function F_X^{-1} defined as*

  $$F_X^{-1}(u) = \inf\{x : F_X(x) = u\}, \quad 0 \leq u \leq 1.$$

  If U is a uniformly distributed random variable on $[0,1]$, then $F_X^{-1}(U)$ has the distribution function F_X. Moreover, F_X is uniformly distributed on $[0,1]$.

  Proof. To prove this theorem, we follow [78].
  First, $F_X^{-1}(U)$ has distribution function F_X, which is easy to check as follows

  $$\begin{aligned} \mathbf{P}(F_X^{-1}(U) \leq x) &= \mathbf{P}(U \leq F_X(x)) \\ &= F_X(x) \quad \text{since} \quad \mathbf{P}(U \leq v) = v. \end{aligned}$$

  Given $0 < u < 1$, we have

  $$\begin{aligned} \mathbf{P}(F_X(x) \leq u) &= \mathbf{P}(X \leq F_X^{-1}(u)) \\ &= F_X(F_X^{-1}(u)) \\ &= u. \end{aligned}$$

  Hence, $F_X(x)$ follows the uniform distribution on $[0,1]$. □

  We will explain now how an exponentially distributed random variable X with parameter $\lambda > 0$ can be generated using the uniform random generator. To this end, recall first that the distribution function of X is

  $$F_X(x) = 1 - e^{-\lambda x}, \quad \lambda > 0, \quad x \geq 0.$$

Then the inverse transform method (Theorem A.0.2) implies that

$$F_X(x) = U = 1 - e^{-\lambda x},$$

is uniformly distributed on $[0, 1]$. Consequently

$$1 - U = e^{-\lambda x},$$

which yields

$$\ln(1 - U) = -\lambda x.$$

Thus

$$-\frac{\ln(1-U)}{\lambda} = x = F_X^{-1}(U).$$

Now, since U is uniformly distributed on $[0, 1]$, so is $1 - U$. Therefore, we can generate the exponentially distributed random variable X:

$$X = -\frac{\ln(U)}{\lambda}. \tag{A.20}$$

Definition A.0.10. [57][**error function**]

The error function or Gauss error function is defined as

$$erf(x) = \frac{2}{\sqrt{\pi}} \int_0^x e^{-t^2} dt.$$

Lemma A.0.3. *Suppose X is a real-valued normally distributed random variable defined on $(\Omega, \mathcal{F}, \mathbf{P})$ with mean μ and variance σ^2. Then for $r > 0$, we have*

$$\mathbf{P}(|X - \mu| \leq r) = erf(\frac{r}{\sqrt{2\sigma^2}}). \tag{A.21}$$

Proof. Since X follows a Gaussian distribution ($X \sim N(\mu, \sigma^2)$, its probability density

function is given by

$$p(x) = \frac{1}{\sqrt{2\pi\sigma^2}} \exp(\frac{-(x-\mu)^2}{2\sigma^2}),$$

and consequently

$$\mathbf{P}(|X-\mu| \leq r) = \mathbf{P}(\mu - r \leq X \leq \mu + r) = \frac{1}{\sqrt{2\pi\sigma^2}} \int_{\mu-r}^{\mu+r} \exp(\frac{-(x-\mu)^2}{2\sigma^2})dx.$$

By setting $t = \frac{x-\mu}{\sqrt{2\sigma^2}}$, we get $dx = \sqrt{2\sigma^2}dt$ and the boundaries of the integral become $t = \frac{-r}{\sqrt{2\sigma^2}}$ and $t = \frac{r}{\sqrt{2\sigma^2}}$.
Substituting these quantities into the integral above yields

$$\begin{aligned} \mathbf{P}(|X-\mu| \leq r) &= \frac{1}{\sqrt{\pi}} \int_{\frac{-r}{\sqrt{2\sigma^2}}}^{\frac{r}{\sqrt{2\sigma^2}}} \exp(-t^2)dt \\ &= \frac{2}{\sqrt{\pi}} \int_{0}^{\frac{r}{\sqrt{2\sigma^2}}} \exp(-t^2)dt \\ &= erf(\frac{r}{\sqrt{2\sigma^2}}). \end{aligned}$$

□

Strong law of large numbers [57] Let $X_j, j = 1, \cdots, M$ be independent and identically distributed (i.i.d) real-valued random variables defined on $(\Omega, \mathcal{F}, \mathbf{P})$ with mean μ and variance σ^2 and define

$$\overline{X}_M = \frac{X_1 + X_2 + \cdots + X_M}{M} \tag{A.22}$$

as the sample mean of M independent samples $X_1, X_2, \cdots, X_M$ of X. Then $\overline{X}_M$ converges to μ with probability one as $M \to \infty$. This law is known as *the strong law of large numbers*. [57]

In many applications, the distribution of the random variable X is unknown. Therefore, if one needs to compute one of its moments, namely β, an estimator β_M of β ($\beta_M \to \beta$ as $M \to \infty$) is used. β_M is a random variable with expectation

β and is called an unbiased estimator of β [57]. For example, $\overline{X}_M$ is an estimator of the mean $\mu = E[X]$ as obtained from the strong law of large numbers. $\overline{X}_M$ is also a random variable since it depends on the particular realizations $X_1, X_2, \cdots, X_M$ and so $E(\overline{X}_M) = \mu$. The sample mean $\overline{X}_M$ is thus an unbiased estimator of μ. More information about the convergence of $\overline{X}_M$ to μ and the rate of this convergence can be obtained from *the central limit theorem* and *the Berry-Esseen inequality.*

Theorem A.0.4. ***Central limit theorem*** *[57]*

Suppose $E[|x_j|^2] < \infty$*, where* X_j*,* $j = 1, 2, \cdots, M$*, are i.i.d. real-valued random variables, then*

$$X_M^* = \sqrt{M}(\overline{X}_M - \mu),$$

converges in distribution to a Gaussian random variable Z *with mean* 0 *and variance* σ^2*. Thus,* $X_M^* \to Z \sim N(0, \sigma^2)$*.*

Theorem A.0.5. ***Berry-Esseen inequality*** *[57]*

Let $E[|x_j|^2] < \infty$ *and* $E[|x_j|^3] < \infty$*, where* X_j*,* $j = 1, 2, \cdots, M$*, are i.i.d. real-valued random variables and* $j = 1, 2, \cdots, M$*. Then the rate of convergence of* X_M^* *to* $Z \sim N(0, \sigma^2)$ *is* $O(M^{\frac{-1}{2}})$*. In particular,*

$$\sup_z |\mathbf{P}(X_M^* \leq z) - \mathbf{P}(Z \leq z)| \leq \frac{E[|X_1 - \mu|^3]}{\sigma^3 \sqrt{M}}.$$

Confidence interval

From the Berry-Esseen inequality, we have [57]

$$\mathbf{P}(X_M^* \leq z) = \mathbf{P}(Z \leq z) + O(M^{\frac{-1}{2}}).$$

Given $r > 0$, equation (A.21) yields

$$\mathbf{P}(X_M^* \leq r) = erf(\frac{r}{\sqrt{2\sigma^2}}) + O(M^{\frac{-1}{2}}). \tag{A.23}$$

Taking $r = 2\sigma$ gives

$$\mathbf{P}(X_M^* \leq 2\sigma) = erf(\frac{2\sigma}{\sqrt{2\sigma^2}}) + O(M^{\frac{-1}{2}}).$$

Thus

$$\mathbf{P}(|\overline{X}_M - \mu| \leq \frac{2\sigma}{\sqrt{M}}) = erf(\sqrt{2}) + O(M^{\frac{-1}{2}}).$$

Since $erf(\sqrt{2}) \simeq 0.9545$, we obtain

$$\mathbf{P}(\overline{X}_M - \frac{2\sigma}{\sqrt{M}} < \mu < \overline{X}_M + \frac{2\sigma}{\sqrt{M}}) > 0.95 + O(M^{\frac{-1}{2}}). \tag{A.24}$$

The interval

$$[\overline{X}_M - \frac{2\sigma}{\sqrt{M}}, \overline{X}_M + \frac{2\sigma}{\sqrt{M}}]$$

is known as a 95% *confidence interval* as the probability that μ is contained within it at least 0.95. If σ is unknown, the unbiased estimator

$$\sigma_M^2 = \frac{1}{M-1}\sum_{j=1}^{M}(X_j - \overline{X}_M)^2$$

of σ^2 can be used. The 95% confidence interval is then given by

$$[\overline{X}_M - \frac{2\sigma_M}{\sqrt{M}}, \overline{X}_M + \frac{2\sigma_M}{\sqrt{M}}],$$

where $\frac{\sigma_M}{\sqrt{M}}$ is known as the standard error. [57]

Appendix B

Hilbert space, operator theory and Fourier series

Hilbert space and Fourier Series

Firstly, we present some preliminaries and some material on Hilbert space and Fourier analysis [73, 5]:

Definition B.0.11. [73][**Cauchy sequence, complete space**]
Consider a normed vector space $(X, ||\cdot||)$. A sequence $x_n \in X$, for $n = 1, 2, 3, \cdots$ is said to be *a Cauchy sequence* if for all $\xi > 0$, there exists $N > 0$ such that $||x_m - x_n|| < \xi$ for all $m, n \geq N$. The space X is said to be *complete* if every Cauchy sequence in X converges to a limit point in X.

Definition B.0.12. [73][**Banach space**]
A Banach space is a complete normed vector space.

$(\mathbb{R}, ||.||_2)$ and $(C(\mathbb{R}, \mathbb{R}), ||.||_\infty)$ are examples of Banach spaces.

Definition B.0.13. [73][**inner product**]
Let X be a vector space over $\mathbb{R}$. Then *the inner product* is a function $\langle ., . \rangle : X \times X \rightarrow \mathbb{R}$ such that

1. $\langle x, x\rangle \geq 0$ and $\langle x, x\rangle = 0 \Leftrightarrow x = 0 \quad \forall x \in X$.

2. $\langle x, y\rangle = \langle y, x\rangle \quad \forall x, y \in X$.

3. $\langle \lambda x + \mu y, z\rangle = \lambda\langle x, y\rangle + \mu\langle x, z\rangle \quad \forall x, y, z \in X$ and $\lambda, \mu \in \mathbb{R}$.

Moreover, the inner product defines a norm,

$$||x|| = \langle x, x\rangle^{1/2} \quad \forall x \in X.$$

Definition B.0.14. [73][**Hilbert space**]

A Hilbert space is defined as a Banach space with an inner product. For example, the space of square integrable functions over $[0, 1]$, denoted by $L^2(0, 1)$, with inner product $\langle f, g\rangle = \int_0^1 f(x)g(x)dx$ and norm $||f||_2 = \langle f, f\rangle^{1/2} = (\int_0^1 f(x)^2 dx)^{1/2}$, $\forall f, g \in L^2(0, 1)$, is a Hilbert space.

From now on, $(.,.)$ will be used to denote the inner product on a Hilbert space.

Lemma B.0.6. ***Cauchy-Schwartz inequality***

Suppose H is a Hilbert space. Then

$$|(x, y)| \leq ||x||||y|| \quad \forall x, y \in H.$$

Proof. See [73] for a proof of this lemma. □

Definition B.0.15. [73][**separable Hilbert space**]

A Hilbert space H is called *separable* if it has a countable dense subset.

Definition B.0.16. [73][**orthonormal basis**]

A family $B = \{e_j\}_{j\in\mathbf{N}}$, is said to be *an orthonormal basis* of a separable Hilbert space H, if the following conditions hold:

1. $(e_j, e_k) = 0$ if $j \neq k$ and for all $j, k \in \mathbb{N}$,

2. $||e_j|| = 1$ for all $j \in \mathbb{N}$ and

3. the linear span of the orthonormal set B (i.e.$x = \sum_{j\in\mathbf{N}}(e_j, x)e_j$), is dense in H. Thus, if $(x, e_j) = 0$ for some $x \in H$ and $\forall j \in \mathbb{N}$, then $x = 0$.

It can be shown that every separable Hilbert space has an orthonormal basis [73]. A Hilbert space is said to be separable if it has a countable orthonormal basis. $L^2(0, 1)$ is an example of a separable Hilbert space(see TheoremB.0.9 below). In practice, the solution to the SDEs in Hilbert space can be represented using countably (or finite) elements of the space; separability is very important in such situations.

Theorem B.0.7. *[73]*

Let $\{e_j\}_{j\in\mathbb{N}}$ be an orthonormal set in a separable Hilbert space H. Then

1. *$\sum_{j\in\mathbb{N}} |(e_j, x)|^2 \leq ||x||^2$ for all $x \in H$ (Bessel's inequality) and*
2. *$\sum_{j\in\mathbb{N}} |(e_j, x)|^2 = ||x||^2$(Parseval's equality), if and only if $x = \sum_{j\in\mathbb{N}}(e_j, x)e_j$. That is, Parseval's equality holds if and only if the orthonormal set $\{e_j\}_{j\in\mathbb{N}}$ forms a basis of H.*

Proof. The proof of this theorem can be found in [73]. □

Definition B.0.17. [73][**Fourier series, Fourier coefficient**]

A periodic function f with period $2L$ has a *Fourier series* given by

$$f(x) = \frac{a_0}{2} + \sum_{j=1}^{\infty} a_j \cos\frac{j\pi x}{L} + \sum_{j=1}^{\infty} b_j \sin\frac{j\pi x}{L}, \tag{B.1}$$

where

$$a_0 = \frac{1}{L}\int_{-L}^{L} f(x)dx,$$

$$a_j = \frac{1}{L}\int_{-L}^{L} f(x)\cos\frac{j\pi x}{L}dx,$$

and

$$b_j = \frac{1}{L}\int_{-L}^{L} f(x)\sin\frac{j\pi x}{L}dx.$$

a_0, a_j and b_j are called *Fourier coefficients* of $f(x)$.

In general, Fourier series may not converge, so the equality in the above series does not always hold. In fact, the main work in the field of harmonic analysis is concerned with discussing when this equality holds. For $L^2(0,1)$, the convergence of Fourier series is guaranteed as a result of TheoremB.0.9 and the following theorem which is known as **Riesz-Fisher theorem.**

Theorem B.0.8. *[5]*
For any orthonormal set $\{e_j, j \in \mathbb{N}\}$ *in* $L^2(0,1)$ *and any sequence* $\{c_j\}, j \in \mathbb{N}$ *in* $l^2(0,1)$*, the series* $\sum_{j=1}^{\infty} c_j e_j$ *converges in* $L^2(0,1)$*.*

Proof. For a proof of this theorem, see [5]. □

Definition B.0.18. [73][**even function, odd function**]
A function $f : [-L, L] \to \mathbb{R}$ is said to be an *even function* if

$$f(-x) = f(x) \quad \forall x \in [-L, L]$$

and an *odd function* if

$$f(-x) = -f(x) \quad \forall x \in [-L, L].$$

It is a simple matter to show that if $f(x)$, for all $x \in [-L, L]$, is an even function, then $b_j = 0$ in the Fourier expansion (B.1), for all $j \in \mathbb{N}$. The Fourier expansion of the even function f is then given by

$$f(x) = \frac{a_0}{2} + \sum_{j=1}^{\infty} a_j \cos \frac{j\pi x}{L},$$

where

$$a_0 = \frac{2}{L} \int_0^L f(x) dx,$$

and

$$a_j = \frac{2}{L} \int_0^L f(x) \cos \frac{j\pi x}{L} dx.$$

If $f(x)$, for all $x \in [-L, L]$, is an odd function, then $a_j = 0$, for all $j = 0, 1, 2, \cdots$ and therefore f has the Fourier expansion

$$f(x) = \sum_{j=1}^{\infty} b_j \sin \frac{j\pi x}{L},$$

where

$$b_j = \frac{2}{L} \int_0^L f(x) \sin \frac{j\pi x}{L} dx.$$

Theorem B.0.9. *[73]*

1. *The family* $\{1, e_j = \sqrt{2} \cos j\pi x, j \in \mathbb{N}\}$ *forms an orthonormal basis of* $L^2(0, 1)$.
2. *The family* $\{e_j = \sqrt{2} \sin j\pi x, j \in \mathbb{N}\}$ *also forms an orthonormal basis of* $L^2(0, 1)$.

Proof. See [73] for the proof of this theorem. □

Generally speaking, any function $f \in L^2(0, 1)$ can be written as an expansion of either a sine or a cosine series, depending on the boundary conditions of the problem.

An area of interest within the SPDEs field is operator theory, in particular linear operator theory. These operators act as transformations between normed vector spaces, thus playing an important role in the analysis and study of SPDEs. Here, we touch on only a few aspects of the theory. For more detail, see [70, 71, 73].

Definition B.0.19. [73][**bounded operator**]
The linear operator $T : U \to H$, where U and H are separable Hilbert spaces (or, in general, Banach spaces), is said to be a *bounded operator* if $||Tx||_H \leq C||x||_U$ for all $x \in U$ and some constant C. Throughout this work, we denote the norm on a Hilbert space by $||.||$ instead of $||.||_H$, for simplicity of notation.

The set of all bounded linear operators from U to H, denoted by $L(U,H)$, with the norm $||T||_{op} = ||T||_{L(U,H)} = \sup_{x\in U, x\neq 0} \frac{||Tx||}{||x||_U}$, forms a Banach space [73]. Moreover, if $T \in L(U,H)$, then $||Tx|| \leq ||T||_{op}.||x||_U, \forall x \in U$ [73]. If $U = H$, we abbreviate $L(H,H)$ to $L(H)$. From now on, U and H are assumed to be separable Hilbert spaces, unless otherwise stated.

Definition B.0.20. [71][**symmetric operator**]
Consider $T \in L(H)$. Then T is called a *symmetric operator* if

$$(Tu, v) = (u, Tv), \quad \text{for all} \quad u, v \in H.$$

Moreover, in this case, $||T||_{op} = \sup_{||u||=1} |(Tu, u)|, \quad \text{for all} \quad u \in H.$

Definition B.0.21. [71][**non-negative operator**]
An operator $T \in L(H)$ is a *non-negative operator* if

$$(Lu, u) \geq 0, \quad \text{for all} \quad u \in H.$$

Definition B.0.22. [71][**adjoint, self-adjoint operator**]
The *adjoint* of an operator $T \in L(H)$, where H is a Hilbert space, is an operator $T^* \in L(H)$ such that

$$(u, Tv) = (T^*u, v) \quad \forall u, v \in H.$$

Morover, the definition implies that $(T^*)^* = T$ and $(TS)^* = S^*T^*$. Furthermore, if $T = T^*$ then the operator T is called *self-adjoint or Hermitian.*

The existence and uniqueness of the adjoint operator T^* of T holds as a result of the following foundation theorem of Hilbert space theory, which is known as the **Riesz representation theorem.**

Theorem B.0.10. *[73]*
Let H be a Hilbert space and let H^* be its dual space (i.e. H^* is the space of all bounded linear functionals from H to $\mathbb{R}$). Then $\forall \varphi \in H^*$ there exists a unique $y \in H$

such that

$$\varphi(x) = (x, y), \quad \textit{for all} \quad x \in H.$$

Proof. The proof of this theorem can be found in [73]. □

Definition B.0.23. [70, 71][**nuclear operator**]

An operator $T \in L(U, H)$ is said to be a *nuclear operator* if there exists a sequence $(a_j)_{j\in\mathbb{N}}$ in H and a sequence $(b_j)_{j\in\mathbb{N}}$ in U such that

$$Tx = \sum_{j=1}^{\infty} a_j (b_j, x)_U, \quad \text{for all} \quad x \in U$$

and

$$\sum_{j=1}^{\infty} ||a_j|| ||b_j||_U < \infty.$$

The space of all nuclear operators from U to H, denoted by $L_1(U, H)$, forms a Banach space with norm [70]

$$||T||_{L_1} = \inf\{\sum_{j=1}^{\infty} ||a_j|| ||b_j||_U : Tx = \sum_{j=1}^{\infty} a_j (b_j, x)_U, \quad x \in U\}.$$

Furthermore, if $U = H$ and $T \in L_1(H)$ is a non-negative and symmetric operator, then T is called a *trace class* operator [70].

Definition B.0.24. [70, 71][**trace of operator**]

Let $T \in L(H)$ and $\{e_j, j \in \mathbb{N}\}$ be an orthonormal basis of H. Then *a trace* T is defined as

$$trT := \sum_{j=1}^{\infty} (Te_j, e_j).$$

We now introduce two propositions about the traces of nuclear operators, the proofs of which can be found in Appendix C in [70].

Proposition B.0.11. *[70, 71]*

Trace T *(*trT*), where* $T \in L_1(H)$*, is a well defined number, independent of the choice of orthonormal basis* $\{e_j, j \in N\}$*. Moreover,* $|trT| \leq ||T||_{L_1}$.

Proposition B.0.12. *[70]*

Let $T \in L(H)$ be a non-negative operator. T is then a nuclear operator if and only if, for an orthonormal basis $\{e_j, j \in \mathbb{N}\}$ on H, we have

$$trT = \sum_{j=1}^{\infty} (Te_j, e_j) < \infty.$$

Also, if this is the case, $trT = ||T||_{L_1}$.

Definition B.0.25. [70, 71][**Hilbert-Schmidt operator**]

An operator $T \in L(U, H)$ is called the *Hilbert-Schmidt operator* if

$$\sum_{j=1}^{\infty} ||Te_j||^2 < \infty,$$

where $\{e_j, j \in \mathbb{N}\}$ is an orthonormal basis of U. $L_2(U, H)$ denotes the space of all Hilbert-Schmidt operators from U to H. The definition of the Hilbert-Schmidt operator and the number

$$||T||_{L_2} = (\sum_{j=1}^{\infty} ||Te_j||^2)^{1/2}$$

are both independent of the choice of orthonormal basis [71].

Moreover, $||T||_{L_2} = ||T^*||_{L_2}$, where T^* is the adjoint operator of T [71].

Proposition B.0.13. *[70, 71]*

1. *Consider $L_2(U, H)$ and define*

$$(S, T)_{L_2} = \sum_{j=1}^{\infty} (Se_j, Te_j),$$

where $S, T \in U$ and $\{e_j, j \in \mathbb{N}\}$ is an orthonormal basis of U. Then $(L_2(U, H), (., .)_{L_2})$ is a separable Hilbert space. Moreover, if $\{f_k, k \in \mathbb{N}\}$ is an orthonormal basis of H, then the set of operators $f_k \otimes e_j := f_k(e_j, .)_U$, where $j, k \in \mathbb{N}$, is an orthonormal basis of $L_2(U, H)$.

2. Let $(G, (.,.)_G)$ be a further separable Hilbert space. If $T \in L_2(U, H)$ and $S \in L_2(H, G)$ then $ST \in L_1(U, G)$ and

$$||ST||_{L_1(U,G)} \leq ||S||_{L_2}.||T||_{L_2}.$$

Proof. See [70] for the proof of this proposition. □

Appendix C

Computer simulation codes

C.1 SDELab codes for simulating the stochastic FHN system

Code C.1.1: The FHN model with additive space-time noise

```
%%%%%%%%%%%%%%%%%%%%%%%%%%%%%%%%%%%%%%%%%%%%%%%%%%%%%%%%%%%%%%%%%%%%%%%%%%%%
% M-file for simulating the FHN  model with additive space-time     %
% white noise presented in Chapter2 using SDELab package            %
%%%%%%%%%%%%%%%%%%%%%%%%%%%%%%%%%%%%%%%%%%%%%%%%%%%%%%%%%%%%%%%%%%%%%%%%%%%%
d = 9;   %dimension of y
p = 9;   %dimension of w
tspan = [0,200];  %time interval
%%%%%%%%%%%%%%%%%%%%%%%%%%%%%%%%%%%%%%%%%%%%%%%%%%%%%%%%%%%%%%%%%%%%%%%%%%%%
%Compute the initial condition
a0_n=0.1/(exp(1)-1); b0_n=0.125; v0=a0_n/(a0_n+b0_n);
y0=[zeros(d,1);v0*ones(d,1)];
%%%%%%%%%%%%%%%%%%%%%%%%%%%%%%%%%%%%%%%%%%%%%%%%%%%%%%%%%%%%%%%%%%%%%%%%%%%%
% Define the drift and diffusion functions
```

```
fcn.drift='spdefh_drift'; fcn.diff_noise='spdefh_diff_noise';
%%%%%%%%%%%%%%%%%%%%%%%%%%%%%%%%%%%%%%%%%%%%%%%%%%%%%%%%%%%%%%%%%%%%%%%%
%Define the parameters of drift and diffusion functions
params.D=0.01; params.a=0.05; params.Mu=0.5; params.b=0.008;
params.gamma=0.5; params.sigma=0.005;
%%%%%%%%%%%%%%%%%%%%%%%%%%%%%%%%%%%%%%%%%%%%%%%%%%%%%%%%%%%%%%%%%%%%%%%%
%Choice the integration method and other options
opt.IntegrationMethod ='StrongItoEuler'; opt.MaxStepSize=1e-2;
opt.StrongItoEuler.Alpha=0.5; opt.MSIGenRNG.SeedZig = 23;
%%%%%%%%%%%%%%%%%%%%%%%%%%%%%%%%%%%%%%%%%%%%%%%%%%%%%%%%%%%%%%%%%%%%%%%%
 %Strong numerical solutions stored in [t,y]
[t,y]= sdesolve_strong_solutions (fcn,tspan,y0,m,opt,params)
%%%%%%%%%%%%%%%%%%%%%%%%%%%%%%%%%%%%%%%%%%%%%%%%%%%%%%%%%%%%%%%%%%%%%%%%
```

Code C.1.2: The drift function of the FHN model

```
%%%%%%%%%%%%%%%%%%%%%%%%%%%%%%%%%%%%%%%%%%%%%%%%%%%%%%%%%%%%%%%%%%%%%%%%
% M-file for the drift function of the SPDEs of the FHN  model      %
%%%%%%%%%%%%%%%%%%%%%%%%%%%%%%%%%%%%%%%%%%%%%%%%%%%%%%%%%%%%%%%%%%%%%%%%
function z=spdefh_drift(t,y,varargin)
%%%%%%%%%%%%%%%%%%%%%%%%%%%%%%%%%%%%%%%%%%%%%%%%%%%%%%%%%%%%%%%%%%%%%%%%
%Extract parameters
D=varargin{2}.D; Mu=varargin{2}.Mu; a=varargin{2}.a;
b=varargin{2}.b; q=varargin{2}.gamma; d=length(y)/2;
%%%%%%%%%%%%%%%%%%%%%%%%%%%%%%%%%%%%%%%%%%%%%%%%%%%%%%%%%%%%%%%%%%%%%%%%
%Compute drift function
A=-gallery('tridiag',d); %tridiagonal matrix A
u=y(1:d);          % u fast variable
v=y(d+1:end);      % v recovery variable
F=(u.*(1-u).*(u-a))-v;
```

```
B=D*((d+1)^2)*A*u;     % Approximation of Laplacian
z1=B+F+Mu; z2=b*(u-(gamma*v));
z=[z1;z2];             %Return values of drift
%%%%%%%%%%%%%%%%%%%%%%%%%%%%%%%%%%%%%%%%%%%%%%%%%%%%%%%%%%%%%%%%%%%%%%%%%%%
```

Code C.1.3: The diffusion function of FHN model

```
%%%%%%%%%%%%%%%%%%%%%%%%%%%%%%%%%%%%%%%%%%%%%%%%%%%%%%%%%%%%%%%%%%%%%%%%%%%
% M-file for the diffusion function of SPDEs of the FHN  model      %
%%%%%%%%%%%%%%%%%%%%%%%%%%%%%%%%%%%%%%%%%%%%%%%%%%%%%%%%%%%%%%%%%%%%%%%%%%%
function z=spdefh_diff_noise(t,y,dw,flag,varargin)
sigma=varargin{2}.sigma;    % Extract parameter
p=length(dw); d=p;
%%%%%%%%%%%%%%%%%%%%%%%%%%%%%%%%%%%%%%%%%%%%%%%%%%%%%%%%%%%%%%%%%%%%%%%%%%%
% Compute Q_ij=sqrt(2)*sin(i*j*pi/(d+1)),i,j=1,2,...,d.
Q=sqrt(d+1)*gallery('orthog', d,1);
%%%%%%%%%%%%%%%%%%%%%%%%%%%%%%%%%%%%%%%%%%%%%%%%%%%%%%%%%%%%%%%%%%%%%%%%%%%
%Compute the diffusion function
if(flag)
    z=[sigma*Q;zeros(m)];
else
    z=[sigma*(Q*dw);zeros(m,1)];
end
%%%%%%%%%%%%%%%%%%%%%%%%%%%%%%%%%%%%%%%%%%%%%%%%%%%%%%%%%%%%%%%%%%%%%%%%%%%
```

C.2 MATLAB M-files for simulation of FET of one-dimensional neural diffusion models

Code C.2.1: The exponential time-stepping Euler method with boundary test

```
%%%%%%%%%%%%%%%%%%%%%%%%%%%%%%%%%%%%%%%%%%%%%%%%%%%%%%%%%%%%%%%%%%%%%%%%%%%%
% The exponential time-stepping Euler method with boundary test     %
% for simulating the mean first exit time of one dimensional        %
% diffusion represented by the space-clamped FitzHugh Nagumo        %
% system with additive noise presented in Chapter3.                 %
%%%%%%%%%%%%%%%%%%%%%%%%%%%%%%%%%%%%%%%%%%%%%%%%%%%%%%%%%%%%%%%%%%%%%%%%%%%%
Lp=100;
%Define mean, variance and standard deviation of the FET
Tm=zeros(Lp,1); Vm=zeros(Lp,1); stdev=zeros(Lp,1);
err=zeros(Lp,1); Verr=zeros(Lp,1); % Error and the variance of error
%%%%%%%%%%%%%%%%%%%%%%%%%%%%%%%%%%%%%%%%%%%%%%%%%%%%%%%%%%%%%%%%%%%%%%%%%%%%
a=0.1;b=0.6;I=1.5; y0=1;%The physical parameters of the system
exact=0.1287;%Analytical solutions of (3.77).
%%%%%%%%%%%%%%%%%%%%%%%%%%%%%%%%%%%%%%%%%%%%%%%%%%%%%%%%%%%%%%%%%%%%%%%%%%%%
 Delta_t=0.0005; % The mean of exponential time step delta_t
 lambda=1/Delta_t; % The parameter of the exponential time step delta_t
 sigma_t=5; % Noise intensity
%%%%%%%%%%%%%%%%%%%%%%%%%%%%%%%%%%%%%%%%%%%%%%%%%%%%%%%%%%%%%%%%%%%%%%%%%%%%
for nerr=1:Lp % Loop to calculate average of the error
M=100000; K=zeros(M,1); V=zeros(M,1);
for j=1:M  %Loop to simulate the MFET
    x0=0;
    i=0;
```

```
for i=1:Inf %Loop to calculate the FET
    u=rand;v=rand;w=rand; %Uniformly distributed random variables
    p=-log(v);  %Exponentially distributed random variable
%%%%%%%%%%%%%%%%%%%%%%%%%%%%%%%%%%%%%%%%%%%%%%%%%%%%%%%%%%%%%%%%%%%%%%%%%%%%
% The quantities required to calculate x(delta t), see Chapter3
    Mu=0.5*x0*(x0-a)*(1-x0);
    f_t=Mu-y0+I;
    F_t=f_t/(sigma_t^2);
    N_t=sqrt((2*lambda/(sigma_t^2))+(F_t^2));
    s=sign(0.5*(1+(F_t/N_t))-u);
    x1=x0+((1/(N_t-s*F_t))*s*p); %Generate x(delta t)
    m=max(x0,x1);
%%%%%%%%%%%%%%%%%%%%%%%%%%%%%%%%%%%%%%%%%%%%%%%%%%%%%%%%%%%%%%%%%%%%%%%%%%%%
%The probability that b was hit before the end of the time step
    r=exp(-2*N_t*(b-m));
%Boundary test if b was hit during the time step
    if (x1>b)||(w<r)
      %if (x1>b)
       K(j)=i/lambda; %Elapsed time after i time steps
        break;
end
%%%%%%%%%%%%%%%%%%%%%%%%%%%%%%%%%%%%%%%%%%%%%%%%%%%%%%%%%%%%%%%%%%%%%%%%%%%%
    x0=x1;
end
%%%%%%%%%%%%%%%%%%%%%%%%%%%%%%%%%%%%%%%%%%%%%%%%%%%%%%%%%%%%%%%%%%%%%%%%%%%%
end
%%%%%%%%%%%%%%%%%%%%%%%%%%%%%%%%%%%%%%%%%%%%%%%%%%%%%%%%%%%%%%%%%%%%%%%%%%%%
Tm(nerr)=mean(K); %The mean of FET for each nerr
%%%%%%%%%%%%%%%%%%%%%%%%%%%%%%%%%%%%%%%%%%%%%%%%%%%%%%%%%%%%%%%%%%%%%%%%%%%%
```

```
for j=1:M
        V(j)=(K(j)-Tm(nerr))^2;
end
Vm(nerr)=sum(V)/(M-1); %Variance of FET for each nerr
stdev(nerr)=sqrt(Vm(nerr)/M);%Standard deviation of FET for each nerr
%%%%%%%%%%%%%%%%%%%%%%%%%%%%%%%%%%%%%%%%%%%%%%%%%%%%%%%%%%%%%%%%%%%%%%%%%%%
err(nerr)=(Tm(nerr)-exact); %calculate the systematic error for each nerr
end
%%%%%%%%%%%%%%%%%%%%%%%%%%%%%%%%%%%%%%%%%%%%%%%%%%%%%%%%%%%%%%%%%%%%%%%%%%%
%TmC=mean(Tm); VmC=mean(Vm); stdevC=mean(stdev);
errC=abs(mean(err)) % Calculate the mean of systematic error
for i=1:Lp
    Verr(i)=(err(i)-errC)^2; %Calculate the variance of systematic error
end
%The unbiased estimator of variance of error.
VerrC=sum(Verr)/(Lp-1);
%The bound of 95% confidence interval of error.
stdeverrC=sqrt(VerrC/Lp)
%%%%%%%%%%%%%%%%%%%%%%%%%%%%%%%%%%%%%%%%%%%%%%%%%%%%%%%%%%%%%%%%%%%%%%%%%%%
```

Code C.2.2: The fixed timestepping Euler method with boundary test

```
%%%%%%%%%%%%%%%%%%%%%%%%%%%%%%%%%%%%%%%%%%%%%%%%%%%%%%%%%%%%%%%%%%%%%%%%%%%
% The fixed time-stepping Euler method with boundary test           %
% for simulating the mean first exit time of one dimensional        %
% diffusion represented by the space-clamped FitzHugh Nagumo        %
% system with additive noise defined in Chapter3.                   %
%%%%%%%%%%%%%%%%%%%%%%%%%%%%%%%%%%%%%%%%%%%%%%%%%%%%%%%%%%%%%%%%%%%%%%%%%%%
Lp=100;
%Define mean, variance and standard deviation of the FET
```

```
Tm=zeros(Lp,1); Vm=zeros(Lp,1); stdev=zeros(Lp,1);
err=zeros(Lp,1); Verr=zeros(Lp,1); % Error and the variance of error
%%%%%%%%%%%%%%%%%%%%%%%%%%%%%%%%%%%%%%%%%%%%%%%%%%%%%%%%%%%%%%%%%%%%%%%%
a=0.1;b=0.6;I=1.5; y0=1;%The physical parameters of the system
exact=0.1287;%Analytical solutions of (3.77).
%%%%%%%%%%%%%%%%%%%%%%%%%%%%%%%%%%%%%%%%%%%%%%%%%%%%%%%%%%%%%%%%%%%%%%%%
Delta_t=0.0005;sigma=5; %Fixed time step and noise intensity
%%%%%%%%%%%%%%%%%%%%%%%%%%%%%%%%%%%%%%%%%%%%%%%%%%%%%%%%%%%%%%%%%%%%%%%%
for nerr=1:Lp % Loop to calculate average of the error
M=100000;
T=zeros(M,1);V=zeros(M,1);
for j=1:M %Loop to simulate the MFET
    x0=0; %Initial data
    for k=1:Inf %Loop to calculate the FET
        n=sqrt(Delta_t)*randn; %Generate the Gaussian samples
         w=rand; %Uniformly distributed random variable
        f=0.5*x0*(x0-a)*(1-x0);
        Mu=f-y0+I; % Calculate the drift term
        x1=x0+Mu*Delta_t + (sigma*n); %Generate x1(Delta_t)
%%%%%%%%%%%%%%%%%%%%%%%%%%%%%%%%%%%%%%%%%%%%%%%%%%%%%%%%%%%%%%%%%%%%%%%%
%The probability that b was hit before the end of the time step
       B=exp(-2*(b-x0)*(b-x1)/((sigma^2)*delta));
%Boundary test if b was hit during the time step
       if (x1>=b)||(w<B)
        %if (x1>b)
            T(j)=k*delta; %Elapsed time after k time steps
            break;
        end
%%%%%%%%%%%%%%%%%%%%%%%%%%%%%%%%%%%%%%%%%%%%%%%%%%%%%%%%%%%%%%%%%%%%%%%%
```

```
        x0=x1;
    end
%%%%%%%%%%%%%%%%%%%%%%%%%%%%%%%%%%%%%%%%%%%%%%%%%%%%%%%%%%%%%%%%%%%%%%%%%%%%
end
%%%%%%%%%%%%%%%%%%%%%%%%%%%%%%%%%%%%%%%%%%%%%%%%%%%%%%%%%%%%%%%%%%%%%%%%%%%%
 Tm(nerr)=mean(T); %The mean of FET for each nerr
    for j=1:M
        V(j)=(T(j)-Tm(nerr))^2;
    end
%The variance and standard deviation of FET for each nerr
Vm(nerr)=sum(V)/(M-1);stdev(nerr)=sqrt(Vm(nerr)/M);
 err(nerr)=(Tm(nerr)-exact);
end
%%%%%%%%%%%%%%%%%%%%%%%%%%%%%%%%%%%%%%%%%%%%%%%%%%%%%%%%%%%%%%%%%%%%%%%%%%%%
TmC=mean(Tm);VmC=mean(Vm);stdevC=mean(stdev);
errC=mean(err)%Calculate the mean of systematic error
for i=1:Lp
    Verr(i)=(err(i)-errC)^2;
end
%The unbiased estimator of variance of error.
VerrC=sum(Verr)/(Lp-1);
%The bound of 95% confidence interval of error.
stdeverrC=sqrt(VerrC/Lp)
%%%%%%%%%%%%%%%%%%%%%%%%%%%%%%%%%%%%%%%%%%%%%%%%%%%%%%%%%%%%%%%%%%%%%%%%%%%%
```

C.3 MATLAB M-files of the simulation of the stochastic Barkley system and the reduced model

Code C.3.1: Numerical simulation of the stochastic Barkley system

```
%%%%%%%%%%%%%%%%%%%%%%%%%%%%%%%%%%%%%%%%%%%%%%%%%%%%%%%%%%%%%%%%%%%%%%%%%%%%
%Simulation of the Barkley model with additive noise, white         %
%in time and correlated in space using numerical technique          %
%presented in Chapter 4 (Section 4.4).                              %
%%%%%%%%%%%%%%%%%%%%%%%%%%%%%%%%%%%%%%%%%%%%%%%%%%%%%%%%%%%%%%%%%%%%%%%%%%%%
params=[];
M=2000; % Number of samples
N=1024;delta=0.01;L=400;sigma=0.09; %Parameters of the system
params.delta=delta; %Time step
params.sigma=sigma; %Noise intensity
params.L=L;         % Length of space domain
params.xi=2;        % Length of spatial correlation
b1=0.275; % Threshold of nucleation of a single wave
b2=0.008 % small boundary layer
x1=zeros(N,1); % The activator variable
Wdiff=zeros(N,1); % The noise
T=zeros(M,1); % First exit times (nucleation times)
V=zeros(M,1); %Variance of FET
Tnuc=zeros(M,1); % Nucleation times of a single wave
Tann=zeros(M,1); % Annihilation times of a single wave
Tlif=zeros(M,1); % Lifetimes of a single wave
Vlif=zeros(M,1); % Variance of lifetimes
% count=0; lambdasum=0;
%%%%%%%%%%%%%%%%%%%%%%%%%%%%%%%%%%%%%%%%%%%%%%%%%%%%%%%%%%%%%%%%%%%%%%%%%%%%
```

```
for j=1:M
    r3=0;r4=0;
    u0=r3*ones(N,1);
    v0=r4*ones(N,1);
    x0=[u0;v0];   %initial condition
   Maxtime=500000;
  x1norm=zeros(Maxtime,1);
  %lambda1=zeros(Maxtime,1);
    for k=1:Maxtime
%%%%%%%%%%%%%%%%%%%%%%%%%%%%%%%%%%%%%%%%%%%%%%%%%%%%%%%%%%%%%%%%%%%%%%%%%%%%
        %Recall subroutine SPTBKBC (code C.3.1.1)
        % to generate updates and to generate the noise
       [x1,Diffw]=SPTBKBC(x0,params);
      % L*norm(Diffw)^2
%%%%%%%%%%%%%%%%%%%%%%%%%%%%%%%%%%%%%%%%%%%%%%%%%%%%%%%%%%%%%%%%%%%%%%%%%%%%
      %Maximum values of the activator over x
        %x1norm(k)=max(x1(1:N));
        %u(:,k)=x1(1:N);
%%%%%%%%%%%%%%%%%%%%%%%%%%%%%%%%%%%%%%%%%%%%%%%%%%%%%%%%%%%%%%%%%%%%%%%%%%%%
  % To calculate the probability of the excitable part of
  %the phase space of the system
        %ux=x1(1:N);
     %lambda1(k)=sum(ux>=0.9)/length(ux);
      %  lambdasum=lambdasum+lambda1(k); count=count+1;
       %  [k*delta,lambda1(k),lambdasum/count];
%%%%%%%%%%%%%%%%%%%%%%%%%%%%%%%%%%%%%%%%%%%%%%%%%%%%%%%%%%%%%%%%%%%%%%%%%%%%
%Plot the activator variable along space domain
     % subplot(1,2,1);
   %plot(x1);     axis([0,N,0,1]); grid on
```

```
%Plot the maximum value of u over x as a function of time
    %  subplot(1,2,2); plot(x1norm); grid on
     %   drawnow;
%%%%%%%%%%%%%%%%%%%%%%%%%%%%%%%%%%%%%%%%%%%%%%%%%%%%%%%%%%%%%%%%%%%%%%%%%%%%
% The criteria of FET or the nucleation time of a traveling single wave
      % if x1norm(k)>b1
       %     T(j)=k*delta;
        %    break;
        %end
%%%%%%%%%%%%%%%%%%%%%%%%%%%%%%%%%%%%%%%%%%%%%%%%%%%%%%%%%%%%%%%%%%%%%%%%%%%%
         x0=x1;
   end
%%%%%%%%%%%%%%%%%%%%%%%%%%%%%%%%%%%%%%%%%%%%%%%%%%%%%%%%%%%%%%%%%%%%%%%%%%%%
  % Calculate the lifetime of a single wave
    %Tannc=find(x1norm>=b1);
    %Tnuc(j)=Tannc(1)*delta;
    %for i=Tannc(1):Maxtime
     % if x1norm(i)<b2
    %Tann(j)=i*delta;
   % break;
    %  end
    %end
     %Tlif(j)=Tann(j)-Tnuc(j);
end
%%%%%%%%%%%%%%%%%%%%%%%%%%%%%%%%%%%%%%%%%%%%%%%%%%%%%%%%%%%%%%%%%%%%%%%%%%%%
%Calculate the MFET or the mean nucleation time
%Tm=mean(T)
%for j=1:M
 %       V(j)=(T(j)-Tm)^2;
```

```
%end
%Vm=sum(V)/(M-1)%The unbiased estimator of variance of FET
%stdev=sqrt(Vm/M) %The bound of 95% confidence interval of FET.
%%%%%%%%%%%%%%%%%%%%%%%%%%%%%%%%%%%%%%%%%%%%%%%%%%%%%%%%%%%%%%%%%%%%%%%%%%%%
%Calculate the mean lifetime of a single wave
%Tmlif=mean(Tlif)
%for j=1:M
 %       Vlif(j)=(Tlif(j)-Tmlif)^2;
%end
%Vmlif=sum(Vlif)/(M-1)%The unbiased estimator of variance of lifetime
%stlif=sqrt(Vmlif/M)%The bound of 95% confidence interval of lifetime.
%%%%%%%%%%%%%%%%%%%%%%%%%%%%%%%%%%%%%%%%%%%%%%%%%%%%%%%%%%%%%%%%%%%%%%%%%%%%
```

Code C.3.1.1: Subroutine of the simulation of the Barkley model

```
%%%%%%%%%%%%%%%%%%%%%%%%%%%%%%%%%%%%%%%%%%%%%%%%%%%%%%%%%%%%%%%%%%%%%%%%%%%%
%The subroutine SPTBKBC to generate updates                              %
% and to generate the noise                                              %
%%%%%%%%%%%%%%%%%%%%%%%%%%%%%%%%%%%%%%%%%%%%%%%%%%%%%%%%%%%%%%%%%%%%%%%%%%%%
  function [z,Diff]=SPTBKBC(y,varargin);
delta=varargin{1}.delta; %Time step
sigma=varargin{1}.sigma; %Noise intensity
    L=varargin{1}.L;    % The length of space domain
    xi=varargin{1}.xi; % Length of spatial correlation
 N=length(y)/2;
 u0=y(1:N); % Activator variable
 v0=y(N+1:end); % Inhibitor variable
%%%%%%%%%%%%%%%%%%%%%%%%%%%%%%%%%%%%%%%%%%%%%%%%%%%%%%%%%%%%%%%%%%%%%%%%%%%%
  a=0.75; b=0.01; eps=0.02; D=1; %The physical parameters of the system
%%%%%%%%%%%%%%%%%%%%%%%%%%%%%%%%%%%%%%%%%%%%%%%%%%%%%%%%%%%%%%%%%%%%%%%%%%%%
```

```
  %Generate eigenvalues of Laplacian
  %using spectral method (see Chapter4,Section 4.3)
%%%%%%%%%%%%%%%%%%%%%%%%%%%%%%%%%%%%%%%%%%%%%%%%%%%%%%%%%%%%%%%%%%%%%%%%%%%%
  lambda=zeros(N,1);
  for k=1:N
  lambda(k)=(2*(k-1)*pi/L)^2;
  end
  diffus1=zeros(N,1);
  for j=1:N
  %Geometric integrator to preserve the eigenvalues
 diffus1(j)=exp(-(D*delta)*lambda(j));
  end
%%%%%%%%%%%%%%%%%%%%%%%%%%%%%%%%%%%%%%%%%%%%%%%%%%%%%%%%%%%%%%%%%%%%%%%%%%%%
% Generating the noise using FFT method: (see Chapter4, Section 4.2)
%%%%%%%%%%%%%%%%%%%%%%%%%%%%%%%%%%%%%%%%%%%%%%%%%%%%%%%%%%%%%%%%%%%%%%%%%%%%
  % (1)Calculate alpha
  alph=zeros(N,1);
  alph(1)=1;
  alph(N/2+1)=((1/(2*sqrt(2))))*exp((-(xi^2)*lambda(N/2+1))/2*pi);
  for j=2:N/2
       alph(j)=((1/(2*sqrt(2))))*exp((-(xi^2)*lambda(j))/2*pi);
       alph(N-j+2)=alph(j);
  end
%%%%%%%%%%%%%%%%%%%%%%%%%%%%%%%%%%%%%%%%%%%%%%%%%%%%%%%%%%%%%%%%%%%%%%%%%%%%
  % (2)Generate complex numbers with random variables parts
  zcom=zeros(N,1);
  zcom(1)=((sigma/sqrt(L))*sqrt(delta))*randn;
  zcom(N/2+1)=((sigma/sqrt(L))*sqrt(delta))*complex(randn,-randn);
  for j=2:N/2
```

```
      zcom(j)=((sigma/sqrt(L))*sqrt(delta))*complex(randn,-randn);
      zcom(N-j+2)=conj(zcom(j));
  end
%%%%%%%%%%%%%%%%%%%%%%%%%%%%%%%%%%%%%%%%%%%%%%%%%%%%%%%%%%%%%%%%%%%%%%%%%%%%
  %(3)Approximate of sigma*W(t,x)
   Diff=alph.*zcom;
%Diffw=ifft(Diff,'symmetric')*length(Diff); %The approximation of noise
%%%%%%%%%%%%%%%%%%%%%%%%%%%%%%%%%%%%%%%%%%%%%%%%%%%%%%%%%%%%%%%%%%%%%%%%%%%%
%Updating the activator and inhibitor variables (see Chapter4,Section 4.4)
%%%%%%%%%%%%%%%%%%%%%%%%%%%%%%%%%%%%%%%%%%%%%%%%%%%%%%%%%%%%%%%%%%%%%%%%%%%%
  z0=fft(u0); %Using FFT
  z3=(z0.*diffus1)+(Diff*length(Diff));
  u05=ifft(z3,'symmetric');
  %Apply the modified reaction terms
  f=(u05.*(1-u05).*(u05-((v0+b)/a)))/eps;
  g=u05-v0;
  for j=1:N
    if u05(j)>=1
      f(j)=-abs(f(j));
    end
  if v0(j)<0
     g(j)=abs(g(j));
  end
  end
  z1=u05+(f*delta); %Generate the activator
  z2=v0+(g*delta);  %Generate the inhibitor
  z=[z1;z2];
%%%%%%%%%%%%%%%%%%%%%%%%%%%%%%%%%%%%%%%%%%%%%%%%%%%%%%%%%%%%%%%%%%%%%%%%%%%%
```

Code C.3.2: The reduced model of the dynamics of the Barkley system

```
%%%%%%%%%%%%%%%%%%%%%%%%%%%%%%%%%%%%%%%%%%%%%%%%%%%%%%%%%%%%%%%%%%%%%%%%%%%%
% Simple, reduced model of the dynamics of the traveling waves      %
% of the Barkley model                                              %
%%%%%%%%%%%%%%%%%%%%%%%%%%%%%%%%%%%%%%%%%%%%%%%%%%%%%%%%%%%%%%%%%%%%%%%%%%%%
lambda=1/17.78;Tdiff=1.44;
%lambda=10/31.4;Tdiff=1.7;
L=400;N=30;v_m=0.75;T_fin=30;
a=0.75; b=0.01; eps=0.02; %The physical parameters of the system
c=(1-2*(b/a))/sqrt(2*eps); % The asymptotic wave speed
w=c*log(1/(1-v_m));      %The analytical value of wave width
M=1000;                  %The number of samples
%LLT=zeros(2*N,M);
%RLT=zeros(2*N,M);
mkink=zeros(M,1);
mantik=zeros(M,1);
Vkink=zeros(M,1);
%%%%%%%%%%%%%%%%%%%%%%%%%%%%%%%%%%%%%%%%%%%%%%%%%%%%%%%%%%%%%%%%%%%%%%%%%%%%
for k=1:M
x=zeros(3*N,1);
x_f=zeros(6*N,1);
T=zeros(3*N,1);
T1=zeros(3*N,1);
T_f=zeros(6*N,1);
%figure(2);clf;hold on
%%%%%%%%%%%%%%%%%%%%%%%%%%%%%%%%%%%%%%%%%%%%%%%%%%%%%%%%%%%%%%%%%%%%%%%%%%%%
%simulate the exponential distributed random variable: time T
u=rand;
```

```
T(1)=-(1/lambda)*log(u);
T1(1)=T(1)+Tdiff;
T(1+N)=T(1)+1e-10;
T1(1+N)=T1(1)+1e-12;
T(1+2*N)=T(1)+1e-11;
T1(1+2*N)=T1(1)+1e-13;
for i=2:N;
    u=rand;
    T(i)=T(i-1)-(1/lambda)*log(u);
    T1(i)=T(i)+Tdiff;
    T(i+N)=T(i)+1e-10;
    T1(i+N)=T1(i)+1e-12;
    T(i+2*N)=T(i)+1e-11;
    T1(i+2*N)=T1(i)+1e-13;
end
for i=1:3*N
    T_f(2*i-1)=T(i);
    T_f(2*i)=T1(i);
end
%%%%%%%%%%%%%%%%%%%%%%%%%%%%%%%%%%%%%%%%%%%%%%%%%%%%%%%%%%%%%%%%%%%%%%%%%%%%
%simulate uniformly distributed random variable: position x on [0,L]
y=L*rand(N,1);
x(1:N)= y;
x(N+1:2*N)=y-L;
x(2*N+1:3*N)=y+L;
for i=1:N-1
    for j=i+1:N
        r=abs(x(i)-x(j));
        while(r<w)
```

```
            r=abs(x(i)-x(j));
            x(j)=L*rand;
            x(j+N)=x(j)-L;
            x(j+2*N)=x(j)+L;
        end
    end
end
%%%%%%%%%%%%%%%%%%%%%%%%%%%%%%%%%%%%%%%%%%%%%%%%%%%%%%%%%%%%%%%%%%%%%%%%%%%%
for i=1:3*N
    x_f(2*i-1)=x(i);
    x_f(2*i)=x(i);
end
%%%%%%%%%%%%%%%%%%%%%%%%%%%%%%%%%%%%%%%%%%%%%%%%%%%%%%%%%%%%%%%%%%%%%%%%%%%%
N1=6*N;
% mark all nucleation points
%plot(x_f, T_f, 'r.','MarkerSize',10);
%%%%%%%%%%%%%%%%%%%%%%%%%%%%%%%%%%%%%%%%%%%%%%%%%%%%%%%%%%%%%%%%%%%%%%%%%%%%
tc1=zeros(N1);
xc1=zeros(N1);
Lann=Inf(N1,1); %times of annihilation of left wave
Rann=Inf(N1,1); % times of annihilation of right wave
%axis([0 L 0 100]);
%box on
Tann=0;
%%%%%%%%%%%%%%%%%%%%%%%%%%%%%%%%%%%%%%%%%%%%%%%%%%%%%%%%%%%%%%%%%%%%%%%%%%%%
for i=1:2*N1
% Subroutine code3 (code C.3.2.1)
    [tc1,  xc1]=code3(T_f,x_f,c,N1,Tann,Lann,Rann);
    % compute crossing points
```

```
    [tminrow, row_X]=min(tc1);
    [T_LR,col]=min(tminrow);
    row=row_X(col) ;
%%%%%%%%%%%%%%%%%%%%%%%%%%%%%%%%%%%%%%%%%%%%%%%%%%%%%%%%%%%%%%%%%%%%%%%%%%%%
    % find first crossing point and position in matrix (row,col)
    if(T_LR<Inf)
        Tann=T_LR;
        Xann=xc1(row,col); %annihilation position
        Lann(col)=Tann;
        Rann(row)=Tann; % these waves are annihilated
        T_L=T_f(row); X_L=x_f(row); % creation of left wave
        T_R=T_f(col); X_R=x_f(col); % creation of right wave
    end
    %if (Tann<Inf)
     %   plot([X_R, Xann],[T_R, Tann]);
      %  plot([X_L, Xann],[T_L, Tann]);
       % plot(Xann,Tann,'g*');
    %end
end
%%%%%%%%%%%%%%%%%%%%%%%%%%%%%%%%%%%%%%%%%%%%%%%%%%%%%%%%%%%%%%%%%%%%%%%%%%%%
% plot all still alive
Textra=80;
%for i=1:N1,
 %   if Lann(i)==Inf
  %      plot([x_f(i),x_f(i)-c*(Textra)],[T_f(i),T_f(i)+Textra]);
   %     plot(x_f(i)-c*(Textra),T_f(i)+Textra,'y*');
    %end
     % if Rann(i)==Inf
      %    plot([x_f(i),x_f(i)+c*(Textra)],[T_f(i),T_f(i)+Textra]);
```

```
       %   plot(x_f(i)+c*(Textra),T_f(i)+Textra,'y*');
      %end
%end
%for i=1:2*N
 %   RLT(i,k)=Rann(i)-T_f(i);%compute lifetime of right wave
  %  LLT(i,k)=Lann(i)-T_f(i);%compute lifetime of left wave
%end
%%%%%%%%%%%%%%%%%%%%%%%%%%%%%%%%%%%%%%%%%%%%%%%%%%%%%%%%%%%%%%%%%%%%%%%%%%%%
%Calculate the number of kinks
numkink=0;
for i=1:2*N
    if Rann(i)>=T_fin && T_f(i)<=T_fin
        numkink=numkink+1;
    end
end
numantik=0;
for i=1:2*N
    if Lann(i)>=T_fin && T_f(i)<=T_fin
        numantik=numantik+1;
    end
end
mkink(k)=numkink;
mantik(k)=numantik;
end
%%%%%%%%%%%%%%%%%%%%%%%%%%%%%%%%%%%%%%%%%%%%%%%%%%%%%%%%%%%%%%%%%%%%%%%%%%%%
Meankink=mean(mkink)
Meanantik=mean(mantik)
for j=1:M
        Vkink(j)=(mkink(j)-Meankink)^2;
```

```
end
Vmkink=sum(Vkink)/(M-1)
stkink=sqrt(Vmkink/M)
%%%%%%%%%%%%%%%%%%%%%%%%%%%%%%%%%%%%%%%%%%%%%%%%%%%%%%%%%%%%%%%%%%%%%%%%%%%%
%MRLT=zeros(N,1);
%MLLT=zeros(N,1);
 %   MRLT=mean(RLT,2);
  %  MLLT=mean(LLT,2);
   % MRLT'
    %MLLT'
%hold off;
%%%%%%%%%%%%%%%%%%%%%%%%%%%%%%%%%%%%%%%%%%%%%%%%%%%%%%%%%%%%%%%%%%%%%%%%%%%%
```

Code C.3.2.1: The subroutine of the reduced model of the dynamics of the Barkley system

```
%%%%%%%%%%%%%%%%%%%%%%%%%%%%%%%%%%%%%%%%%%%%%%%%%%%%%%%%%%%%%%%%%%%%%%%%%%%%
 function [tc1,  xc1]=code3(T,x,c,N, tcurrent, Lann, Rann)
% T nucleation times at positions given in x
% c wave speed.
% N number of particles
% tcurrent current time
% Lann, Rann are annihilation times of left,right waves.
% tc1 matrix of crossing of i moving left, j moving right
%   infinity indicates no crossing after tcurrent
% xc1 position of crossing
%%%%%%%%%%%%%%%%%%%%%%%%%%%%%%%%%%%%%%%%%%%%%%%%%%%%%%%%%%%%%%%%%%%%%%%%%%%%
tc1=zeros(N);
xc1=zeros(N);
for i=1:N,
```

```
    if (Rann(i) > tcurrent) % right wave allive
        for j=1:N
            if (Lann(j)>tcurrent)% left wave allive
                tc(i,j)=(T(i)+T(j))/2-((x(i)-x(j))/(2*c));
                xc(i,j)=x(i)+(c*tc(i,j))-(c*T(i));
                if (tc(i,j)>T(i) && tc(i,j)>T(j))
                    tc1(i,j)=tc(i,j);
                    xc1(i,j)=xc(i,j);
                end
            end
        end
    end
end
tc1   (tc1<=tcurrent)=Inf;
%%%%%%%%%%%%%%%%%%%%%%%%%%%%%%%%%%%%%%%%%%%%%%%%%%%%%%%%%%%%%%%%%%%%%%%%%%%%%%%
```

Bibliography

[1] Hasan Alzubaidi, Hagen Gilsing, and Tony Shardlow. Numerical simulations of SDEs and SPDEs from neural systems. In Carlo Laing and Gabriel Lord, editors, *Stochastic methods in neuroscience*, chapter 12, pages 346–366. Oxford University Press, UK, 2010.

[2] D. Barkley. A model for fast computer simulation of waves in excitable media. *Physica D: Nonlinear Phenomena*, 49:61–70, 1991.

[3] R. Bhattacharya and E. C. Waymire. *Stochastic processes with applications*. John Wiley and Sons, Inc, USA, 1990.

[4] E. Bibbona, G. Panfilo, and P. Tavella. The Ornstein-Uhlenbeck process as a model of a low pass filtered white noise. *Metrologia*, 45:S117–S126, 2008.

[5] V. Bogachev. *Measure Theory*, volume I, chapter 4. Springer-Verlag Berlin, 2007.

[6] A. N. Borodin and P. Salminen. *Handbook of Brownian motion: facts and formulae*. Birkhäuser Verlage, Basel, 2002.

[7] M. Bttiker and T. Christen. Nucleation of weakly driven kinks. *Physical Review Letters*, 75(10):1895–1898, 1995.

[8] F.M. Buchmann. Computing exit times with Euler scheme. Technical Report 2003-02, Seminar für Angewandte Mathematik, Eidgenössische Technische Hochschule, 2003.

[9] F.M. Buchmann. Simulation of stopped diffusions. *Journal of Computational Physics*, 202:446–462, 2005.

[10] R. Bürger, R. Ruiz-Baier, and K. Schneider. Adaptive multiresolution methods for the simulation of waves in excitable media. *Journal of Scientific Computing*, 43(2):261–290, 2010.

[11] G. Cerbone, L. M. Ricciardi, and L. Sacerdote. Mean variance and skewness of the first passage time for the Ornstein-Uhlenbeck process. *Cybernetics and Systems*, 12:395–429, 1981.

[12] P. J. Collins. *Differential and integral equations.* Oxford University Press,UK, 2006.

[13] J. W. Cooley and J. W. Tukey. An algorithm for the machine calculation of complex Fourier series. *Mathematics of Computation*, 19(90):297–301, 1965.

[14] B. Costa. Spectral methods for partial differential equations. *CUBO,A Mathematical Journal*, 6(34):1–32, 2004.

[15] A. M. Davie and J. G. Gaines. Convergence of numerical schemes for the solution of parabolic stochastic partial differential equations. *Mathematics of Computation*, 70(233):121–134, 2001.

[16] S. Ditlevsen and O. Ditlevsen. Parameter estimation from observations of first-passage times of the Ornstein-Uhlenbeck process and the feller process. *Probabilistic Engineering Mechanics*, 23:170–179, 2008.

[17] P. Duhamel and M. Vetterli. Fast Fourier transforms: A tutorial review and a state of the art. *Signal Processing*, 19:259–299, 1990.

[18] A. Etheridge. *A Course in Financial Calculus.* Cambridge University Press, UK, 2002.

[19] R. FitzHugh. Thresholds and plateaus in the Hodgkin-Huxley nerve equations. *Journal of General Physiology*, 43:867–896, 1960.

[20] R. FitzHugh. Impulses and physiological states in theoretical models of nerve membrane. *Biophysical Journal*, 1:445–466, 1961.

[21] M. Frigo and S. G. Johnson. FFTW: An adaptive software architecture for the FFT. In *IEEE International Conference on Acoustics Speech and Signal Processing*, volume 3, pages III–1381–III–1384, 1998.

[22] M. Frigo and S. G. Johnson. The design and implementation of FFTW3. In *Proceedings of the IEEE*, volume 93, pages 216–231, 2005.

[23] J. G. Gaines. Numerical experiments with S(P)DEs. In A. M. Etheridge, editor, *Stochastic Partial Differential Equations*, London Mathematical Society Lecture Note Series 216, pages 55–71. Cambridge University Press, Cambridge, 1995.

[24] J. García-Ojalvo, F. Sagués, L. Schimansky-Geier, and J. M. Sancho. Noise-enhanced excitability in bistable activator-inhibitor media. *Physical Review E*, 65(1):011105, 2002.

[25] J. García-Ojalvo and J. M. Sancho. *Noise in spatially extended systems*. Springer Verlag, 1999.

[26] J. García-Ojalvo and L. Schimansky-Geier. Noise-induced spiral dynamics in excitable media. *Europhysics Letters*, 47(3):298–303, 1999.

[27] J. García-Ojalvo and L. Schimansky-Geier. Excitable structures in stochastic bistable media. *Journal of Statistical Physics*, 101(1/2):473–481, 2000.

[28] C. W. Gardiner. *Handbook of stochastic methods for physics, chemistry and the natural sciences*. Springer-Verlag, Berlin, 1985.

[29] H. Gilsing and T. Shardlow. SDELab: A package for solving stochastic differential equations in MATLAB. *Journal of Computational and Applied Mathematics*, 205(2):1002–1018, 2007.

[30] M. Giraudo and L. Sacerdote. An improved technique for the simulation of first passage times for diffusion processes. *Communications in Statistics Simulation and Computation*, 28:1135–1163, 1999.

[31] M. Giraudo, L. Sacerdote, and C. Zucca. A Monte Carlo method for the simulation of first passage times of diffusion processes. *Methodology and Computing in Applied Probability*, 3:215–231, 2001.

[32] E. Gobet. Weak approximation of killed diffusion using Euler schemes. *Stochastic Processes and Their Applications*, 87:167–197, 2000.

[33] R. Guttman, S. Lewis, and J. Rinzel. Control of repetitive firing in squid axon membrane as a model for a neuroneoscillator. *Journal of Physiology*, 305:377–395, 1980.

[34] I. Gyöngy. Lattice approximations for stochastic quasi-linear parabolic partial differential equations driven by space-time white noise I. *Potential Analysis*, 9:1–25, 1998.

[35] S. Habib and G. Lythe. Dynamics of kinks: Nucleation, diffusion and annihilation. *Physical Review Letters*, 84(6):1070–1073, 2000.

[36] B. Hassard. Bifurcation of periodic solutions of the Hodgkin-Huxley model for the squid giant axon. *Journal of Theoretical Biology*, 71:401–420, 1978.

[37] D. J. Higham. An algorithmic introduction to numerical simulation of stochastic differential equations. *SIAM Review*, 43(3):525–546, 2001.

[38] A. L. Hodgkin and A. F. Huxley. A quantitative description of membrane current and its application to conduction and excitation in nerve. *Journal of Physiology*, 117:500–544, 1952.

[39] Y. Horikawa. Noise effects on spike propagation in the stochastic Hodgkin Huxley models. *Biological Cybernetics*, 66:19–25, 1991.

[40] K. Itô and H. P. McKean. *Diffusion processes and their sample paths*. Springer-Verlag, Berlin, 1965.

[41] E. M. Izhikevich. Neural excitability, spiking and bursting. *International Journal of Bifurcation and Chaos*, 10:1171–1266, 2000.

[42] K. M. Jansons and G. D. Lythe. Efficient numerical solution of stochastic differential equations using exponential timestepping. *Journal of Statistical Physics*, 100(5), 2000.

[43] K. M. Jansons and G. D. Lythe. Exponential timestepping with boundary test for stochastic differential equations. *SIAM Journal on Scientific Computing*, 24(5):1809–1822, 2003.

[44] P. Jung and G. Mayer-Kress. Noise controlled spiral growth in excitable media. *Chaos*, 5(2):458–462, 1995.

[45] S. Kádár, J. Wang, and K. Showalter. Noise-supported travelling waves in sub-excitable media. *Nature*, 391:770–772, 1998.

[46] S. Karlin and H. M. Taylor. *A second course in stochastic processes*. Academic Press, London, 1981.

[47] P. E. Kloeden and E. Platen. Stratonovich and Itô stochastic Taylor expansion. *Mathematische Nachrichten*, 151:33–50, 1991.

[48] P. E. Kloeden, E. Platen, and H. Schurz. *Numerical Solution of SDE Through Computer Experiments*. Springer-Verlag, Berlin, Heidelberg, 1994.

[49] P.E. Kloeden and E. Platen. *Numerical Solution of Stochastic Differential Equations*. Springer-Verlag, Berlin, 1999.

[50] C. Koch. *Biophysics of computation: Information processing in single neurons*, chapter 6. Oxford University Press, 1999.

[51] P. Lánský and S. Ditlevsen. A review of the methods for signal estimation in stochastic diffusion leaky integrate-and-fire neuronal models. *Biological Cybernetics*, 99:253–262, 2008.

[52] P. Lánský and V. Lánská. First-passage-time problem for simulated stochastic diffusion processes. *Computers in Biology and Medicine*, 24(2):91–101, 1994.

[53] P. Lánský and J. P. Rospars. Ornstein–Uhlenbeck model neuron revisited. *Biological Cybernetics*, 72:397–406, 1995.

[54] P. Lánský and L. Sacerdote. The Ornstein-Uhlenbeck neuronal model with signal-dependent noise. *Physics Letters A*, 285:132–140, 2001.

[55] P. Lánský, P. Sanda, and J. He. The parameters of the stochastic leaky integrate-and-fire neuronal model. *Journal of Computational Neuroscience*, 21:211–223, 2006.

[56] B. Lindner, J. García-Ojalvo, A. Neimand, and L. Schimansky-Geier. Effects of noise in excitable systems. *Physics Reports*, 392:321–424, 2004.

[57] G. Lord, C. Powell, and T. Shardlow. *An introduction to computational stochastic PDEs*. Cambridge University Press. In preparation.

[58] G. Lythe and S. Habib. Kink stochastics. *Computing in Science and Engineering*, 8(3):10–15, 2006.

[59] R. Mannella. Absorbing boundaries and optimal stopping in a stochastic differential equation. *Physics Letters A*, 254:257–262, 1999.

[60] R.I. McLachlan, G.R.W. Quispel, and P.S.P. Tse. Linearization-preserving self-adjoint and symplectic integrators. *BIT Numerical Mathematics*, 49(1):177–197, 2009.

[61] A. S. Mikhailov. *Foundations of Synergetics I.* Springer Verlag, Berlin, 1994.

[62] B. V. Minchev and W. M. Wright. A review of exponential integrators for first order semi-linear problems. Technical report, The Norwegian University of Science and Technology, Norway, 2005.

[63] D. Mishra, A. Yadav, R. Sudipta, and P. K. Kalra. Effects of noise on the dynamics of biological neuron models. In Takeshi Furuhashi Azuma Ohuchi Yukio Ohsawa Ajith Abraham, Yasuhiko Dote, editor, *Soft Computing as Transdisciplinary Science and Technology*, Advances in Soft Computing, pages 61–69. Springer Berlin / Heidelberg, 2005.

[64] C. Moler. *Numerical computing with MATLAB.* Philadelphia : Society for Industrial and Applied Mathematics, 2004.

[65] P. Mörters and Y. Peres. *Brownian Motion.* Cambridge University Press, UK, 2010.

[66] J. D. Murray. *Mathematical Biology II.* Springer Verlag, Berlin, 1993.

[67] M. Musila, D. Suta, and P. Lánský. Computation of first passage time moments for stochastic diffusion processes modelling nerve membrane depolarization. *Computer Methods and Programs in Biomedicine*, 49:19–27, 1996.

[68] J. Nagumo, S. Arimoto, and S. Yoshizawa. An active pulse transmission line simulating nerve axon. *Proceedings of the IRE*, 50:2061–2070, 1962.

[69] E. V. Pankratova, A. V. Polovinkin, and E. Mosekilde. Resonant activation in a stochastic Hodgkin-Huxley model: Interplay between noise and suprathreshold driving effects. *The European Physical Journal B*, 45:391–397, 2005.

[70] G. Da Prato and J. Zabczyk. *Stochastic equations in infinite dimensions*, volume 44 of *Encyclopedia of Mathematics and its applications.* Cambridge University Press, Cambridge, 1992.

[71] C. Prévôt and M. Rockner. *A concise course on Stochastic Partial Differential Equations*. Springer-Verlag, Berlin, Heidelberg, 2007.

[72] C. E. Rasmussen and C. Williams. *Gaussian processes for machine learning*. The MIT Press,Cambridge, UK, 2006.

[73] M. Renardy and R. Rogers. *An Introduction to Partial Differential Equations*, chapter 6,12. Springer-Verlag New York, 2004.

[74] L.M. Ricciardi and S. Sato. Diffusion processes and first-passage-time problems. In L.M. Ricciardi, editor, *Lectures in Applied Mathematics and Informatics*. Manchester University Press, 1999.

[75] J. Rinzel and R. Miller. Numerical calculation of stable and unstable periodic solutions to the Hodgkin-Huxley equations. *Mathematical Biosciences*, 49:27–59, 1980.

[76] L.C. G. Rogers and D. Williams. *Diffusions, Markov processes and martingale II*. Cambridge University Press, Cambridge, 2000.

[77] P. Rowat. Interspike interval statistics in the stochastic Hodgkin-Huxley model: Coexistence of gamma frequency bursts and highly irregular firing. *Neural Computation*, 19:1215–1250, 2007.

[78] R. Y. Rubinstein and D. P. Kroese. *Simulation and the Monte Carlo method*. New York ; Chichester : Wiley 2008, 2 edition, 2008.

[79] L. Grüne S. Cyganowski and P.E. Kloeden. Maple for stochastic differential equations. In *Theory and Numerics of Differential Equations*, Universitext, pages 127–178. Springer-Verlag, Berlin 2001, University of Durham, UK.

[80] A. C. Scott. The electrophysics of a nerve fiber. *Reviews of Modern Physics*, 47(2):487–533, 1975.

[81] T. Shardlow. Numerical methods for stochastic parabolic PDEs. *Numerical Functional Analysis and Optimization*, 20(1), 1999.

[82] T. Shardlow. Nucleation of waves in excitable media by noise. *Multiscale Modeling and Simulation*, 3(1):151–167, 2005.

[83] T. Shardlow. Numerical simulation of stochastic PDEs for excitable media. *Journal of Computational and Applied Mathematics*, 175:429–446, 2005.

[84] R. B. Stein. The frequency of nerve action potentials generated by applied currents. *Proceeding of the Royal Society B*, 167:64–86, 1967.

[85] D. Sundararajan. *The Discrete Fourier Transform: Theory, Algorithms and Applications*. World Scientific Publishing Company, 2001.

[86] H. C. Tuckwell. Stochastic equations for nerve membrane potential. *Journal of Theoretical Neurobiology*, 5:87–99, 1986.

[87] H. C. Tuckwell. Spike trains in a stochastic Hodgkin-Huxley system. *BioSystems*, 80:25–36, 2005.

[88] H. C. Tuckwell and R. Rodriguez. Analytical and simulation results for stochastic FitzHugh-Nagumo neurons and neural networks. *Journal of Computational Neuroscience*, 5:91–113, 1998.

[89] H. C. Tuckwell, R. Rodriguez, and F. Y. M. Wan. Determination of firing times for the stochastic FitzHugh-Nagumo neuronal model. *Neural Computation*, 15:143–159, 2003.

[90] H. C. Tuckwell and F. Y. Wan. Time to first spike in stochastic Hodgkin-Huxley systems. *Physica A: Statistical Mechanics and its Applications*, 351:427–438, 2005.

[91] H.C. Tuckwell. *Introduction to Theoretical Neurobiology: Volume 2, Nonlinear and Stochastic Theories*. Cambridge University Press, 1988.

[92] A. T. Winfree. Varieties of spiral wave behavior: An experimentalist's approach to the theory of excitable media. *Chaos*, 1(3):303–334, 1991.

[93] A. M. Zhabotinsky. A history of chemical oscillations and waves. *Chaos*, 1(4):379–386, 1991.

[94] C. Zhou and J. Kurths. Noise-induced synchronization and coherence resonance of a Hodgkin-Huxley model of thermally sensitive neurons. *Chaos*, 13(1):401–409, 2003.

[95] V. S. Zykov and A. T. Winfree. *Simulation of Wave Processes in Excitable Media*. Manchester University Press, Manchester, 1987.